European Commission

JRC TECHNICAL REPORTS

JRC – Ispra Atmosphere – Biosphere – Climate Integrated monitoring Station
2013 Report

J. P. Putaud, P. Bergamaschi, M. Bressi, F. Cavalli, A. Cescatti, D. Daou, A. Dell'Acqua, K. Douglas, M. Duerr, I. Fumagalli, I. Goded, F. Grassi, C. Gruening, J. Hjorth, N. R. Jensen, F. Lagler, G. Manca, S. Martins Dos Santos, M. Matteucci, R. Passarella, V. Pedroni, O. Pokorska, D. Roux

2 0 1 4

Joint Research Centre

Abstract

The Institute for Environment and Sustainability provides long-term observations of the atmosphere within international programs and research projects. These observations are performed from the research infrastructure named ABC-IS: Atmosphere – Biosphere – Climate Integrated monitoring Station. Most measurements are performed at the JRC-Ispra site, but observations are also carried out from two other platforms: the forest station in San Rossore, and a ship cruising in the Western Mediterranean sea. This document reports about the measurement programs, the equipment which is deployed, the data quality assessment, and the results obtained for each site. Our observations are presented, compared to each other, as well as to historical data obtained over more than 25 years at the Ispra site.

Contents

Executive Summary

The ABC-IS annual report 2013 provides an overview of the Atmosphere-Biosphere-Climate integrated monitoring activities performed by the Air and Climate Unit of the Joint Research Centre (H02). It presents results obtained in 2013 on long lived greenhouse gases concentrations (CO_2, CH_4, N_2O, SF_6), air $\leftrightarrows$ biosphere fluxes (CO_2, H_2O, heat, O_3), short lived climate forcers (O_3, aerosols) and their precursors (NOx, SO_2, CO), as well as other regulated species (PM_{10}, $PM_{2.5}$, heavy metals). These data extend the long time series in key pollution metrics (> 25 years) and climate forcers (5-10 years), in one of the most polluted areas in Europe.

We measure greenhouse gas concentrations and ^{222}Rn activity in Ispra (regional background in Northern Italy), atmosphere $\leftrightarrows$ terrestrial biosphere fluxes in Ispra (unmanaged temperate forest) and San Rossore (semi-managed Mediterranean forest), and O_3, aerosols and their precursors in Ispra and from a cruise ship in Western Mediterranean. Data quality is our priority. It is assured through our participation in international projects (ICOS, InGOS, ECLAIRE, ACTRIS) and programs (EMEP, GAW, AQUILA), in which standard operating procedures are applied, certified scales are used and inter-laboratory comparisons are organized regularly.

Our data can be downloaded from international data bases (www.europe-fluxdata.eu, www.ingos-infrastructure.eu, ebas.nilu.no, www.eclaire-fp7.eu), and can also be directly obtained from ABC-IS' staff.

Six years of continuous greenhouse gas monitoring show that CO_2, CH_4, N_2O, and SF_6 concentrations are close to marine background under clean air conditions. Deviations from background concentrations provide key information about regional and larger scale European greenhouse gas sources.

Analyses of rainwater revealed 9 very acid (pH<4.6) rain event in 2013, but deposition fluxes of acidifying and eutrophying substances remain low compared to the 1990's.

Measurements of PM mass concentrations confirm the high level of particulate air pollution in the area of Ispra (Northwest of the Po Valley): 38 exceedances of the 24hr limit value (50 µg m^{-3}) were observed in 2013. However, PM concentrations have decreased by 1 µg m^{-3} yr^{-1} on average for more than 25 years. The main constituents of $PM_{2.5}$ are currently organic matter (49%), ammonium sulfate (21%), ammonium nitrate (17%), and elemental carbon (7%). On-line measurements of the sub-micron aerosol chemistry allowed us to determine to contribution of wood burning, primary, and secondary species to the organic aerosol.

Ozone concentration decreased during 2001 – 2008, but increased for the 4th consecutive year in 2013. As a consequence, several indicators (e.g. SOMO35) reached or exceeded their historical maximums record at Ispra since 1988. In contrast, SO_2 concentrations remained as low as during the few last years.

Atmosphere $\leftrightarrows$ vegetation flux measurements in the forest on the JRC-Ispra premises were initiated in June 2012. During 2013, atmospheric turbulence was such that 60 to 67% of the

flux measurements were of good to acceptable quality. "Our" forest is clearly a sink for CO_2 in summer, and for O_3 the whole year round. In contrast, the forest soil is a significant source of NO in summer, and a sink of NO_2 especially in winter. In San Rossore, pests' attacks led to massive tree cutting which forced us to set up a new site 700 m away in autumn 2012. In 2013, micrometeorological conditions were such that 72% of the CO_2 flux measurements performed were of good to acceptable quality. Over the year, the pine forest in San Rossore was a larger CO_2 sink than the deciduous forest in Ispra (630 g C m^{-2} vs 400 g C m^{-2}).

The measurements from the cruise ship were resumed on board Costa Concordia in June this year. They clearly show the impact of ship emissions on SO_2 concentrations in the Western Mediterranean. In 2013, ozone concentrations were larger than during past years. A week of ^{7}Be measurements did not reveal significant intrusions of upper atmosphere at sea level.

Long-term accurate measurements produce datasets which are essential to assess the impact of European Directives and international protocols, and develop future air quality and climate change mitigation policies. Conclusions arising from further analyses of our measurements include:

- evaluation of regional greenhouse gas emissions using inverse modeling and model-independent analyses using the ^{222}Rn tracer.

- abatement in sulfur emissions have been efficient in solving the acid rain issue and decreasing PM levels in our area. PM levels still remains too high though

- air quality policies are dimming the climate cooling effect of aerosols at our site (Putaud et al., 2014).

- measures for abating tropospheric ozone, which had a positive impact on concentrations and various indicators in the early 2000's, were not sufficient to keep O_3 concentrations low during the 4 last years

- temperate and Mediterranean forest are important sinks for CO_2 and O_3. In contrast, the emission of NO from forest soils is significant.

- The scope of these conclusions is certainly limited by the spatial representativeness of our measurements, which depends on the atmospheric lifetime of the studied species. This is why our measurements are performed in the framework of international collaborations. This ensures a privileged near real time access to the data produced on regional and global scales by the networks in which we participate.

ABC-IS mission

The aim of the Atmosphere-Biosphere-Climate Integrated monitoring Station (ABC-IS) is to measure changes in atmospheric variables to obtain data that are useful for the conception, development, implementation, and monitoring of the impact of European policies and International conventions on air pollution and climate change. Measurements include greenhouse gas concentrations, forest ⇆ atmosphere fluxes, and concentrations of pollutants in the gas phase, the particulate phase and precipitations, as well as aerosol physical and optical characteristics. The goal of ABC-IS is to establish real world interactions between air pollution, climate change and the biosphere, for highlighting possible trade-offs and synergies between air pollution and climate change related policies. Interactions include the role of pollutants in climate forcing and CO_2 uptake by vegetation, the impact of climate change and air pollution on CO_2 uptake by vegetation, the effect of biogenic emission on air pollution and climate forcing, etc.
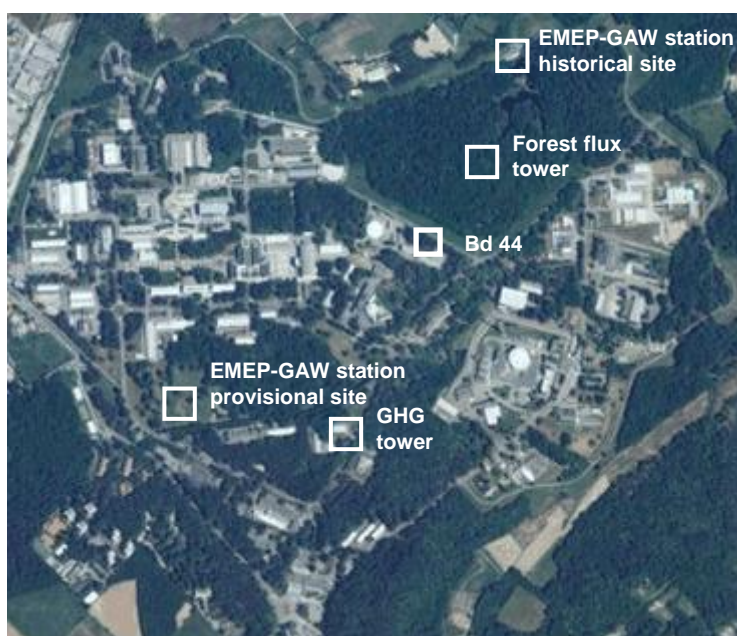
Fig. 1. The *JRC-Ispra site and the location of the laboratory for greenhouse gas (GHG) monitoring, the forest flux tower, the historical and the provisional EMEP-GAW station sites.*

Measurements are performed in the framework of international monitoring programs like the future (from 2014) European Research Infrastructure Consortium project ICOS (Integrated Carbon Observation System), EMEP (Co-operative program for monitoring and evaluation of the long range transmission of air pollutants in Europe of the UN-ECE *Convention on Long-Range Transboundary Air Pollution* CLRTAP) and GAW (the Global Atmosphere Watch program of the World Meteorological Organization). The ABC-IS infrastructure is also used in competitive projects (e.g ACTRIS, ECLAIRE, InGOS). Through the participation of ABC-IS in international networks, inter-laboratory comparisons are conducted and standard methods are developed in the frame of the European Reference Laboratory for Air Pollution of the JRC-IES.

Quality management system

ABC-IS is a research infrastructure of JRC's Institute for Environment and Sustainability. JRC-IES achieved the ISO 9001 re-certification in June 2013, which is also valid for the year 2013 (ISO 9001 is mainly about "project management").

In addition, in Nov. 2010 the JRC-Ispra also achieved the ISO 14001 certificate (ISO 14001 is mainly about "environmental issues"), which is also valid for 2013.

Every year there are internal/external audits for the certificates (ISO 9001 / ISO 14001), which were also performed in 2013.

For information (the links below being accessible to JRC staff only), the "quality management system (QMS) for the ABC-IS regional station" includes server space at the following links:

\\ies.jrc.it\H02\H02QMS_year_2013_

\\ies.jrc.it\H02\LargeFacilities\ABC-IS\

\\ies.jrc.it\H02\Laboratories

\\Lake\lifecyclesheets\

where the following information can be found: list of instruments; information about calibrations; standards used and maintenance; standard operational procedures (SOP's); instrument lifecycle sheets and log-books; manuals for the instruments; *etc*. For additional specific details about QMS, for the year 2013 and the ABC-IS station, see e.g. the file 2013_Instruments'_calibration_&_standards_&_maintenance.xls, that can be found under \\ies.jrc.it\H02\LargeFacilities\ABC-IS\Quality_management.

More QMS information/details can also be found in the sections "Measurement techniques" in this report.

More general QMS information/documentations about how the IES-AC Unit (H02) was run in 2013, the management of all of the projects within the Unit and the running of the ABC-IS station can also be found at

\\ies.jrc.it\H02\H02QMS_year_2013_\1_UNIT\QMS_info\QMS_documents_H02

\\ies.jrc.it\H02\H02QMS_year_2014_\1_UNIT\QMS_info\QMS_documents_H02

and especially in the seven H02 Unit QMS documents listed here:

QMS_H02_SUMM_Scientific_Unit_Management_Manual_v9_0.pdf

QMS_H02_MANPROJ_PROJ_Laboratory_Management_v8_0.pdf

QMS_H02_MANPROJ_PROJ_Model_Management_v8_0.pdf

QMS_H02_MANPROJ_PROJ_Informatics_Management_v8_0.pdf

QMS_H02_MANPROJ_PROJ_Knowledge_Management_v8_0.pdf

QMS_H02_MANPROJ_PROJ_Review_Verification_Validation_Approval_v4_0.pdf

QMS_H02_MANPROJ_PROJ_Administration_Implementation_v2_0.pdf

The latest versions of the documents are available at

\\ies.jrc.it\H02\H02QMS_year_2014_\1_UNIT\QMS_info\QMS_documents_H02

Fig. 2: the laboratory for greenhouse gas concentration monitoring (Bd 5). Air is sampled from the 15m high mast.
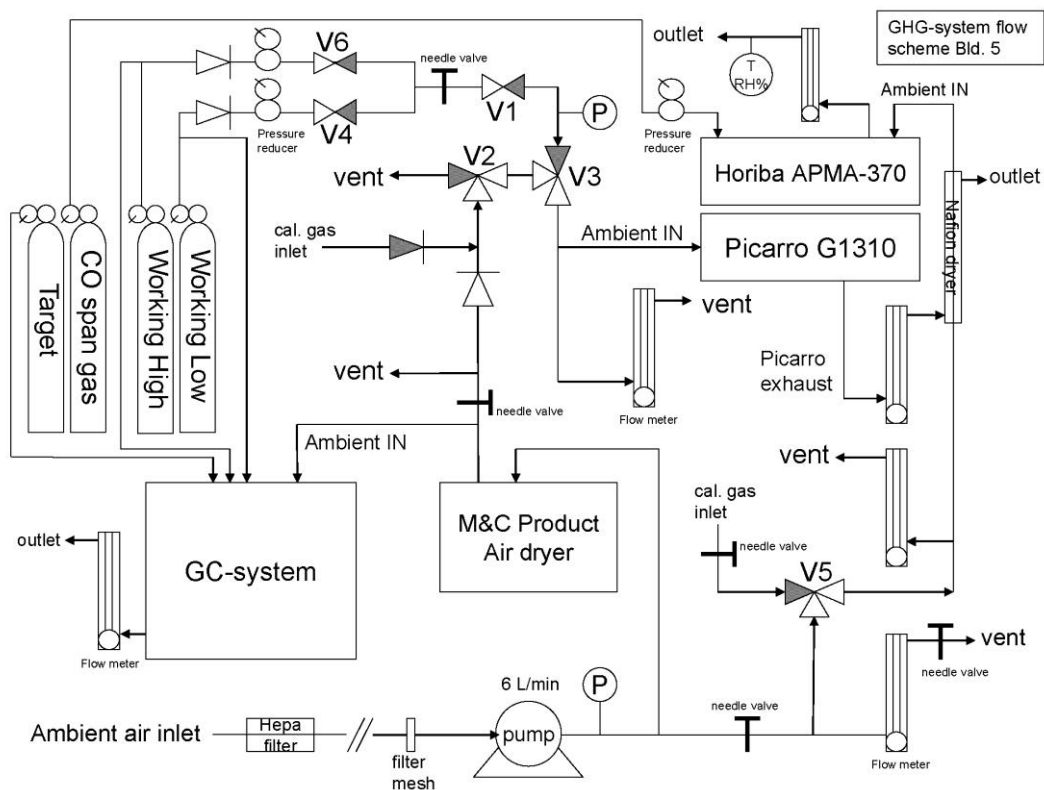

Fig. 3: *Building 5 GHG-system flow scheme.*

Greenhouse gas concentration monitoring at the JRC-Ispra site

Introduction

Location

The GHG monitoring station is located at Building 5 of the JRC site Ispra (45.807°N, 8.631°E, 223 m asl). The station is currently the only low altitude measurement site for greenhouse gases near the Po Valley. The unique location of the station at the South-Eastern border of Lake Maggiore in a semi-rural area at the North-Western edge of the Po Valley allows sampling of highly polluted air masses from the Po Valley during meteorological conditions with southerly flow, contrasted by situations with northerly winds bringing relatively clean air to the site. The main cities around are Varese, 20 km to the East, Novara, 40 km South, Gallarate - Busto Arsizio, about 20 km southeast and Milan, 60 km to the south-east. The GHG monitoring station is in operation since October 2007 and is complementary to the JRC-Ispra EMEP-GAW (European Monitoring and Evaluation Programme - Global Atmospheric Watch) air quality station, which started in 1985 (Putaud et al., 2014). Both activities together are referred to as ABC-IS (Atmosphere, Biosphere, Climate Integrated Monitoring Station).

Measurement program

The GHG monitoring station is in operation since October 2007 and is complementary to the JRC-Ispra EMEP-GAW (European Monitoring and Evaluation Programme - Global Atmospheric Watch) air quality station which started in 1985. Both activities together with biosphere atmosphere fluxes are referred to as ABC-IS (Atmosphere, Biosphere, Climate Integrated Monitoring Station), and will be merged in 2015 into a single monitoring and research platform with a new station building and tall tower for atmospheric sampling. The measurement program follows the recommendations of ICOS (www.ICOS-infrastructure.eu) for level 2 stations.

Instrumentation

Here we summarize the most important aspects of the GHG and ^{222}Radon measurement system. A more detailed description is given by Scheeren et al. (2010).

Sampling

Air is sampled from a 15 m high mast using a 50 m ½" Teflon tube at a flow rate of ~6 L /min using a KNF membrane pump (KNF N811KT.18). The sampled air is filtered from aerosols by a Pall Hepa filter (model PN12144) positioned 10 m downstream of the inlet and dried cryogenically by a commercial system from M&C products (model EC30 FD) down to a water vapour content of <0.015%v before being directed to the different instruments. The remaining water vapour is equivalent to a maximum 'volumetric error' of <0.06 ppmv of CO_2 or <0.3 ppbv of CH_4 or <0.05 ppbv N_2O. A schematic overview of the sample flow set-up is shown in Figure 4.

Gas Chromatograph Agilent 6890N (S/N US10701038*)*

For continuous monitoring at 6 minute time resolution of CO_2, CH_4, N_2O, and SF_6 we apply an Agilent 6890N gas chromatograph equipped with a Flame Ionization Detector (FID) and micro-Electron Capture Detector (µECD) based on the set-up described by Worthy el al. (1998). The calibration strategy has been adopted from Pepin et al. (2001) and is based on applying a Working High (WH) and Working Low (WL) standards (bracketing standards), which are calibrated regularly using NOAA primary standards. The WH and WL are both measured 2 times per hour for calculating ambient mixing ratios and a Target (TG) sample is measured every 6 hours for quality control (purchased from Deuste Steininger GmbH, Germany). N_2O concentrations were also calculated using a second calibration strategy that is based on a one-point-reference method with a correction for non-linearity of µECD. The non-linear response of the µECD was estimated using NOAA primary standards and then it was applied to the entire time series. This second method improves the quality of the time series when the bracketing standards do not cover well the range for N_2O ambient concentrations (i.e. range too large or range that does not include the ambient concentration). GHG measurements are reported as dry air mole fractions (mixing ratios) using the WMO NOAA2004 scale for CO_2 and CH_4, the NOAA2006 scale for N_2O and SF_6. We apply a suite of five NOAA tanks ranging from 369-523 ppm for CO_2, 1782-2397 ppb for CH_4, 318-341 ppb for N_2O, and 6.1-14.3 ppt for SF as primary standards. The GC control and peak integration runs on *ChemStation* commercial software. Further processing of the raw data is based on custom built software developed in C language and named GC_6890N_Pro. A schematic of the GC-system set-up and typical chromatograms are shown in Figure 4, while Figure 5 shows the graphical user interface of the GC_6890N_Pro software..
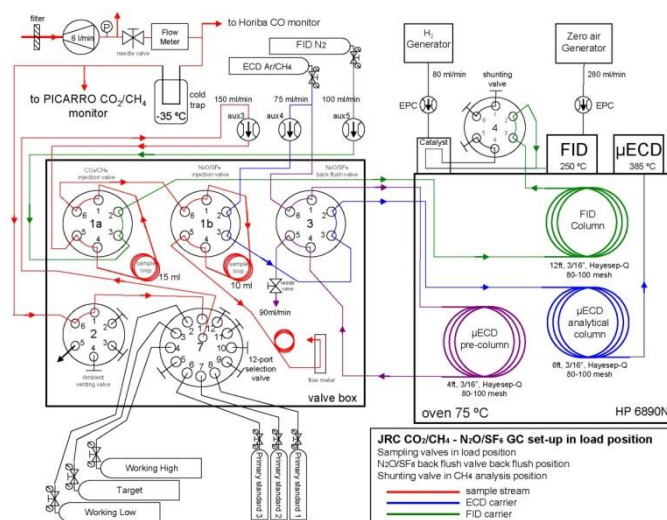

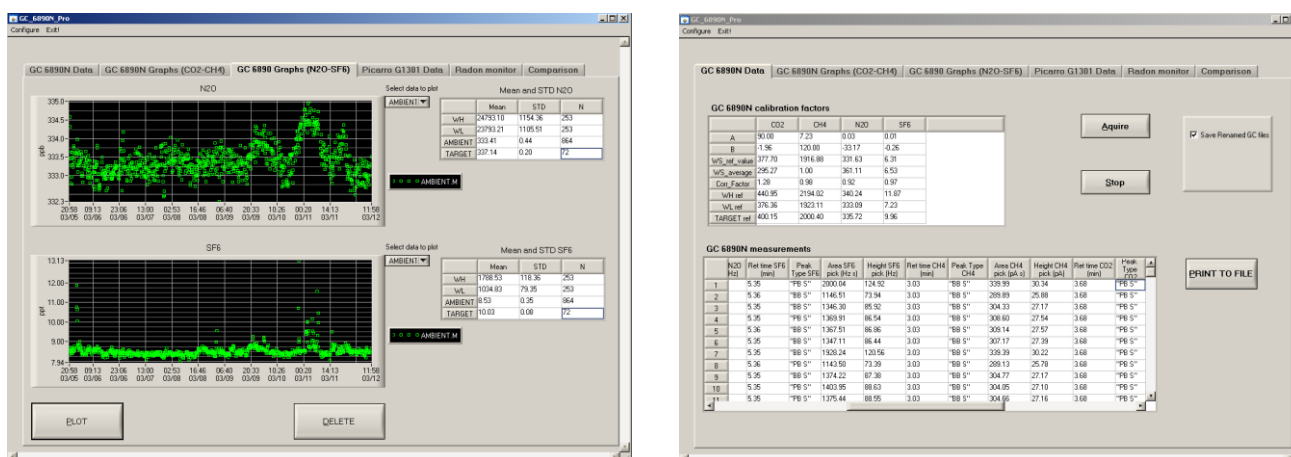*Fig.4: Schematic of the GC-system set-up for greenhouse gas concentration measurements*

Fig. 5: *Graphical User Interface of GC_6890N_Pro software, developed for data processing of GC raw data*

Cavity Ring-Down Spectrometer (Picarro G1301) (S/N CFDAS-42)

In addition to the low time resolution GC-system we have been operating a fast Picarro G1301 Cavity Ring-Down Spectrometer (Picarro CRDS) for CO_2 and CH_4 since February 2009. The Picarro instrument collected air samples from the same inlet used for the GC at a time resolution of 12 seconds until July 2013. Since August 2013 the Picarro instrument is measuring at the flux tower in Ispra with an air sample inlet at 36 m height. From March 24, 2009 onwards we applied a commercial M&C Products Compressor gas Peltier cooler type EC30/FD for drying of the sampling air to below 0.02%v. This corresponds to a maximum 'volumetric error' of about 0.08 ppm CO_2 and 0.4 ppb CH_4. To compensate for the remaining water vapor fraction we apply an empirically determined instrument specific water vapor correction factor. From May 27, 2009 onwards, the monitor received a WL and WH standard for 10 minutes each once every two days which was reduced to once every 4 days from September 2011 onwards, to serve as a Target control sample and to allow for correction of potential instrumental drift. A full scale calibration with 5 NOAA standards is performed 2 to 3 times per year. The monitor response has shown to be highly linear and the calibration factors obtained with the 5-point calibration have shown negligible changes within the precision of the monitor over the course of a year. The monitor calibration factors to calculate raw concentration values have been set to provide near real-time raw data with an accuracy of <0.5 ppm for CO_2 and <2 ppb for CH_4.

Radon analyser ANSTO (custom built)

[222]Radon activity concentrations in Bq m^{-3} have been semi-continuously monitored (30 minute time integration) applying an ANSTO dual-flow loop two-filter detector (Zahorowski et al., 2004) since October of 2008. The monitor is positioned close to the GHG-sampling mast and used a separate inlet positioned at 3.5 m above the ground. A 500 L decay tank was placed in the inlet line to allow for the decay of Thoron ([220]Rn with a half-life of 55.6 s) before reaching the [222]Radon monitor. The ANSTO [222]Radon monitor is calibrated once a month using a commercial passive [226]Radium source from Pylon Electronic Inc. (Canada) inside the calibration unit with an activity of 21.99 kBq, which corresponds to a [222]Radon delivery rate of 2.77 Bq min^{-1}. The lower limit of detection is 0.02 Bq m^{-3} for a 30% precision (relative counting error). The total measurement uncertainty is estimated to be <5% for ambient [222]Radon activities at Ispra.

Table 1: Precision and reproducibility for the different gas species measured by PICARRO G1301.

Species-method	Precision	Reproducibility Long-term	WMO [1] compatibility goal
CO_2-CRDS	0.03 ppm	0.04 ppm	0.1 ppm
CH_4-CRDS	0.2 ppb	0.3 ppb	2 ppb

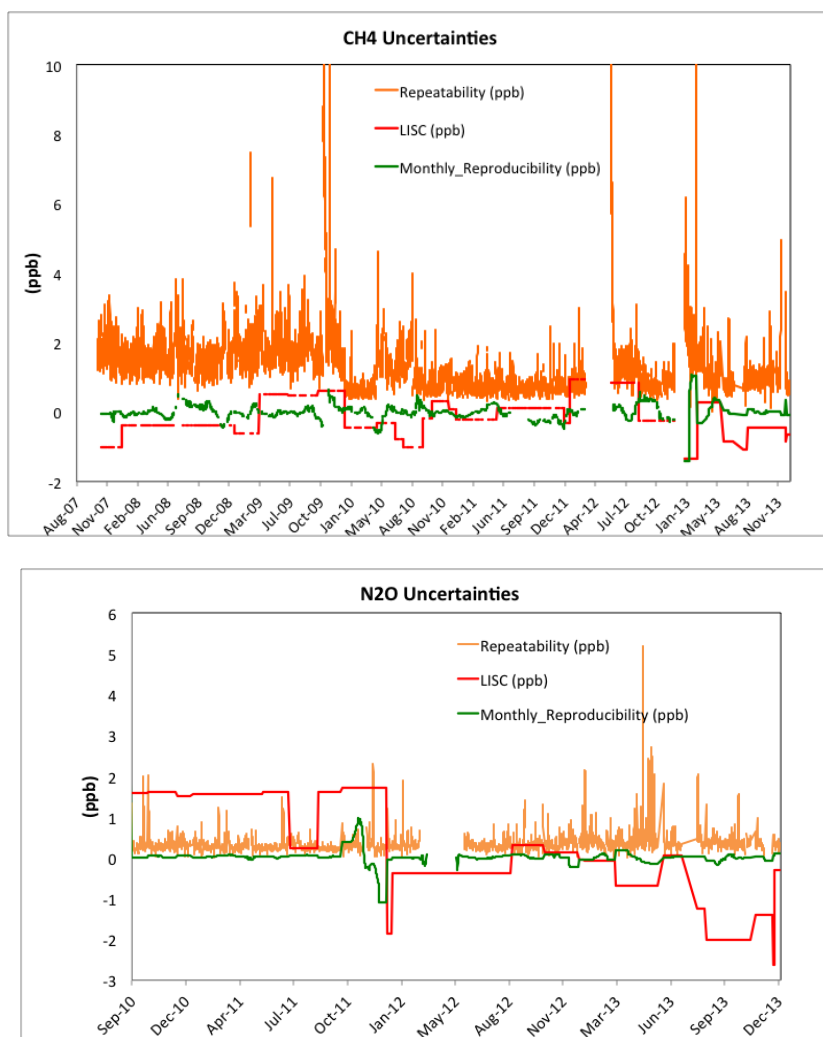*(1)* *WMO-GAW Report No. 194, 2010.*

Fig. 6: *Uncertainties affecting CH$_4$ and N$_2$O measurements performed by the GC system.*

Measurement uncertainties

The different types of uncertainties affecting the GC measurements (Fig. 6) have been estimated using the algorithms developed in the InGOS ("Integrated non-CO2 Greenhouse gas Observing System") project (http://www.ingos-infrastructure.eu/). These uncertainties are defined as follows:

- Working standard repeatability is calculated as the 24-hours centered moving, 1σ standard deviation of the bracketing standards (or reference standard in case of the one-point-reference method).
- Laboratory internal scale consistency uncertainty (LISC) is the median of the difference between measured and assigned values of the target gas. The median is calculated for different time periods.
- Monthly reproducibility represents the values of the smoothed target residuals. Smoothing is performed with a centered running median with a window length of 30 days.
- Scale transfer and non-linearity uncertainty is calculated as one-sigma confidence bands of the fit used to estimate the response function of the GC. Errors of the reference standards and primary standards used to estimate the response function must be taken into account in the fitting procedure. This error is not yet estimated for the GC measurements.

Uncertainties values are presented in the following section. For the PICARRO G1301 we define the precision by the 1σ standard deviation of the average of a 10 minutes dry standard measurement. To determine the long-term reproducibility we evaluated the deviations of the Target from the assigned value over a period of about 7 months. We found that the reproducibility over this period was <0.04 ppm for CO_2 and <0.3 ppb for CH_4. The precision and reproducibility for the PICARRO measurements are presented in Table 1.
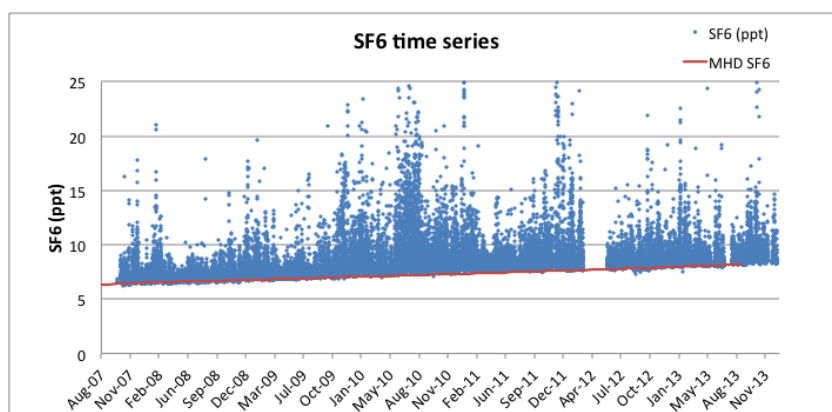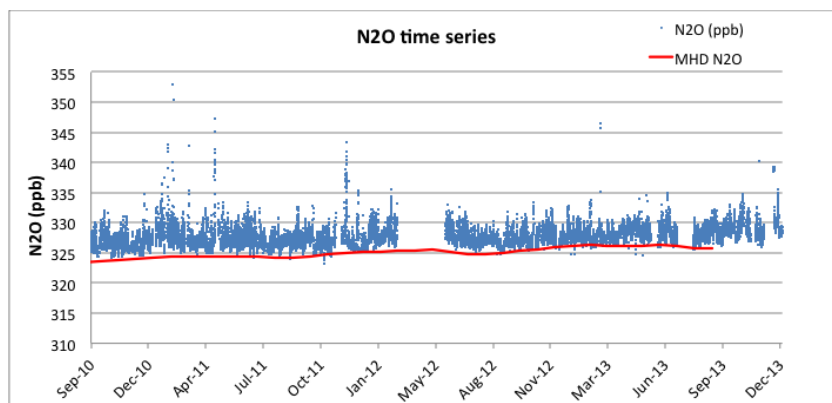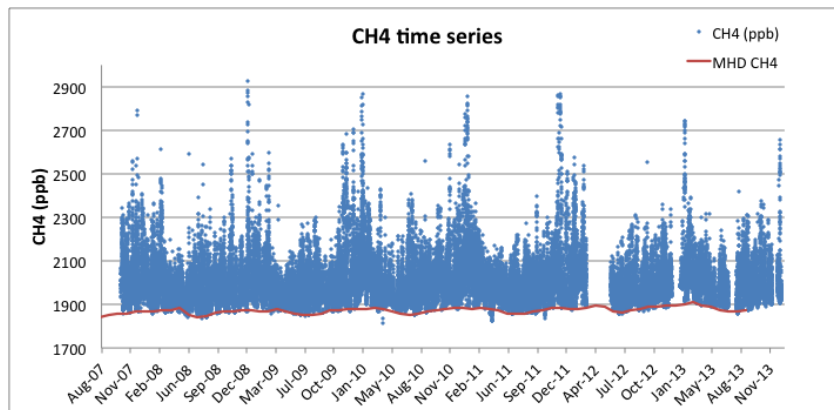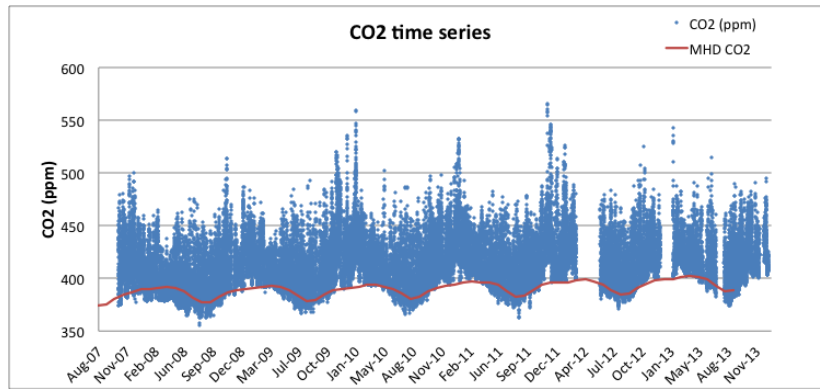
Fig. 7 *Time series of continuous CO₂, CH₄, N₂O, SF₆, measurements at Ispra between October 2007 and December 2012. The figure shows hourly mean values of dry air mole fractions (blue points). Monthly mean concentrations from the background station Mace Head on the West coast of Ireland are also included (red points).*

Overview of measurement results

Figure 7 gives an overview of the GC greenhouse gas measurements since the start of the measurements in October 2007 until December 2013. For N_2O only date after 15/09/2010 based on the one-point-reference method are shown. Before this date there was a dilution problem of the sample loop connected to the column of µECD detector. The flushing of the sample loop during ambient measurement was not sufficient to remove completely the carrier gas used in the previous analysis. Work is on-going to try to recover data collected before 15/09/2010.

Figure 7 shows hourly averages concentrations. Furthermore, continuous measurements from the Mace Head (Ireland) station are included in the Figure to illustrate the Atlantic background mixing ratios. Minimum values of CH_4, N_2O and SF_6 measured at the JRC-Ispra site are close to the Mace Head baseline, while CO_2 mixing ratios can be lower than the Mace Head baseline due to the continental biospheric CO_2 sink.

At the end of February 2012 GC measurement were stopped because of the end of the working contract of Bert Scheeren. Measurements restarted at the end of May 2012 when Giovanni Manca took over from Bert Scheeren. Shorter gaps in the GC measurements during 2013 were mainly due to the failure of the electronic pressure control connected to the FID detector and due to delays to get appropriate working standards from the market.

Figure 6 shows three types of uncertainties as defined in the InGOS project for CH_4 and N_2O. Working standard repeatability and laboratory internal scale consistency (LISC) uncertainty are the major contributors to the overall uncertainty affecting the GC.

Figure 8 shows hourly mean [222]Radon activities since October 2008.

In Figure 9a we show the CO_2 and CH_4 hourly mean time series from both the GC-system and the Picarro CRDS for 2013. Gaps in the time series are due to the failure of the Picarro instrument in November 2012 that required a long time to be solved and due to the technical problems during the installation of the instrument at the flux tower in Ispra. Figure 9b shows the absolute difference between the hourly mean values of the Picarro and the GC-system. Until July 2013 there is an excellent agreement between the two instruments. Since August 2013 a systematic difference is evident due to the different location of the two instruments.
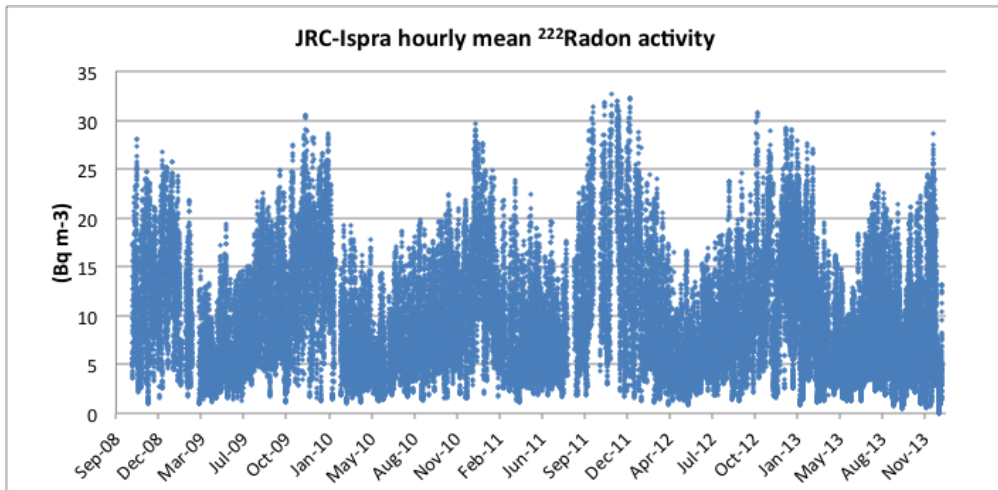
Fig. 8: *Time series of hourly mean ^{222}Radon activity from Oct. 2008 to Dec. 2012.*
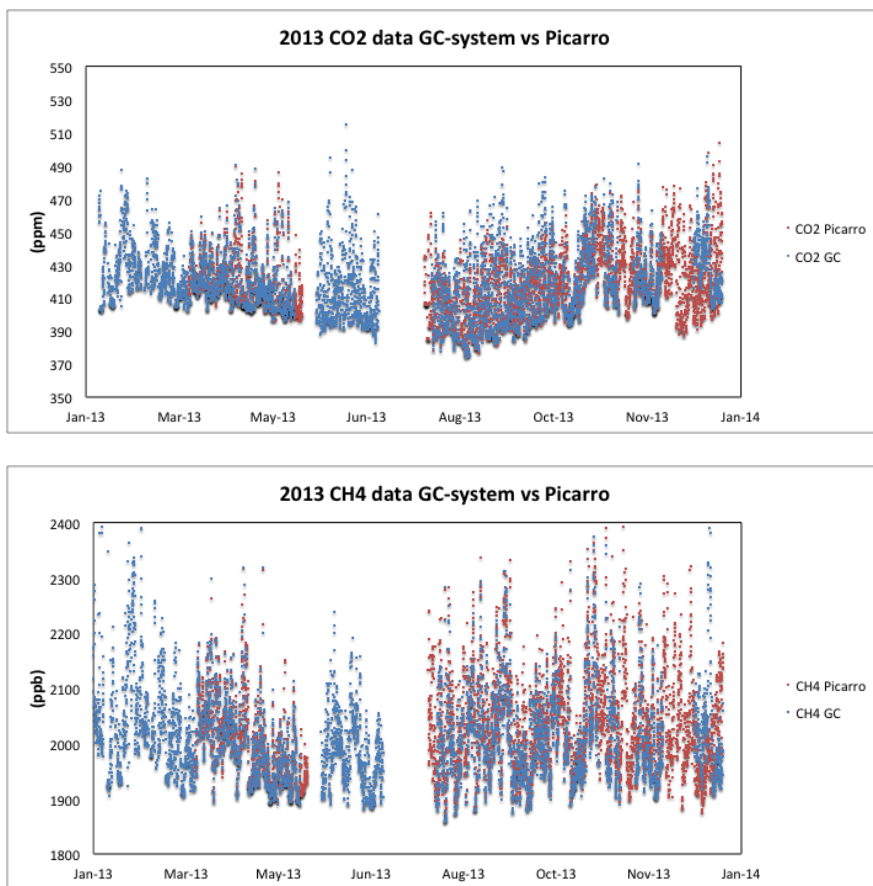
Fig. 9a: *Time series of hourly mean CH_4 and CO_2 dry air mole fractions at Ispra during 2013 from the GC-system and the Picarro CRDS.*

Focus on 2013 data

In Figure 9a we show the CO_2 and CH_4 hourly mean time series from both the GC-system and the Picarro CRDS for 2013. In Figure 9b the excellent agreement between both measurements system is illustrated by the fact that the absolute difference between the hourly mean values of the Picarro and the GC-system is usually well within the variability (depicted as the 1-σ standard deviation) of the hourly mean data from the Picarro instrument.
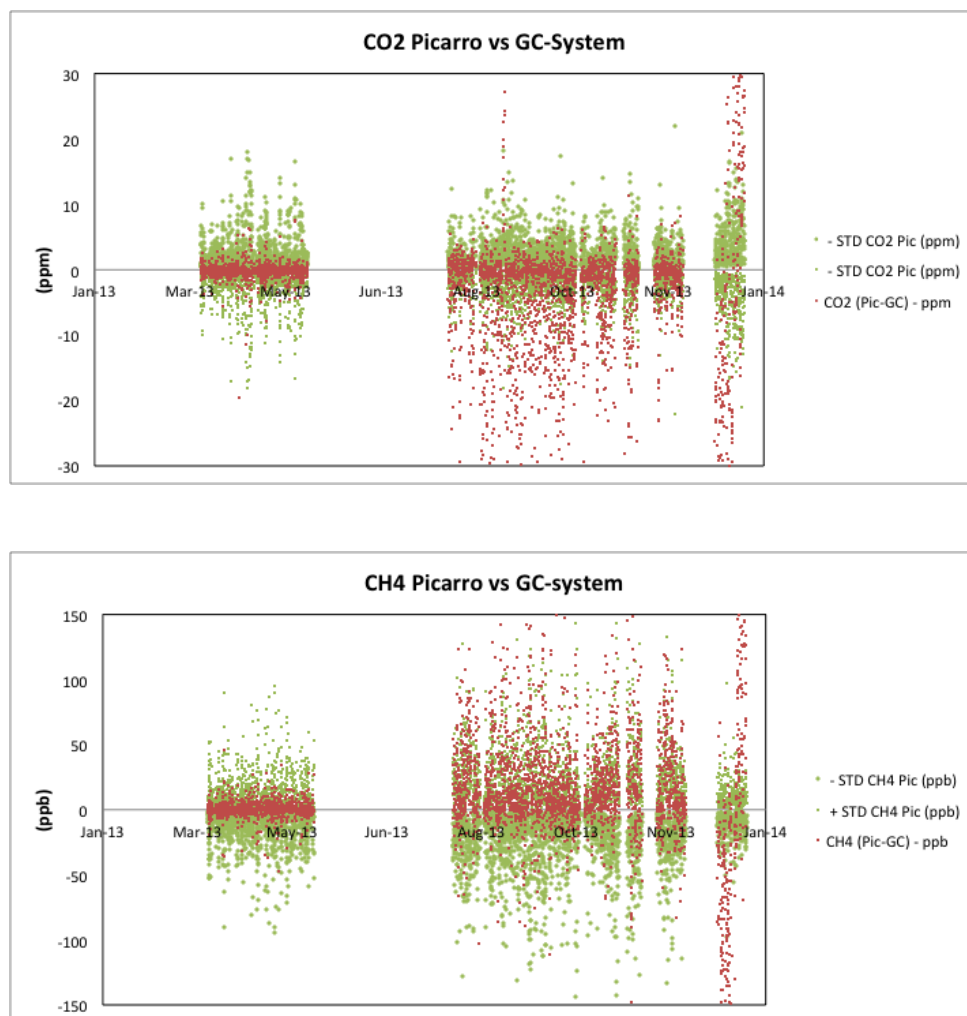
Fig. 9b: *Comparison between the absolute difference of the hourly mean values of the Picarro and the GC-system and the variability (depicted as the 1-σ standard deviation) of the hourly mean data from the Picarro instrument.*
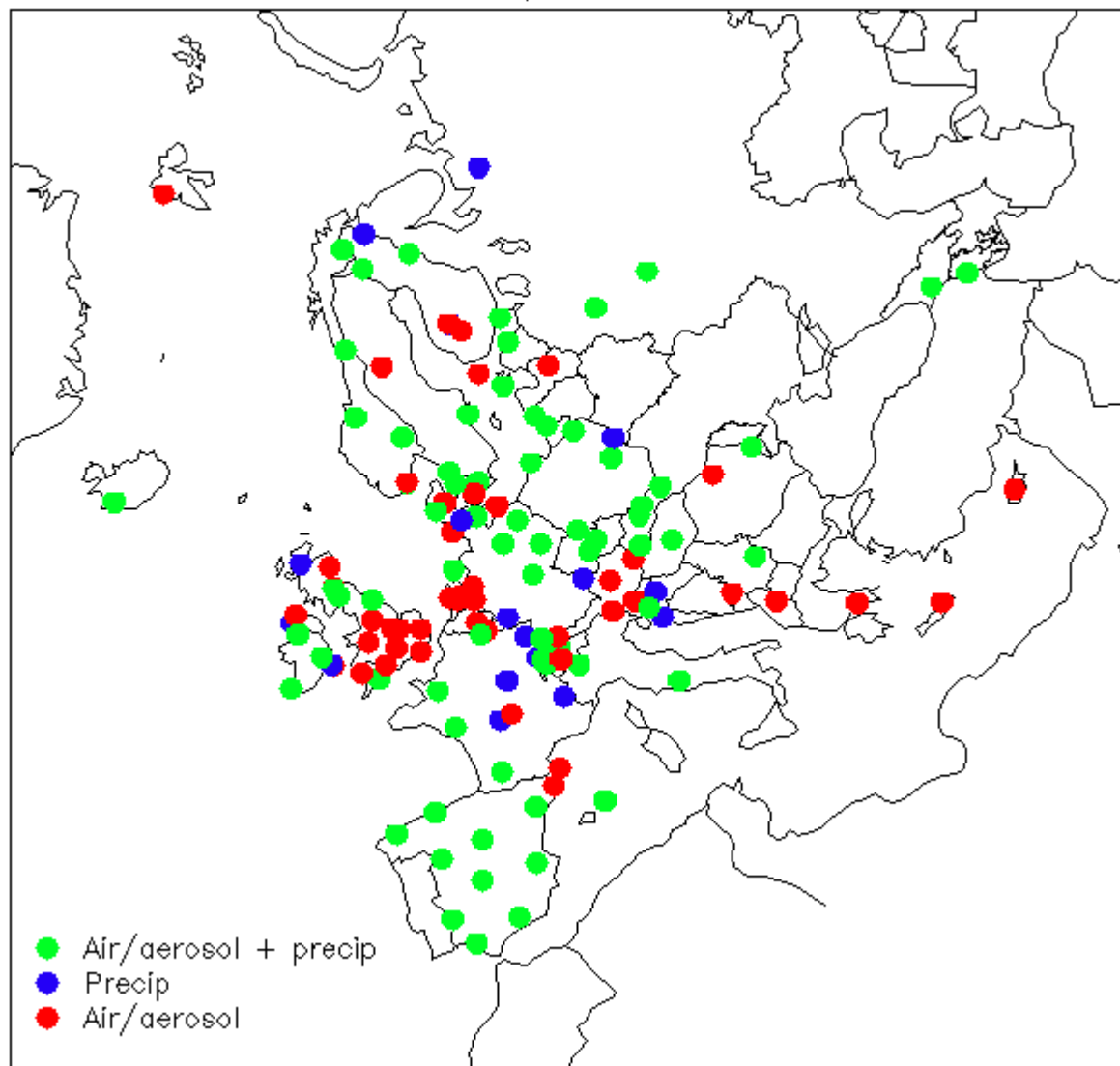
Fig 10: *most recent available map of the EMEP stations across Europe.*

Short-lived atmospheric species at the JRC-Ispra site

Introduction

Location

Air pollution has been monitored since 1985 at the EMEP and regional GAW station for atmospheric research (45°48.881'N, 8°38.165'E, 209 m a.s.l.) located by the Northern fence of the JRC-Ispra site (see Fig. 1), situated in a semi-rural area at the NW edge of the Po valley in Italy. The main cities around are Varese (20 km east), Novara (40 km south), Gallarate - Busto Arsizio (about 20 km south-east) and the Milan conurbation (60 km to the south-east). Busy roads and highways link these urban centers. Emissions of pollutants reported for the four industrial large point sources (CO_2 emissions $>$ 1500 tons d^{-1}) located between 5 and 45 km NE to SE from Ispra also include 2 and 3 tons of CO per day, plus 3 and 5 tons of NOx (as NO_2) per day for the 2 closest ones (PRTR emissions, 2010).

Underpinning programs

The EMEP program (*http://www.emep.int/*)

Currently, about 50 countries and the European Community have ratified the CLRTAP. Lists of participating institutions and monitoring stations (Fig. 10) can be found at: *http://www.nilu.no/projects/ccc/network/index.html*

The set-up and running of the JRC-Ispra EMEP station resulted from a proposal of the Directorate General for Environment of the European Commission in Brussels, in agreement with the Joint Research Centre, following the Council Resolution N° 81/462/EEC, article 9, to support the implementation of the EMEP programme.

The JRC-Ispra station operates on a regular basis in the extended EMEP measurement program since November 1985. Data are transmitted yearly to the EMEP Chemical Coordinating Centre (CCC) for data control and statistical evaluation, and available from the EBAS data bank (Emep dataBASe, *http://ebas.nilu.no/*).

The GAW program (*http://www.wmo.int/web/arep/gaw/gaw_home.html*)

WMO's Global Atmosphere Watch (GAW) system was established in 1989 with the scope of providing information on the physico-chemical composition of the atmosphere. These data provide a basis to improve our understanding of both atmospheric changes and atmosphere-biosphere interactions. GAW is one of WMO's most important contributions to atmosphere-biosphere the study of environmental issues, with about 80 member countries participating in GAW's measurement program. Since December 1999, the JRC-Ispra station is also part of the GAW coordinated network of regional stations. Aerosol data submitted to EMEP and GAW are available from the World Data Centre for Aerosol (WDCA).
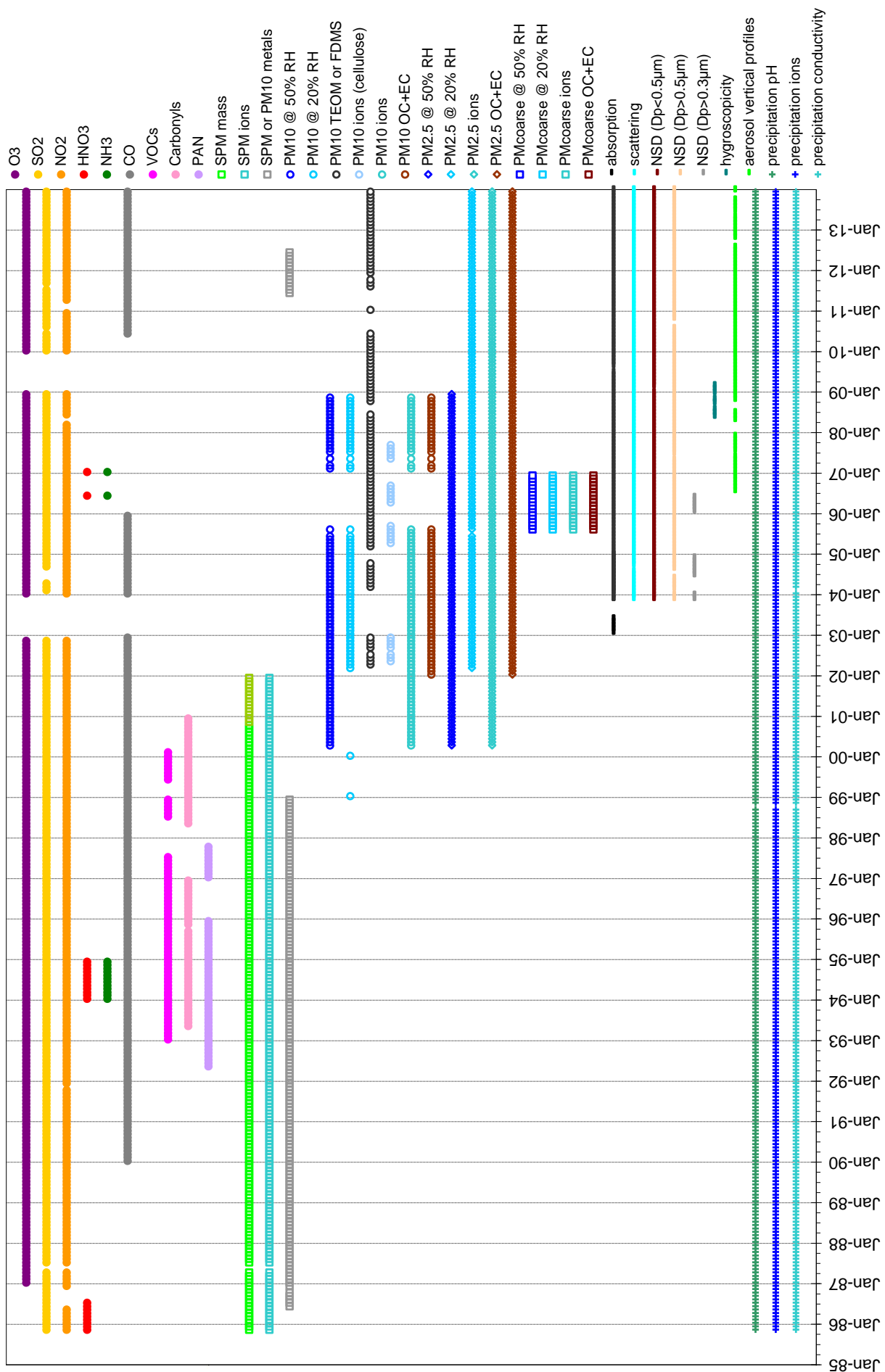
Fig. 11. Measurements performed at the JRC-Ispra station for atmospheric research since 1985.

The institutional program (***http://ccaqu.jrc.ec.europa.eu***)

Since 2002, the measurement program of the air pollution monitoring station of JRC-Ispra has gradually been focused on short-lived climate forcers such as tropospheric ozone and aerosols, and their precursors (Fig. 11). Concretely, more sensitive gas monitors were introduced, as well as a set of new measurements providing aerosol characteristics that are linked to radiative forcing. In 2012, the station's duty as listed in the Airclim action work plan was to deliver "data on regulated and non-regulated pollutants delivered to EMEP and the World Data Centre for Aerosols international databases"

The site is also being used for research and development purposes. Regarding particulate organic and elemental carbon, techniques developed in Ispra are implemented and validated by international research station networks (EUSAAR, ACTRIS), recommended in the EMEP sampling and analytical procedure manual, and considered by the European Committee for Standardisation (CEN) as possible future standard methods.

Additional information about the JRC-Ispra air monitoring station and other stations from the EMEP network can also be found in the following papers: Van Dingenen et al., 2004; Putaud et al., 2004; Mira-Salama et al., 2008; Putaud et al., 2010). Nowadays, all validated monitoring data obtained at the JRC-Ispra station within the EMEP and the GAW program and other international projects (EUSAAR, ACTRIS) can be retrieved from the EBAS database (*http://ebas.nilu.no/*), selecting Ispra as the station of interest.

Table 2. Parameters measured during 2013

METEOROLOGICAL PARAMETERS	Pressure, temperature, humidity, wind, solar radiation
GAS PHASE	SO_2, NO, NO_X, O_3, CO
PARTICULATE PHASE	For $PM_{2.5}$: PM mass and Cl^-, NO_3^-, SO_4^{2-}, $C_2O_4^{2-}$, Na^+, NH_4^+, K^+, Mg^{2+}, Ca^{2+}, OC, and EC
	For PM_{10}: PM mass and Cl^-, NO_3^-, SO_4^{2-}, $C_2O_4^{2-}$, Na^+, NH_4^+, K^+, Mg^{2+}, Ca^{2+}, OC, and EC + 31 trace elements (till June)
	Number size distribution (10 nm - 10 µm)
	Aerosol absorption, scattering and back-scattering coefficient
	Altitude-resolved aerosol back-scattering
PRECIPITATION	Cl^-, NO_3^-, SO_4^{2-}, $C_2O_4^{2-}$, Na^+, NH_4^+, K^+, Mg^{2+}, Ca^{2+} pH, conductivity
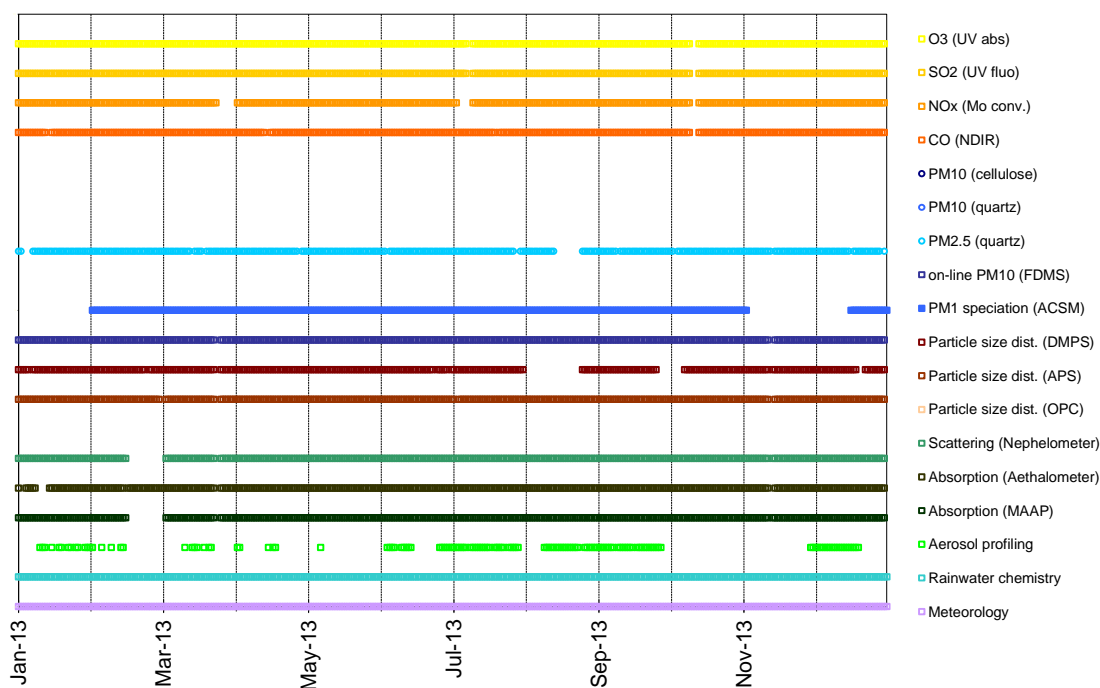
Fig. 12. *The year 2013 data coverage at the JRC EMEP-GAW station.*

22

Measurements and data processing

The air pollution monitoring program at the JRC- Ispra station in 2013

Since 1985, the JRC-Ispra air monitoring station program evolved significantly (Fig. 11). The variables measured at the JRC-Ispra station in 2013 are listed in Table 2. Fig. 12 shows the data coverage for 2013.

Meteorological parameters were measured during the whole year 2013, except from April 10th to 22nd, and after Dec. 19th, for which data measured at the JRC flux tower were used.

SO_2, O_3 and NOx were measured almost continuously during the year 2013..

Particulate matter (PM2.5) samples were collected daily and analyzed for PM2.5 mass (at 20% RH), main ions, OC (organic carbon) and EC (elemental carbon), except for a few days in August (sampler breakdown during holidays).

On-line PM10 measurements (FDMS-TEOM, Filter Dynamics Measurement System - Tapered Element Oscillating Microbalance) were carried out continuously, except from March 25th to 26th (when moving the station to provisional site)

Particle number size distribution (10 nm < Dp < 10 μm) were measured continuously except from Aug.2nd to Aug. 25th (DMPS sampling line leaking) and from Sep. 27th to Oct 10th (DMPS calibration workshop at the WCAPC). Aerosol absorption and scattering coefficients were measured continuously, except from Feb. 15th to March 4th (participation in the Nephelometer calibration 2013).

The CIMEL LiDAR (Light Detection and Ranging) provided altitude resolved aerosol backscattering profiles during favourable weather conditions till June, with several significant gaps during to various breakdowns. The Raymetrics Raman LiDAR took over from November 2012. All LiDAR data have been processed till December 2013.

Precipitation was collected throughout the year and analyzed for pH, conductivity, and main ions (collected water volume permitting).

Measurement techniques

On-line Monitoring

Meteorological Parameters

Meteorological data and solar radiation were measured directly at the EMEP station with the instrumentation described below.

WXT510 (S/N: A1410009 & A1410010)

Two WXT510 weather transmitters from Vaisala recorded simultaneously the six weather parameters temperature, pressure, relative humidity, precipitation and wind speed and direction from the top of a 10 m high mast.

The wind data measurements utilise three equally spaced ultrasonic transducers that determine the wind speed and direction from the time it takes for ultrasound to travel from one transducer to the two others. The precipitation is measured with a piezoelectrical sensor that detects the impact of individual raindrops and thus infers the accumulated rainfall. For the pressure, temperature and humidity measurements, separate sensors employing high precision RC oscillators are used.

CM11 (S/N: 058911) & CMP 11 (S/N: 070289)

To determine the solar radiation, a Kipp and Zonen CM11 was used. From 23.06.2008 and onwards an additional CMP11 Pyranometer have been installed that measures the irradiance (in W/m^2) on a plane surface from direct solar radiation and diffuse radiation incident from the hemisphere above the device. Both devices were ca. 1.5 m above the ground till Apr 10th, 2013. From Apr. 22nd, the CMP11 S/N 070289 only is installed on the top of the container (3 m above ground). The measurement principle is based on a thermal detector. The radiant energy is absorbed by a black disc and the heat generated flows through a thermal resistance to a heat sink. The temperature difference across the thermal resistance is then converted into a voltage and precisely measured. Both the CM11 & CMP11 feature a fast response time of 12 s, a small non stability of +/-0.5 % and a small non linearity of +/-0.2 %.

Gas Phase Air Pollutants

Sampling

From January to March, SO_2, NO, NO_x, O_3 and CO were sampled from a common inlet situated at about 3.5 m above the ground on the roof of the gas phase monitors' container (see Fig. 13 and Fig. 1) at ABC-IS EMEP/GAW site of JRC-Ispra, or from a mobile lab. (plate number CM328CN) parked at the same place. The sampling line in the container consists in an inlet made of a PVC semi-spherical cap (to prevent rain and bugs to enter the line), a PTFE tube (inner diameter = 2.7 cm, height = 150 cm), and a "multi-channel distributor" glass tube, with nine 14 mm glass connectors. This inlet is flushed by an about 60 L min^{-1} flow with a fan-coil (*measured with RITTER 11456*). Each instrument samples from the glass tube with its own pump through a 0.25 inch Teflon line and a 5 μm pore size 47 mm diameter Teflon filter (to eliminate particles from the sampled air).

From April to June 2013, SO_2, NO, NO_x, O_3 and CO were sampled from a common inlet situated at about 3.5 m above the ground on the roof of a mobile laboratory (plates number CM328CN) at building 44 at JRC-Ispra (see Fig. 1) about 300 meter from the old site. The inlet is flushed by an about 45 L min^{-1} flow with a fan-coil and also has a "multi-channel distributor" glass tube. Each instrument samples from the glass tube with its own pump through a 0.25 inch Teflon line and a 5 μm pore size 47 mm diameter Teflon filter (to eliminate particles from the sampled air).

From July to December 2013, SO_2, NO, NO_x, O_3 and CO were measured from the mobile laboratory (plates number CM328CN), moved to EMEP/GAW provisional station at JRC-Ispra (see Fig. 1) about 500 meter from the old site.

More details about the mobile lab and instruments (where exactly they were measuring and when) can be found in sections below.

SO₂: *UV Fluorescent SO₂ Analyser*

Thermo 43iTL (S/N 1021443379) and 43CTL (S/N 0401904668)

43iTL (S/N 1021443379): 01.01-06.02.2013: ABC-IS station, mobile lab.
43CTL (S/N 0401904668): 07.02-09.04.2013: ABC-IS station, container.
43iTL (S/N 1021443379): 10.04-08.07.2013: Building 44, mobile lab.
43iTL (S/N 1021443379): 11.07-31.12.2013: Provisional station, mobile lab.

At first, the air flow is scrubbed to eliminate aromatic hydrocarbons. The sample is then directed to a chamber where it is irradiated at 214 nm (UV), a wavelength where SO_2 molecules absorb. The fluorescence signal emitted by the excited SO_2 molecules going back to the ground state is filtered between 300 and 400 nm (specific of SO_2) and amplified by a photomultiplier tube. A microprocessor receives the electrical zero and fluorescence reaction intensity signals and calculates SO_2 based on a linear calibration curve.

Calibration was performed with a certified SO_2 standard at a known concentration in N_2. Zero check was done, using a zero air gas cylinder from Air Liquide, Alphagaz 1, CnHm < 0.5 ppm).

The specificity of the trace level instrument (TEI 43C-TL) is that it uses a pulsed lamp. The 43C-TL's detection limit is 0.2 ppb (about 0.5 µg m^{-3}) according to the technical specifications and for 43i-TL's detection limit is 0.05 ppb (about 0.13 µg m^{-3}) over 300 second averaging time, according to the technical specifications.

The 43C-TL (S/N 0401904668) was used from 07.02 to 09.04.2013, and data were corrected for consistency with the data from 43iTL (S/N 1021443379), based on regressions observed during overlapping periods.

For more details about the instruments, manuals are available on \\ies.jrc.it\H02\lLargefacilities\ABC-IS\Quality_management\Manuals
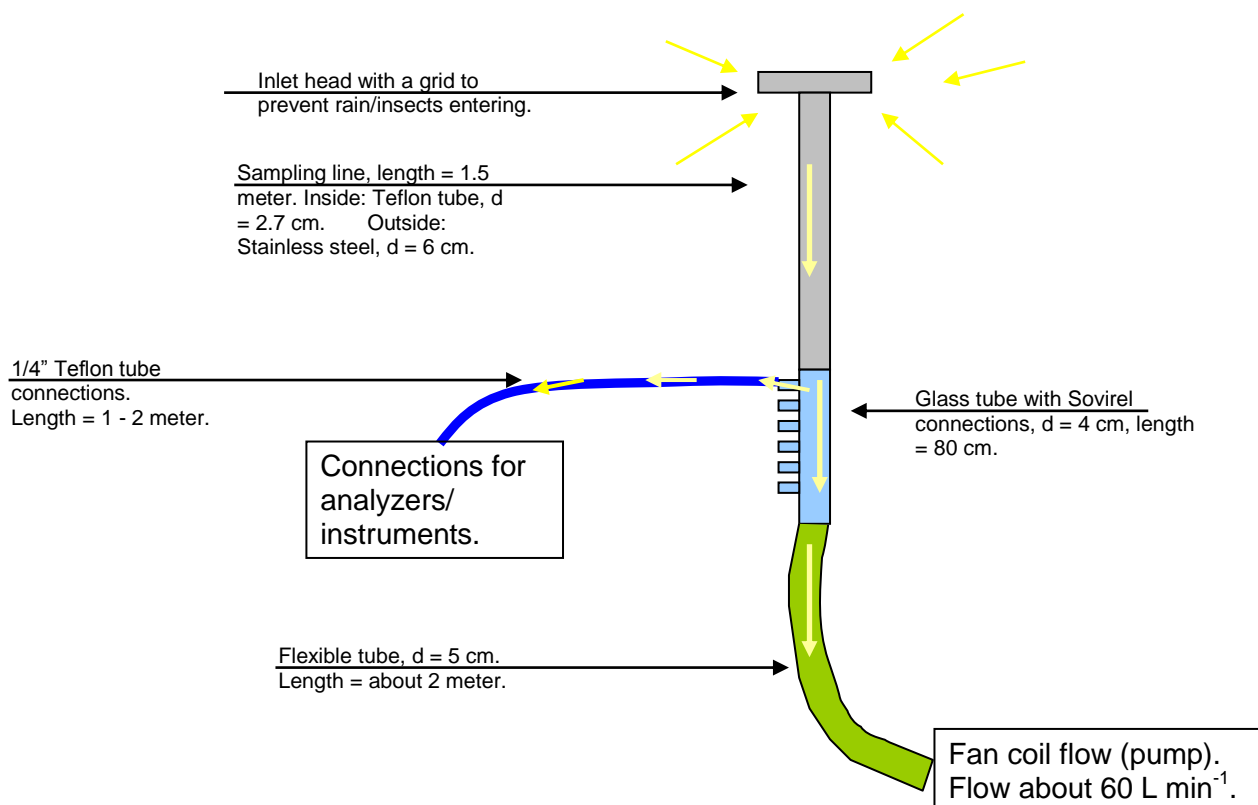

Fig. 13. *Sampling inlet system for the gaseous air pollutant.*

In 2013, the gas phase monitors were calibrated about every month with suitable span gas cylinders and zero air (see below for more details). Sampling flow rates are as follow:

Compounds	Flow rates ($L\ min^{-1}$)
SO_2	0.5
NO, NO_x	0.6
O_3	0.7
CO	1.5

NO + NO_X: Chemiluminescent Nitrogen Oxides Analyzer ($NO_2 = NO_x - NO$)

Thermo 42iTL (S/N 936539473) and 42C (S/N 0401304317) /
*42iTL (S/N 936539473): 01.01-24.01.2013: ABC-IS station, mobile lab.*
42C (S/N 0401304317): 25.01-26.03.2013: ABC-IS station, container.
42C (S/N 0401304317): 03.04-04.07.2013: Building 44, mobile lab.
42C (S/N 0401304317): 11.07-31.12.2013: Provisional station, mobile lab.

This nitrogen oxide analyser is based on the principle that nitric oxide (NO) and ozone react to produce excited NO_2 molecules, which emit infrared photons when going back to lower energy states:

$$NO + O_3 \rightarrow [NO_2]^* + O_2 \rightarrow NO_2 + O_2 + h\nu$$
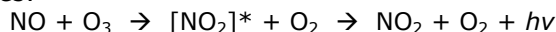
A stream of purified air (dried with a Nafion Dryer) passing through a silent discharge ozonator generates the ozone concentration needed for the chemiluminescent reaction. The specific luminescence signal intensity is therefore proportional to the NO concentration. A photomultiplier tube amplifies this signal.
NO_2 is detected as NO after reduction in a Mo converter heated at about 325 °C.
The ambient air sample is drawn into the analyzer, flows through a capillary, and then to a valve, which routes the sample either straight to the reaction chamber (NO detection), or through the converter and then to the reaction chamber (NO_X detection). The calculated NO and NO_X concentrations are stored and used to calculate NO_2 concentrations ($NO_2 = NO_x - NO$), assuming that only NO_2 is reduced in the Mo converter.
Calibration was performed using a zero air gas cylinder (Air Liquide, Alphagaz 1, CnHm<0.5 ppm) and a NO span gas. Calibration with a span gas was performed with a certified NO standard at a known concentration in N_2.
For more details about the instruments, manuals are available on \\ies.jrc.it\H02\LargeFacilities\ABC-IS\Quality_management\Manuals

O_3:   UV Photometric Ambient Analyzer

Thermo 49C (S/N 0503110499 and S/N 0503110398)
49C (S/N 0503110499): 01.01-09.04.2013: ABC-IS station, container.
49C (S/N 0503110398): 10.04-09.07.2013: Building 44, mobile lab.
49C (S/N 0503110398): 11.07-31.12.2013: Provisional station, mobile lab.
The UV photometer determines ozone concentrations by measuring the absorption of O_3 molecules at a wavelength of 254 nm (UV light) in the absorption cell, followed by the use of Bert-Lambert law. The concentration of ozone is related to the magnitude of the absorption. The reference gas, generated by scrubbing ambient air, passes into one of the two absorption cells to establish a zero light intensity reading, I_0. Then the sample passes through the other absorption cell to establish a sample light intensity reading, I. This cycle is reproduced with inverted cells. The average ratio $R = I/I_0$ between 4 consecutive readings is directly related to the ozone concentration in the air sample through the Beer-Lambert law. Calibration is performed using externally generated zero air and external span gas. Zero air is taken from a gas cylinder (Air Liquide, Alphagaz 1, CnHm < 0.5 ppm). Span gas normally in the range 50 - 100 ppb is generated by a TEI 49C-PS transportable primary standard ozone generator (S/N 0503110396) calibrated/check by ERLAP (European Reference Laboratory of Air Pollution) and/or TESCOM annually. A Nafion Dryer system is connected to the O_3 instruments.

For more details about the instruments, the manual is available on
[\\ies.jrc.it\H02\LargeFacilities\ABC-IS\Quality_management\Manuals](\\ies.jrc.it\H02\LargeFacilities\ABC-IS\Quality_management\Manuals)

CO: Non-Dispersive Infrared Absorption CO Analyzer

Horiba AMPA-370 (S/N WYHEOKSN)
from 01.01 to 09.04.2013: ABC-IS station, mobile lab.
from 10.04 to 09.07.2013: Building 44, mobile lab.
from 10.07 to 31.12.2013: Provisional station, mobile lab.

In 2013, carbon monoxide (CO) has been continuously monitored using a commercial Horiba AMPA-370 CO monitor based on the principle of non-dispersive infrared absorption (NDIR). The Horiba APMA-370 uses solenoid valve cross flow modulation applying the same air for both the sample and the reference, instead of the conventional technique to apply an optical chopper to obtain modulation signals. With this method the reference air is generated by passing the sample air over a heated oxidation catalyst to selectively remove CO which is then directly compared to the signal of the untreated sample air at a 1 Hz frequency. The result is a very low zero-drift and stable signal over long periods of time.

To reduce the interference from water vapor to about 1% the sample air was dried to a constant low relative humidity level of around 30% applying a Nafion dryer (Permapure MD-070-24P) tube in the inlet stream. The detection limit of the Horiba AMPA-370 is ~20 ppbv for a one minute sampling interval, and the overall measurement uncertainty is estimated to be ±5%, which includes the uncertainty of the calibration standards, the H_2O interference, and the instrument precision (~2%).

For more details about the instrument, see the manual available from
[\\ies.jrc.it\H02\LargeFacilities\ABC-IS\Quality_management\Manuals](\\ies.jrc.it\H02\LargeFacilities\ABC-IS\Quality_management\Manuals)

Atmospheric Particles

Sampling conditions

Since 2008, all instruments for the physical characterization of aerosols (Aethalometer, Nephelometer, Aerodynamic Particle Sizer, Differential Mobility Particle Sizer) sample isokinetically from an inlet pipe (Aluminium), diameter = 15 cm, length of horizontal part ~280 cm and vertical part ~220 cm (see Jensen et al., 2010). The Tapered Element Oscillating Mass balance (FDMS-TEOMs) and the Multi-Angle Absorption Photometer (MAAP) used their own inlet systems. On April 10th, 2013, the MAAP started to sample from the main inlet through Nafion dryers at a flow rate of 498 L hr^{-1} (8.3 L min^{-1}).

The size dependent particle losses along the pipe radius were determined by measuring the ambient aerosol size distribution with two DMPS at the sampling points P0 and P2 for different radial positions relative to the tube centre (0, 40 and 52 mm) at P2 (Gruening et al., 2009). Data show a small loss of particles towards the rim of the tube can be observed, but it stays below 15 %. The bigger deviation for particles smaller than 20 nm is again a result of very small particle number concentrations in this diameter range and thus rather big counting errors.

PM10 mass concentration: Tapered Element Oscillating Mass balance (TEOM), Series 1400a

Thermo FDMS – TEOM (S/N 140AB233870012 & 140AB253620409)

The Series 1400a TEOM® monitor incorporates an inertial balance patented by Rupprecht & Patashnick, now Thermo. It measures the mass collected on an exchangeable filter cartridge by monitoring the frequency changes of a tapered element. The sample flow passes through the filter, where particulate matter is collected, and then continues through the hollow tapered element on its way to an electronic flow control system and vacuum pump. As more mass collects on the exchangeable filter, the tube's natural frequency of oscillation decreases. A *direct* relationship exists between the tube's change in frequency and mass on the filter. The TEOM mass transducer does not require recalibration because it is designed and constructed from non-fatiguing materials. However, calibration is yearly verified using a filter of known mass.

The instrument set-up includes a Sampling Equilibration System (SES) that allows a water strip-out without sample warm up by means of Nafion Dryers. In this way the air flow RH is reduced to < 30%, when TEOM® operates at 30 °C only. The Filter Dynamic Measurement System (FDMS) is based on measuring changes of the TEOM filter mass when sampling alternatively ambient and filtered air. The changes in the TEOM filter mass while sampling filtered air is attributed to sampling (positive or negative) artefacts, and is used to correct changes in the TEOM filter mass observed while sampling ambient air.

Particle number size distribution: Differential Mobility Particle Sizer (DMPS)

DMPS "B, DMA serial no. 158", CPC TSI 3010 (S/N 2051) or CPC TSI 3772 (S/N 70847419 and 3772133103), neutraliser ^{85}Kr 10 mCi (2007)

The Differential Mobility Particle Sizer consists of a home-made medium size (inner diameter 50 mm, outer diameter 67 mm and length 280 mm) Vienna-type Differential Mobility Analyser (DMA) and a Condensation Particle Counter (CPC), TSI 3010 or TSI 3772. Its setup follows the EUSAAR specifications for DMPS systems.
DMA's use the fact that electrically charged particles move in an electric field according to their electrical mobility. Electrical mobility depends mainly on particle size and electrical charge. Atmospheric particles are brought in the bipolar charge equilibrium in the bipolar diffusion charger (Eckert & Ziegler neutralizer with 370 MBq): a radioactive source (^{85}Kr) ionizes the surrounding atmosphere into positive and negative ions. Particles carrying a high charge can discharge by capturing ions of opposite polarity. After a very short time, particles reach a charged equilibrium such that the aerosol carries the bipolar Fuchs-Boltzman charge distribution. A computer program sets stepwise the voltage between the 2 DMA's electrodes (from 10 to 11500 V). Negatively charged particles are so selected according to their mobility. After a certain waiting time, the CPC measures the number concentration for each mobility bin. The result is a particle mobility distribution. The number size distribution is calculated from the mobility distribution by an inversion routine (from Stratmann and Wiedensohler, 1996) based on the bipolar charge distribution and the size dependent DMA transfer function. The DMPS measured aerosol particles in the range 10 – 600 nm during an 8 minute cycle until 12.06.2009 and afterwards in the range 10 to 800 nm with a 10 minute cycle. It records data using 45 size channels for high-resolution size information. This submicrometer particle sizer is capable of measuring concentrations in the range from 1 to 2.4 x 10^6 particles cm^{-3}. Instrumental parameters that are necessary for data evaluation such as flow rates, relative humidity, ambient pressure and temperature are measured and saved as well.
The CPC detection efficiency curve and the particle diffusion losses in the system are taken into account at the data processing stage.

Accessories include:
- FUG High voltage cassette power supplies Series HCN7E – 12500 Volts.
- Rotary vacuum pump vane-type (sampling aerosol at 1 LPM)
- Controlled blower (circulating dry sheath air)
- Sheath air dryer only using silica gel until 27.10.2009, thereafter sheath and sample air dryer using Nafion dryer; this mean that the DMPS started to sample in dry conditions from 27 October 2009 onwards.
- Mass flow meter and pressure transducer (to measure sheath air and sample flows).

Particle number size distribution: Aerodynamic Particle Sizer (APS)

APS TSI 3321 (S/N 70535014 & S/N 1243)

The APS 3321 is a time-of-flight spectrometer that measures the velocity of particles in an accelerating air flow through a nozzle.
Ambient air is sampled at 1 L min^{-1}, sheath air (from the room) at 4 L min^{-1}. In the instrument, particles are confined to the center-line of an accelerating flow by sheath air. They then pass through two broadly focused laser beams, scattering light as they do so. Side-scattered light is collected by an elliptical mirror that focuses the collected light onto a solid-state photodetector, which converts the light pulses to electrical pulses. By electronically timing between the peaks of the pulses, the velocity can be calculated for each individual particle.
Velocity information is stored in 1024 time-of-flight bins. Using a polystyrene latex (PSL) sphere calibration, which is stored in non-volatile memory, the APS Model 3321

converts each time-of-flight measurement to an aerodynamic particle diameter. For convenience, this particle size is binned into 52 channels (on a logarithmic scale).

The particle range spanned by the APS is from 0.5 to 20 µm in both aerodynamic size and light-scattering signal. Particles are also detected in the 0.3 to 0.5 µm range using light-scattering alone, and are binned together in one channel. The APS is also capable of storing correlated light-scattering-signal. *dN/dLogDp* data are averaged over 10 min.

Particle scattering and back-scattering coefficient

Nephelometer TSI 3563 (S/N 1081)

The integrating nephelometer is a high-sensitivity device capable of measuring the scattering properties of aerosol particles. The nephelometer measures the light scattered by the aerosol and then subtracting light scattered by the walls of the measurement chamber, light scattered by the gas, and electronic noise inherent in the detectors.

Dried ambient air is sampled at 5.3 L min^{-1} since 18.11.2009 from a PM10 inlet. .

The three-color detection version of TSI nephelometer detects scattered light intensity at three wavelengths (450, 550, and 700 nm). Normally the scattered light is integrated over an angular range of 7–170° from the forward direction, but with the addition of the backscatter shutter feature to the Nephelometer, this range can be adjusted to either 7–170° or 90–170° to give total scatter and backscatter signals. A 75 Watt quartz-halogen white lamp, with a built-in elliptical reflector, provides illumination for the aerosol. The reflector focuses the light onto one end of an optical pipe where the light is carried into the internal cavity of the instrument. The optical pipe is used to thermally isolate the lamp from the sensing volume. The output end of the optical light pipe is an opal glass diffuser that acts as a *quasi*-cosine (Lambertian) light source. Within the measuring volume, the first aperture on the detection side of the instrument limits the light integration to angles greater than 7°, measured from the horizontal at the opal glass. On the other side, a shadow plate limits the light to angles less than 170°. The measurement volume is defined by the intersection of this light with a viewing volume cone defined by the second and fourth aperture plates on the detection side of the instrument. The fourth aperture plate incorporates a lens to collimate the light scattered by aerosol particles so that it can be split into separate wavelengths. The nephelometer uses a reference chopper to calibrate scattered signals. The chopper makes a full rotation 23 times per second. The chopper consists of three separate areas labeled "signal", "dark", and "calibrate".

The signal section simply allows all light to pass through unaltered. The dark section is a very black background that blocks all light. This section provides a measurement of the photomultiplier tube (PMT) background noise. The third section is directly illuminated this section to provide a measure of lamp stability over time. To reduce the lamp intensity to a level that will not saturate the photomultiplier tubes, the calibrate section incorporates a neutral density filter that blocks approximately 99.9 % of the incident light. To subtract the light scattered by the gas portion of the aerosol, a high-efficiency particulate air (HEPA) filter is switched in line with the inlet for 300 s every hour. This allows compensation for changes in the background scattering of the nephelometer, and in gas composition that will affect Rayleigh scattering of air molecules with time. When the HEPA filter is not in line with the inlet, a small amount of filtered air leaks through the light trap to keep the apertures and light trap free of particles. A smaller HEPA filter allows a small amount of clean air to leak into the sensor end of the chamber between the lens and second aperture. This keeps the lens clean and confines the aerosol light scatter to the measurement volume only.

Nephelometer data are corrected for angular non idealities and truncation errors according to Anderson and Ogren, 1998. From 18.11.2009 onwards, a Nafion dryer has been installed at the inlet to measure dry aerosols. Internal RH ranged from 0 to 50 % (average 18%, 99th percentile 41%), with values > 40% occurring between June 30th and July 22nd. At 40% RH, aerosol scattering is on average increased by 20% compared to 0% RH in Ispra (Adam et al., 2012). However, aerosol particle scattering coefficients presented in this report are **not** corrected for RH effects, except when specified.

Particle absorption coefficient

Aethalometer Magee AE-31 ('A' S/N 408: 0303 & 'B' S/N 740:0609)

The principle of the Aethalometer is to measure the attenuation of a beam of light transmitted through a filter, while the filter is continuously collecting an aerosol sample. Suction is provided by an internally-mounted pump. Attenuation measurements are made at successive regular intervals of a time-base period. The objectives of the Aethalometer hardware and software systems are as follows:

(a) to collect the aerosol sample with as few losses as possible on a suitable filter material;

(b) to measure the optical attenuation of the collected aerosol deposit as accurately as possible;

(c) to calculate the rate of increase of the equivalent black carbon (EBC) component of the aerosol deposit and to interpret this as an EBC concentration in the air stream;

(d) to display and record the data, and to perform necessary instrument control and diagnostic functions.

The optical attenuation of the aerosol deposit on the filter is measured by detecting the intensity of light transmitted through the spot on the filter. In the AE-31, light sources emitting at different wavelengths (370, 470, 520, 590, 660, 880 and 950 nm) are also installed in the source assembly. The light shines through the lucite aerosol inlet onto the aerosol deposit spot on the filter. The filter rests on a stainless steel mesh grid, through which the pumping suction is applied. Light penetrating the diffuse mat of filter fibers can also pass through the spaces in the support mesh. This light is then detected by a photodiode placed directly underneath the filter support mesh. As the EBC content of the aerosol spot increases, the amount of light detected by the photodiode will diminish.

For better accuracy, further measurements are necessary: the amount of light penetrating the combination of filter and support mesh is relatively small, and a correction is needed for the 'dark response signal' of the overall system. This is the electronics' output when the lamps are off: typically, it may be a fraction of a percent of the response when the lamps are on. To eliminate the effect of the dark response, we take 'zero' readings of the system response with the lamps turned off, and subtract this 'zero' level from the response when the lamps are on.

The other measurement necessary is a 'reference beam' measurement to correct for any small changes in the light intensity output of the source. This is achieved by a second photodiode placed under a different portion of the filter that is not collecting the aerosol, on the left-hand side where the fresh tape enters. This area is illuminated by the same lamps. If the light intensity output of the lamps changes slightly, the response of this detector is used to mathematically correct the 'sensing' signal. The reference signal is also corrected for dark response 'zero' as described above.

The algorithm in the computer program (see below) can account for changes in the lamp intensity output by always using the ratio quantity [Sensing]/[Reference]. As the filter deposit accumulates EBC, this ratio will diminish.

In practice, the algorithm can account for lamp intensity fluctuations to first order, but we find a residual effect when operating at the highest sensitivities. To minimize this effect and to realize the full potential of the instrument, it is desirable for the lamps' light output intensity to remain as constant as possible from one cycle to the next, even though the lamps are turned on and off again. The computer program monitors the repeatability of the reference signal, and issues a warning message if the fluctuations are considered unacceptable. When operating properly, the system can achieve a reference beam repeatability of better than 1 part in 10000 from one cycle to the next. The electronics circuit board converts the optical signals directly from small photocurrents into digital data, and passes it to the computer for calculation. A mass flow meter monitors the sampled air flow rate. These data and the result of the EBC calculation are written to disk and displayed on the front panel of the instrument.

Aethalometer data are corrected for the shadowing effect and for multiple-scattering in the filter to derive the aerosol absorption coefficient (Arnott et al., 2005) with a correction factor C = 3.60, 3.65, and 3.95 for green 450, 550 and 660 nm, respectively.

Multi Angle Absorption Photometer (S/N 4254515)

A new Multi Angle Absorption Photometer (MAAP) model 5012 from Thermo Scientific has been installed at the EMEP station in September 2008 and provides equivalent black carbon concentrations (EBC) and aerosol absorption (*a*) data at a nominal wavelength of 670 nm. Note that during a EUSAAR workshop (www.eusaar.org) in 2007 it has been observed that the operating wavelength of all MAAP instruments present at that workshop was 637 nm with a line width of 18 nm fwhm. The operating wavelength of this MAAP instrument has not been measured yet, therefore it is assumed to work at 670 nm as stated by the manufacturer.

The MAAP is based on the principle of aerosol-related light absorption and the corresponding atmospheric equivalent black carbon (EBC) mass concentration. The Model 5012 uses a multi angle absorption photometer to analyze the modification of scattering and absorption in the forward and backward hemisphere of a glass-fibre filter caused by deposited particles. The internal data inversion algorithm of the instrument is based on a radiation transfer model and takes multiple scattering processes inside the deposited aerosol and between the aerosol layer and the filter matrix explicitly into account (see Petzold et al., 2004).

The sample air is drawn into the MAAP and aerosols are deposited onto the glass fibre filter tape. The filter tape accumulates the aerosol sample until a threshold value is reached, then the tape is automatically advanced. Inside the detection chamber (Fig. 14), a 670-nanometer light emitting diode is aimed towards the deposited aerosol and filter tape matrix. The light transmitted into the forward hemisphere and reflected into the back hemisphere is measured by a total of five photo-detectors. During sample accumulation, the light intensities at the different photo-detectors change compared to a clean filter spot. The reduction of light transmission, change in reflection intensities under different angles and the air sample volume are continuously measured during the sample period. With these data and using its proprietary radiation transfer scheme, the MAAP calculates the equivalent black carbon concentration (EBC) as the instruments measurement result.

Using the specific absorption cross section σ_{BC} = 6.6 m^2/g of equivalent black carbon at the operation wavelength of 670 nm, the aerosol absorption (α) at that wavelength can be readily calculated as:
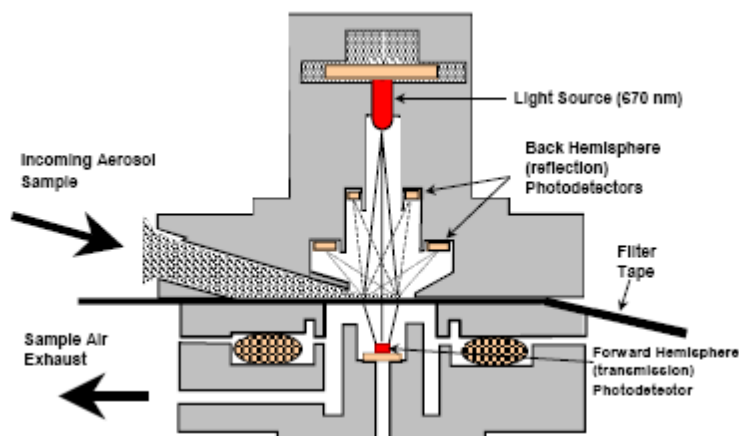
$$\alpha = EBC \times \sigma_{BC} \qquad Eq.\ 1$$

Fig. 14. MAAP detection chamber (sketch from the manual of the instrument).

Aerosol Chemical Speciation Monitor

Aerodyne Research Inc. ACSM#1: S/N 140-105 & ACSM#2: S/N 140-151.

The ACSM is a mass spectrometric technique allowing the chemical speciation (organics, nitrate, sulfate, ammonium and chloride) of non-refractory submicron aerosols (NR-PM$_1$) to be determined with a time-resolution of 30 minutes. Its full description can be found in (Ng et al., 2011). Briefly, PM$_{10}$ are sampled at a flow rate of 3 L/min before passing through a critical orifice of 100 µm diameter, which fixes the sampling flow at ca. 85 mL/min into the ACSM. Aerodynamic lenses are then used to focus submicron particles into the instrument (with a 50% transmission range of 75-650 nm; (Liu et al., 2007). The focused particle beam passes through vacuum chambers (~10^{-5} Pa) before impacting a heated surface (~600 °C) where aerosol particles are vaporized. The resulting vapour is ionized with 70 eV electron impacts and analysed by a quadruple mass spectrometer (Pfeiffer Vacuum Prisma Plus RGA). Mass concentrations of NR-PM$_1$ chemical components are retrieved from mass spectra following the methodology described in the manual of the data analysis software (ftp://ftp.aerodyne.com/ACSM/ACSM_Manuals/ACSM_Igor_Manual.pdf) of the instrument (DAS 1.5.3.0). Additional calibration (e.g. ammonium nitrate) and correction factors (e.g. collection efficiency, Middlebrook et al., 2012) are applied to accurately quantify submicron the aerosol chemical composition (see Bressi et al., in

preparation for more details). Two ACSMs have been used at the ABC-IS provisional site during the year 2013: ACSM #1 operated continuously from 1 February 2013 to 15 August 2013 and ACSM#2 from 15 August to 3 November and from 17 to 31 December 2013. The instrument participated in an inter-ACSM comparison in November-December 2013 (Crenn et al., in preparation).
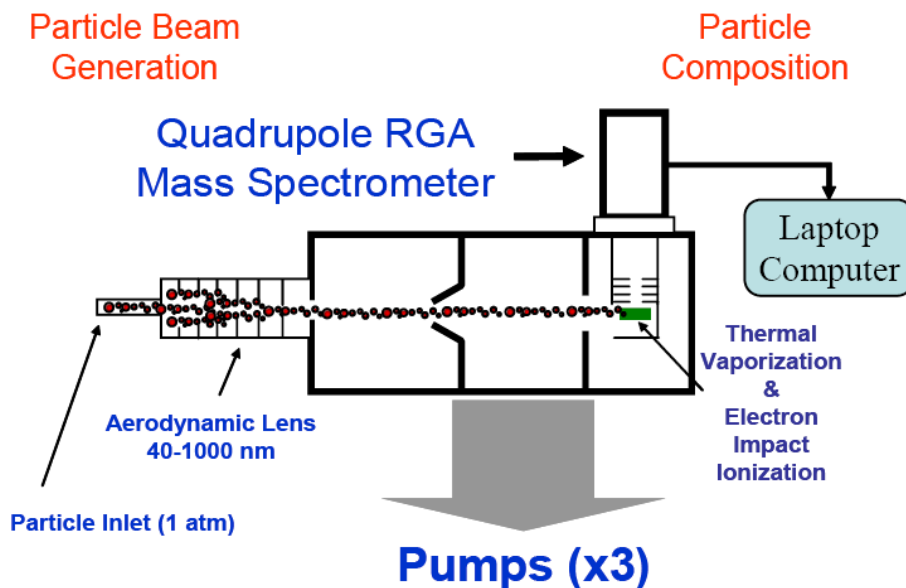

Figure 15: the ACSM principle (© Aerodyne Research Inc.)

Range-resolved aerosol backscattering, extinction and aerosol optical thickness

LIDAR measurements are based on the time resolved detection of the backscattered signal of a short laser pulse that is sent into the atmosphere (for an introduction see Weitkamp , 2005). Using the speed of light, time is converted to the altitude where the backscattering takes place. Utilising some assumptions about the atmospheric composition, aerosol backscattering and extinction coefficients as well as aerosol optical thickness can be derived using the LIDAR equation. The received power P of the detector is therein given as a function of distance and wavelength by *Eq. 2*:

$$P(R, \lambda) = P_0 \frac{c\tau}{2} A \eta \frac{O(R)}{R^2} \beta(R, \lambda) \exp\left(-2\int_0^R \alpha(r, \lambda)dr\right)$$

Eq. 2: P_0: Power of the laser pulse, c: speed of light, τ: laser pulse length, A: area of the telescope, η: system efficiency, R: distance, O: overlap function (between laser beam and receiving optics field of view), λ: wavelength, β: backscatter coefficient, α: absorption coefficient

Cimel Aerosol Micro Lidar (CAML) CE 370-2 (laser & electronics: S/N 0507-846 and telescope: S/N 0507- 847)

The aerosol backscatter LIDAR instrument (LIght Detection And Ranging) from CIMEL (CAML) was installed in 2006 at the EMEP-GAW station for the range-resolved optical remote sensing of aerosols. It serves to bridge the gap between local, in-situ measurements of aerosols at the ground and satellite based characterizations of the aerosol column above ground. To reach this, altitude resolved aerosol backscattering, and estimated aerosol extinction are derived from the LIDAR data with high time resolution.

CAML is an eye-safe, single-wavelength, monostatic aerosol backscatter lidar. The lidar emitter is a diode pumped, frequency doubled Nd:YAG laser operating at a wavelength of 532 nm, with a repetition rate of 4.7 kHz, pulse energy of 8 μJ/pulse and a width of the laser pulse of less than 15 ns. The short integration time of the detector of 100 ns allows for a vertical resolution of 15 m. With 2048 time bins of the detector, the maximum altitude is ~30 km. However, depending on the actual atmospheric conditions and the quality of signal to noise ratio (SNR), the vertical limit for probing the atmosphere usually goes up to 15 km. Eye-safety of the system is reached by

32

expanding the laser beam trough a 20 cm diameter, 1 m focal length refractive telescope. The emission and reception optical paths coincide through a single, 10 m long optical fibre that connects both the laser output and receiving detector with the telescope. The telescope field of view is approximately 50 μrad. The backscatter signal is sent to the receiver passing through a narrow band-pass interference filter (0.2 nm fwhm, centred at 532 nm) to reduce the background level. To avoid saturation of the detector immediately after the laser pulse is emitted and thus reduce the afterpulse signal, an acousto-optical modulator is placed before the detector that blocks the light from the detector that is directly backscattered from optical components in the light path. The detector is an avalanche photodiode photon-counting module with a high quantum efficiency approaching 55 % with maximum count rates near 20 MHz.

Data evaluation is done with an inversion algorithm based on an iteration-convergence method for the LIDAR equation (see *Eq. 2*) that has been implemented in-house using the MATLAB programming environment. Starting with the CAML raw data, the 10 minutes time averages of the backscatter profiles are space–averaged over 60 m. Then the background signal (including afterpulse component) is subtracted. The afterpulse component originates from light that is scattered back to the detector from all surfaces on the optical path to the telescope. As its intensity is rather high compared to the atmospheric backscatter, it influences the raw detector signal. Furthermore, the overlap function O(R) (see *Eq. 2*) is applied to the data before it is range corrected, i.e. multiplied by R^2. The shape of this overlap function varied significantly and thus gives rise to a potentially large error in the evaluation of the lidar data. The range corrected signal constitutes the level 0 data.

Usually, the US standard atmosphere is used to calibrate the molecular backscattering in an aerosol free region and an assumed LIDAR ratio (i.e. extinction-to-backscatter ratio) that is constant with height is used to retrieve the aerosol backscatter, extinction and optical thickness (AOT) profiles (provided as level 1 data). During 2013, the molecular extinction and backscatter profiles were computed using radiosonde measurements (launched from Linate airport) for air number of molecules. The Lidar Ratio (LR) is determined using as a constraint the AOT measured by sun photometer.

The mean (median) estimate of the LIDAR ratios (LR = Lidar Ratios) that have been used for the data inversion was LR = 29.73 sr (with median = 22).

In 2013, CAML was run in automatic mode following the program "running for 20 min, and off for 10 min" till June when the signal dropped and did not recover after the acousto-optical modulator was substituted. Before this, e 30 min-cycle was repeated continuously during favourable weather conditions, i.e. no precipitation and no cloud coverage that would absorb the laser pulse and thus prevent meaningful aerosol LIDAR measurements above clouds.

Raymetrics Aerosol Raman Lidar (S/N 400-1-12, QUANTEL Brilliant B Laser and cooler S/N 120059004 and S/N 120034401, LICEL Transient Recorder & Hi Voltage Supply S/N BS3245 and BS3245b, industrial PC S/N TPL-1571H-D3AE, Radar LS150-24)

The instrument itself was installed on October 8-11th, 2012, and indispensable accessories (including radar) on December 11-13, 2012. This lidar emits at 3 wavelengths from IR to UV (1064 nm, polarised-532 nm, 355 nm) and records at 5 wavelengths, namely the emission wavelengths and two Raman channels 387 and 607 nm. Measurements at 1064 nm, 532 nm, and 355 nm provide aerosol backscatter profiles, while measurements at 687 nm, and 387 nm provide aerosol extinction profiles during the dark hours of the day. The 532 nm signal depolarisation is also measured. In 2013, the instrument was run mainly with a 5 min integration time during time slots covering sunrise, noon, sunset, midnight, and Calipso over passes. Data were inverted using several algorithms, including the online Single Calculus Chain developed by EARLINET. Data were submitted to the ACTRIS-EARLINET data bank for the whole of 2013, except for October and November for which no valid data are available

Sampling and off-line analyses

Particulate Matter

PM2.5 was continuously sampled at 16.7 L min^{-1} on quartz fibre filters with a Partisol sampler equipped with carbon honeycomb denuder. The sampled area is 42 mm. Filters were from PALL Life Sciences (type TISSUEQUARTZ 2500QAT-UP). Filter changes occurred daily at 08:00 UTC.

Filters were weighed at 20 % RH before and after exposure with a microbalance Sartorius MC5 placed in a controlled (dried or moisture added and scrubbed) atmosphere glove box. They were stored at 4 °C until analysis.

Main ions (Cl^-, NO_3^-, SO_4^{2-}, $C_2O_4^{2-}$, Na^+, NH_4^+, K^+, Mg^{2+}, Ca^{2+}) were analysed by ion chromatography (Dionex DX 120 with electrochemical eluent suppression) after extraction of the soluble species in an aliquot of 16 mm Ø in 20 ml 18.2 MOhm cm resistivity water (Millipore mQ).

Organic and elemental carbon (OC+EC) were analysed using a Sunset Dual-optical Lab Thermal-Optical Carbon Aerosol Analyser (S/N 173-5). PM2.5 samples were analysed using the EUSAAR-2 thermal protocol that has been developed to minimize biases inherent to thermo-optical analysis of OC and EC (Cavalli et al., 2010):

Fraction Name Sunset Lab.	Plateau Temperature (°C)	Duration (s)	Carrier Gas
OC 1	200	120	He 100%
OC 2	300	150	He 100%
OC 3	450	180	He 100%
OC 4	650	180	He 100%
cool down		30	He 100%
EC1	500	120	He:O_2 98:2
EC2	550	120	He:O_2 98:2
EC3	700	70	He:O_2 98:2
EC4	850	80	He:O_2 98:2

No measurement of PM_{10} or PM_{coarse} was performed in 2013. Only forty PM_{10} samples were collected in November - December 2013 in the frame of the CEN TC 264 WG35 field validation work, using HiVol samplers provided by Digitel.

Wet-only deposition

For the precipitation collection, two Eigenbrodt wet-only samplers (S/N 3311 and 3312) were used that automatically collect the rainfall in a 1 L polyethylene container. The collection surface is 550 cm^2. 24-hr integrated precipitation samples (if any) are collected every day starting at 8:00 UTC. All collected precipitation samples were stored at 4 °C until analyses (ca. every 3 months).

Analyses include the determinations of pH and conductivity at 25 °C with a Sartorius Professional Meter PP-50 and principal ion concentrations (Cl^-, NO_3^-, SO_4^{2-}, $C_2O_4^{2-}$, Na^+, NH_4^+, K^+, Mg^{2+}, Ca^{2+}) by ion chromatography (Dionex DX 120 with electrochemical eluent suppression).

KOALA

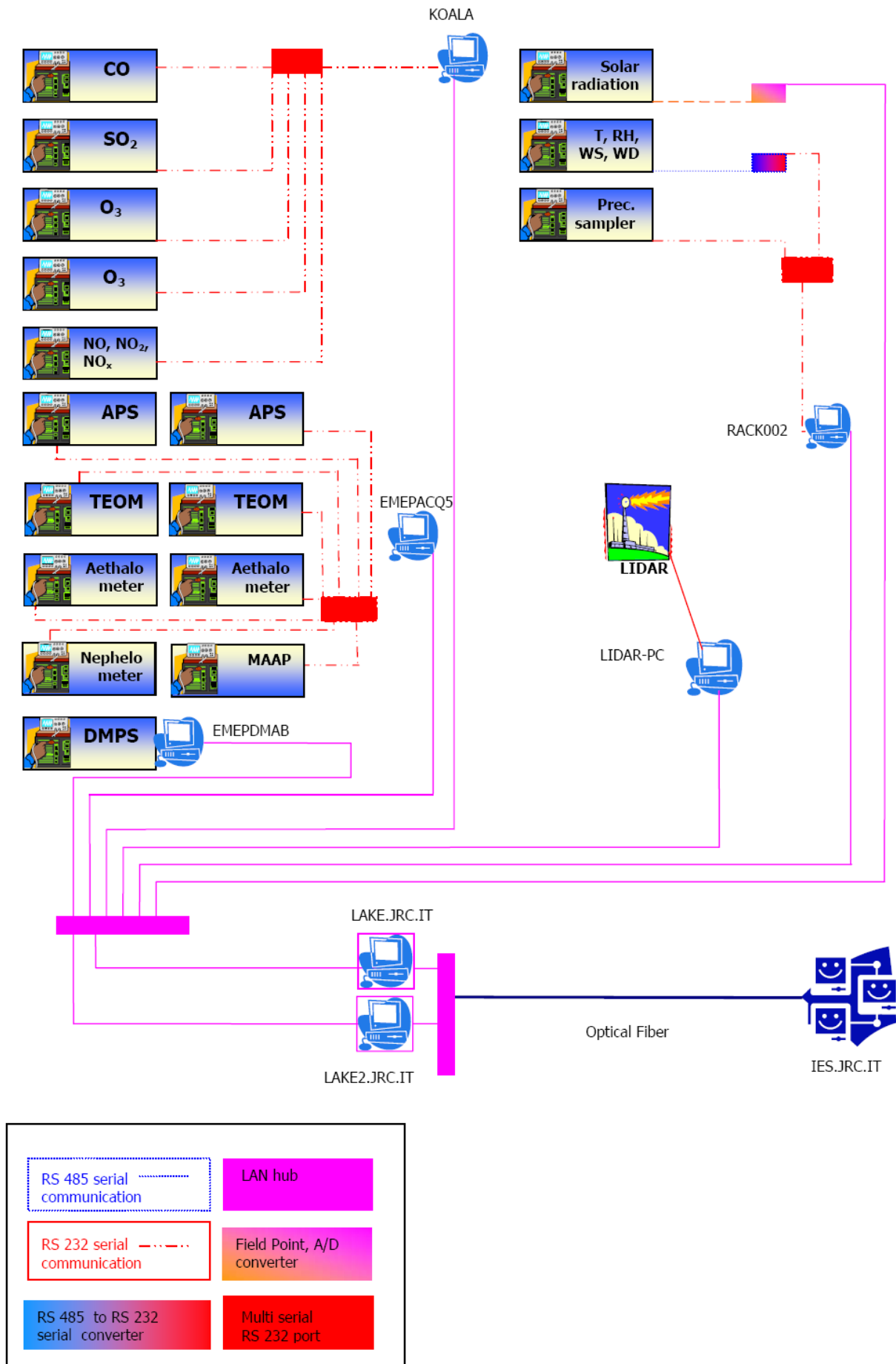CO

SO$_2$

O$_3$

O$_3$

NO, NO$_2$, NO$_x$

APS   APS

TEOM   TEOM

Aethalo meter   Aethalo meter

EMEPACQ5

Nephelo meter   MAAP

DMPS   EMEPDMAB

Solar radiation

T, RH, WS, WD

Prec. sampler

RACK002

LIDAR

LIDAR-PC

LAKE.JRC.IT

LAKE2.JRC.IT

Optical Fiber

IES.JRC.IT

RS 485 serial communication   LAN hub

RS 232 serial communication   Field Point, A/D converter

RS 485 to RS 232 serial converter   Multi serial RS 232 port

Fig. 14. *Set-up of the EMEP- GAW station Data Acquisition System.*

On-line data acquisition system/data management

The JRC EMEP-GAW station Data Acquisition System (DAS) is a specifically tailored set of hardware and software (implemented by [NOS s.r.l](#)), designed to operate instruments, acquire both analog and digital output from instruments and store pre-processed measurement data into a database for further off-line evaluation. The DAS operated and controlled the instrumentation during 2013. No updates were implemented.

The software environment of the DAS is Labview 7.1 from [National Instruments](#) and the database engine for data storage is Microsoft SQL Server 2008.

The DAS is designed to continuously run the following tasks:

- Start of the data acquisition at a defined time (must be full hour);
- Choose the instruments that have to be handled;
- Define the database path where data will be stored (primary in the network, secondary local on the acquisition machine);
- Define the period (10 minutes currently used) for storing averaged data, this is the data acquisition cycle time;
- Obtain data (every 10 seconds currently set) for selected instruments within the data acquisition cycle:
  - For analog instruments (currently only the CM11 and CMP11 Pyranometers), apply the calibration constants to translate the readings (voltages or currents) into analytical values;
  - Send commands to query instruments for data or keep listening the ports for instruments that have self defined output timing;
  - Scan instruments outputs to pick out the necessary data;
- Calculate average values and standard deviations for the cycle period;
- Query instruments for diagnostic data (when available), once every 10 minutes;
- Store all data in a database
  - With a single timestamp for the gas analyzers, FDMS-TEOM and Nephelometer
  - With the timestamp of their respective measurement for all other instruments.

The following instruments are managed with the DAS, using three PCs (currently called Emepacq5, Koala and Rack002):

Emepacq5:

- Number size distribution for particles diameter >0.500 μm, APS
- On-line FDMS-TEOMs
- Aerosol light absorption, Aethalometer
- Aerosol light absorption, MAAP
- Aerosol light scattering, Nephelometer

Koala:

- Reactive gases: CO, SO2, NO, NO_2, NO_x, O_3

Rack002:

- Solar radiation
- Weather transmitter (temperature, pressure, relative humidity, wind speed and direction, precipitation)
- Precipitation data

Data acquired are stored in a Microsoft SQL Server 2008 database on the central database **emep_db** hosted on the pc **Lake2.jrc.it**. If local network is not available, data are stored in a local database on the acquisition pc itself. Each pc has a software for the synchronisation of **emep_db** with **local db.**
The PC "**Lake.jrc.it**" connects the laboratory to the JRC network (*ies.jrc.it* domain) via optical lines. The schematic setup of the data acquisition system is shown in Fig. 14.
The acquisition time is locally synchronized for all PCs via a network time server running on lake and is kept at UTC, without adjustment for summer/winter time. Data are collected, called **emep_db** that runs on "**Lake2.jrc.it**".

Lake is the user gateway for the Station user, to allow granted staff to remotely access the acquisitions computers. This PC is also used to share information (life cycle sheets, lidar data) between IES domain and the Station network.

During 2013 the ABC-IS web site http://abc-is.jrc.ec.europa.eu/ was not updated. The aim of this product is to have of the Station presented as whole on the Internet: measurements distributed over different points within the JRC site, also covering different branches of environmental sciences, long-lived greenhouse gases, short-lived pollutants, and biosphere-atmosphere fluxes. The various sets of preliminary data reported on 24 hours window plots, updated every 10 minutes, are publically available. In the web site the projects to which ABC-IS contributes and contact persons can also be retrieved.

The web site runs over two machines. The first is the web server, **ccuprod2**, in the DMZ (demilitarized zone), where the web page code runs and is managed by the Air and Climate Unit IT staff. The development environment was Python and Ajax. The second computer, **emepimag.jrc.it,** in the JRC network, queries the database for data, generate plots and store plots in a folder in ccuprod2, to make them available to the internet. This second machine is managed by ABC-IS data management team and the software has been developed in C-sharp.
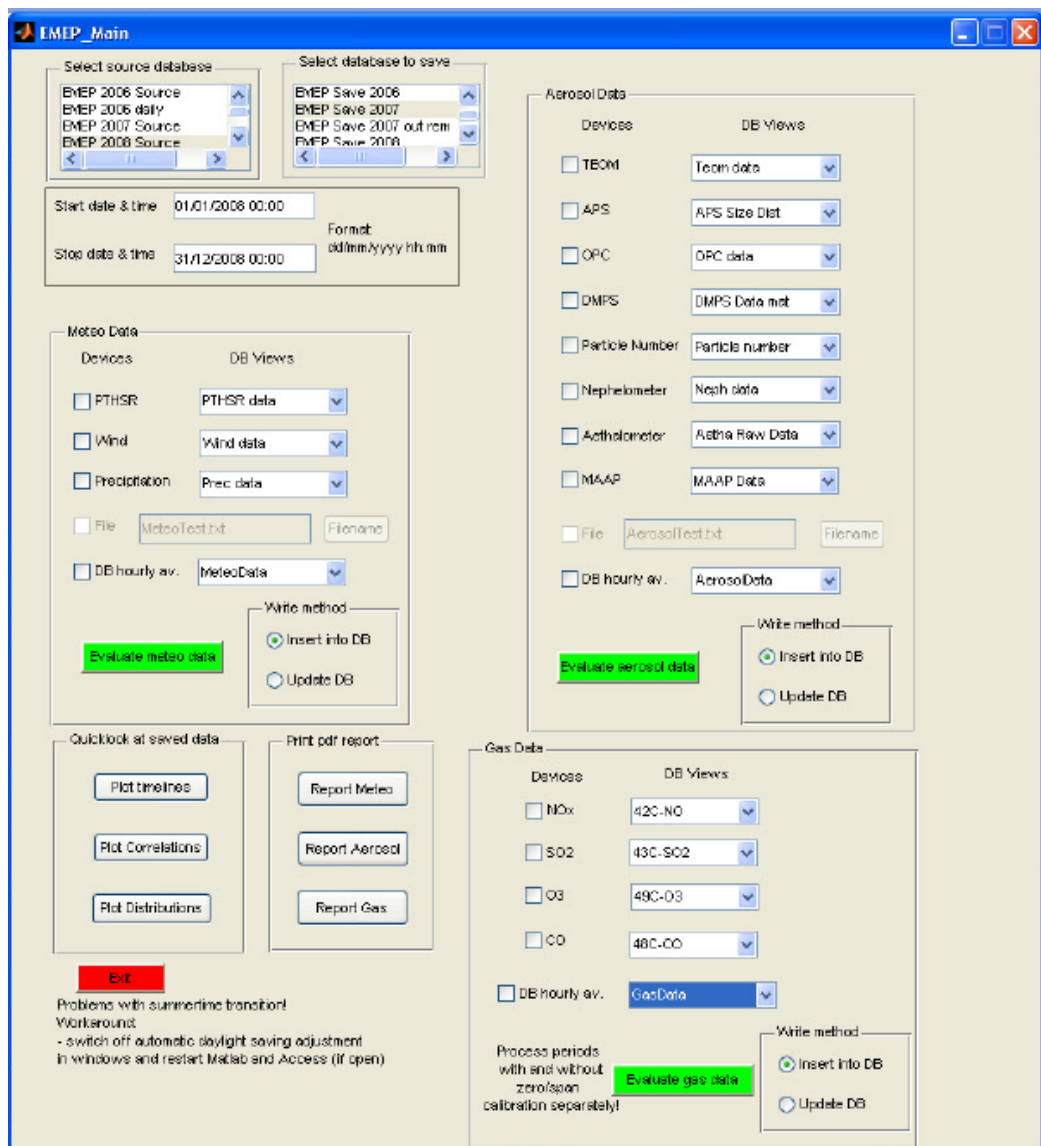

Fig. 16. *Graphic user interface of the EMEP data evaluation program.*

Data evaluation

The structured data evaluation system (EMEP_Main.m) with a graphic user interface (see Fig. 16) has been used with Matlab Release R2007b (www.mathworks.com) as the programming environment. The underlying strategy of the program is:

1) Load the necessary measurement data from all selected instruments from the data acquisition database as stored by the DAS (source database).
2) Apply the necessary individual correction factors, data analysis procedures, etc. specific to each instrument at the time base of the instrument.
3) Perform the calculation of hourly averages for all parameters.
4) Calculate outputs that require data from more than one instrument.
5) Store hourly averages of all results into a single Microsoft Access database, organized into different tables for gas phase, aerosol phase and meteorological data (save database).

Only the evaluation of gas phase data has an automatic removal algorithm for outliers / spikes implemented: d_i = 10 minute average value at time i, std_i = standard deviation for the 10 minute average (both saved in the raw data)

if $std_i > 100 \cdot \overline{std}$ and $|d_i - d_{i\pm1}| > 10 \cdot \overline{std}$

$\Rightarrow d_i = 1/2 (d_{i-1} + d_{i+1})$ for d_{i-1} **and** d_{i+1} **no** outliers,

otherwise $d_i = missig\ data$.

This algorithm corrects for single point outliers and removes double point outliers. All other situations are considered correct data. To check these data and to exclude outliers for all other measurements, a visual inspection of the 10 min data needs to be performed.

In addition, quick looks of evaluated data for selected time periods can be produced as well as printed timelines in the pdf-format for the evaluated data. All database connections are implemented via ODBC calls (Open DataBase Connectivity) to the corresponding Microsoft (MS) Access database files.

With a second program (EMEP_DailyAverages.m), daily averages (8:00 < t ≤ 8:00 +1 day) of all parameters stored in the hourly averages database can be calculated and are subsequently stored in a separate MS Access database.

Station representativeness

The representativeness of the JRC EMEP-GAW IT04 site has been evaluated to check:

- what area are the data acquired at the EMEP-GAW station (Bd 77p) representative for?
- would a move from the actual location to building 51 (or to "Roccolo hill, nido blu" 150 m from building 51 on Rocolo hill) lead to a break in the data series collected during the past 2 decades?

Summarizing the comparisons which are discussed in details in Dell'Acqua et al. (2010): No relevant difference in the daily maximum concentration of the compared parameters was observed. However, daily minimum are generally lower at the current site compared to Bd. 51 on Rocolo hill. The fact that O_3 daytime maximum concentrations are very similar at the EMEP-GAW station compared to the top of JRC Bd. 51 located 50 m higher also indicates that there are no significant local sources of O_3 precursors at the current site. However, O_3 minima and SO_2 concentrations in general are lower at the EMEP-GAW station, suggesting stronger sinks at the EMEP site.

Measurements were stopped at the EMEP IT04 site (Bd 77p) gradually between March 20 and 25th, and resumed at the provisional site or from the mobile laboratory parked at Bd 44 a few days later. All measurements were eventually resumed at the provisional site (Fig. 1) from July 11th.
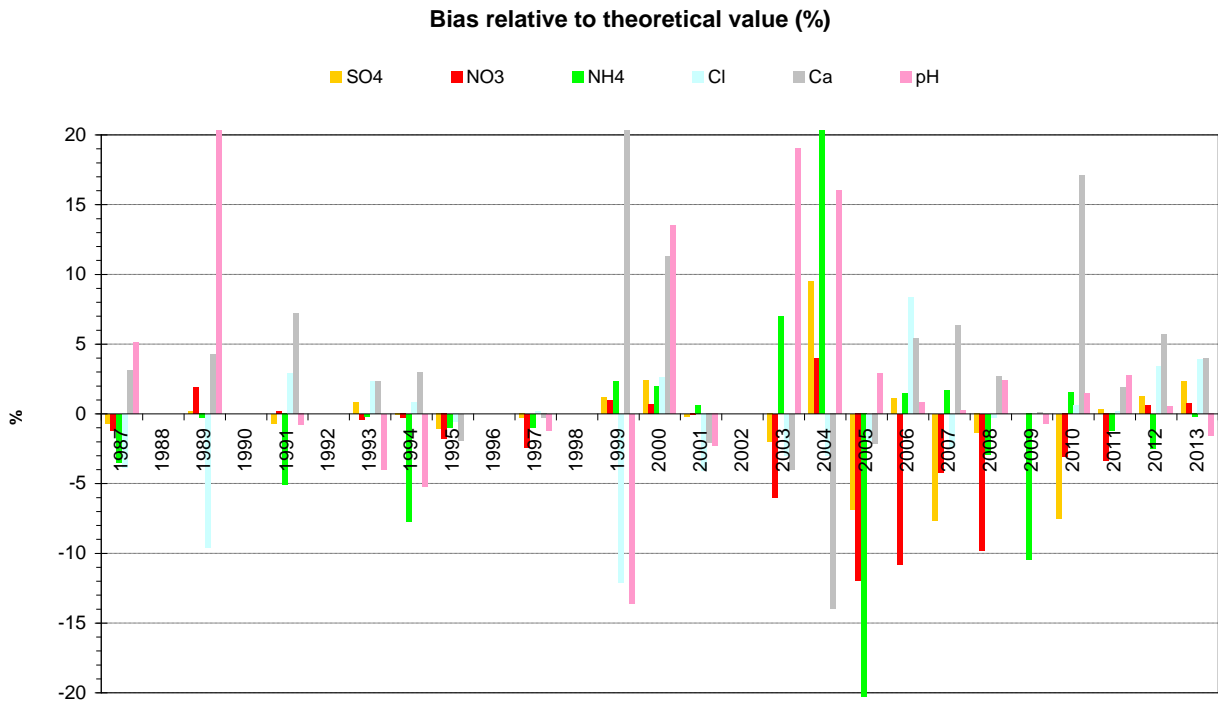
Fig. 17. *EMEP intercomparisons for rainwater analyses (1987-2013): JRC-IES results.*

Fig. 18. *JRC-IES instruments' (15 and 15.B) performance for the determination of (top) total carbon (TC) and (bottom) elemental carbon (EC/TC ratio) during the ACTRIS inter-laboratory comparison 2013.*

Quality assurance

At JRC level the quality system is based on the Total Quality Management philosophy the implementation of which started at the Environment Institute in December 1999. We have been working under ISO 9001 and ISO 14001 since 2010 (more information about our QMS system can also be found in the chapter "Quality management system"). Lacking personnel to specifically follow this business, the JRC-Ispra station for atmospheric research did not renew the accreditation for the monitoring of SO_2, NO, NO_2 and O_3 under EN 45001 obtained in 1999. However, most measurements and standardized operating procedures are based on recommendations of the EMEP manual (1995, revised 1996; 2001; 2002; 2014), WMO/GAW 153, ISO and CEN standards. Moreover, the JRC-Ispra gas monitors and standards are checked by the European Reference Laboratory for Air Pollution (ERLAP) regularly (see specific measurement description for details). For on-line aerosol instruments, intercomparisons took place in February 2013 (Nephelometer, Aethalometer, MAAP) and September 2013 (DMPS and CPC) at the world calibration center for aerosol physics (WCCAP) in Leipzig (D) in the frame of ACTRIS (www.actris.net). In addition, the EMEP-GAW station was favorably audited on March 22-24.03, 2010, in the frame of EUSAAR (www.eusaar.net) by Dr. T. Tuch, World Calibration Centre for Aerosol Physics (WCCAP) as described in a specific report.

Ion analysis quality was checked through the 31th annual EMEP intercomparison (Fig. 17). In the 2013 exercise, all ions measured in the rain water synthetic samples provided by NILU were determined with an error ≤4%, except K^+ and Mg^{2+} (+5% and +8%, respectively). The mean error for pH measurements was -1.6%.

The inter-laboratory comparison for organic and elemental carbon analyses organized in the frame of the competitive action ACTRIS in 2013 indicate no systematic bias for the determination of total carbon, and a slight systematic negative bias in the determination of EC with both our instruments compared to the average of the participants (Fig. 18).

Data quality for other measurements is also checked whenever possible through comparison among different instruments (for gases), mass closure (for PM) and ion balance (for precipitation) exercises. In addition, the Aethalometers AE31 S/N 4080303 and 7400609 (general maintenance) and the Aerodynamic Particle Sizer TSI 3321 S/N 70535014 (revision and calibration) were calibrated by their manufacturers in February and December 2013, respectively.
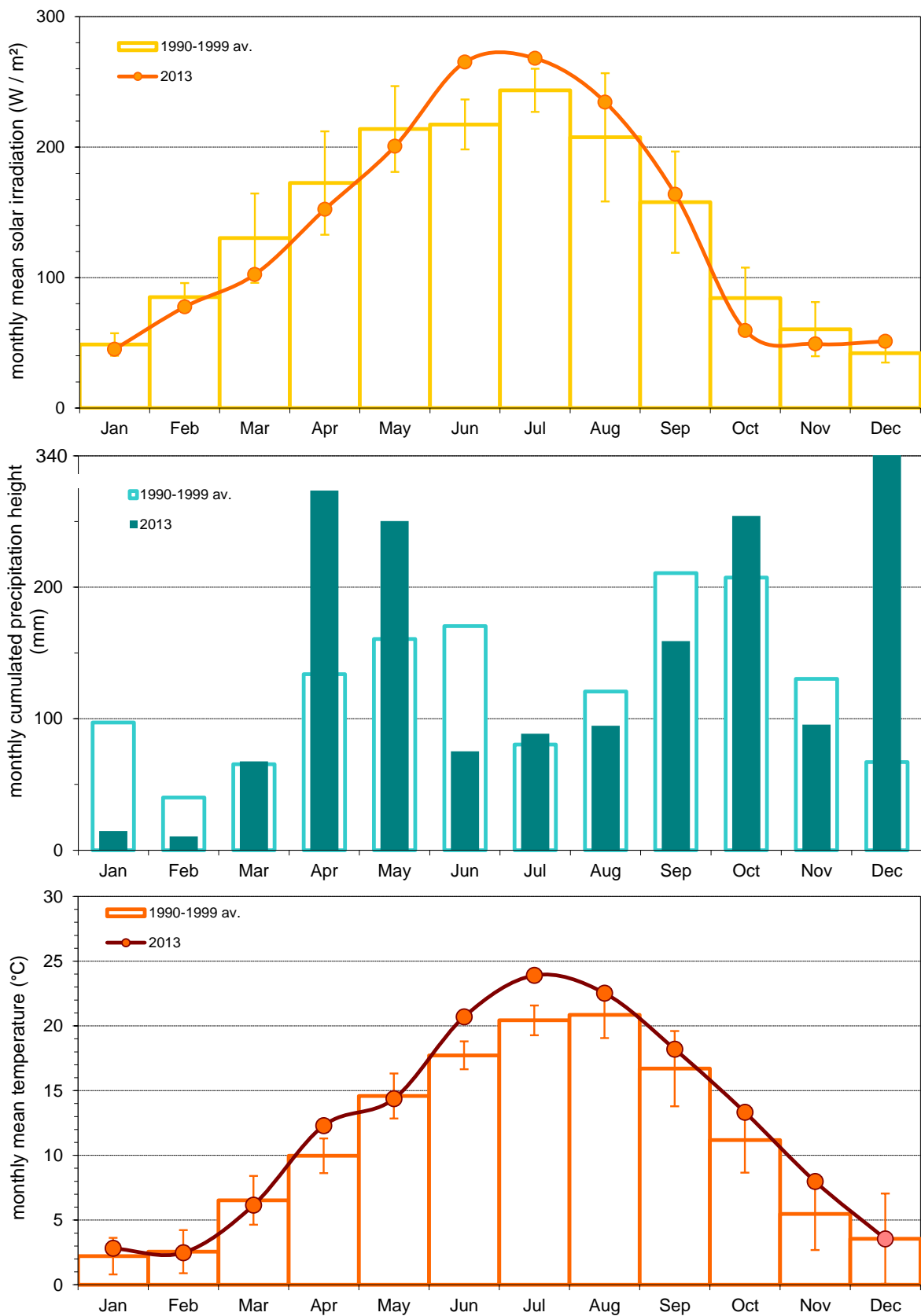
Fig. 19. Solar global irradiation, precipitation amount, and temperature monthly means observed at the EMEP station in the JRC-Ispra in 2013, compared to the 1990-1999 period ± standard deviations.

Results of the year 2013

Meteorology

Meteorological data were acquired directly at the EMEP site using the weather transmitter (T, P, RH) and a pyranometer (solar radiation) at 10 m and 1.5 m (2.5 m at the provisional site) above the ground, respectively. Precipitation data were measured at the forest flux tower of ABC-IS. Also all other meteorological variables were measured at the forest flux tower from December 19th. Fig. 19 shows monthly values of these meteorological variables for 2013 compared to the 1990-1999 average used as reference period.

June and July were exceptionally sunny and warm compared to the reference period.

January and February were particularly dry, while December was much rainier than usual. The total yearly rainfall was 1724 mm, i.e. much larger than the 2012 rainfall (1141 mm), and about 15 % larger compared to the 1990-1999 average (1484 mm), due to the exceptional rainfall in December.

Gas phase air pollutants

SO_2, CO, NOx and O_3 were measured almost continuously during the year 2013. An uncertainty of 15 % may be applied to these data in accordance with the *European Directive 2008/50/EC.* To render the time series comparable to the historical data acquired at the EMEP-GAW site at Bd 77p, 10 min data were flagged for local contamination, and hourly (and daily) averages were computed excluding the data points for which local contamination was identified.

In 2013, seasonal variations in SO_2, NO, NO_2, NO_x and O_3 were similar to those observed over the 1990-1999 period (Fig. 20). Concentrations are generally highest during wintertime for primary pollutants (SO_2, CO, NO_x), and in summertime for O_3. The higher concentrations of SO_2, CO, NO_x in winter result from a least dispersion of pollutant during cold months (low boundary layer height and stagnant conditions), whereas the high concentration of O_3 during summer is due to enhanced photochemical production.

SO_2 concentrations (average = 0.6 µg/m³) were about 7 times less compared to the reference period (1990-1999) and on average 40% lower than in 2012.

Daily mean CO concentrations ranged from 0.14 to 1.30 µg m^{-3} (~0.1 – 1.1 ppmv), which are typical values in a regional background station like the ABC-IS station in Ispra. The lowest values were observed in very clean air masses during Föhn events and windy summer days, and the highest values during cold winter nights.

NO_2 concentrations (annual average = 18 µg m^{-3}) were on average 30% lower than during 1990-1999 but very similar to the 2012 levels, as NO concentrations (annual average = 5.9 µg m^{-3}) were.
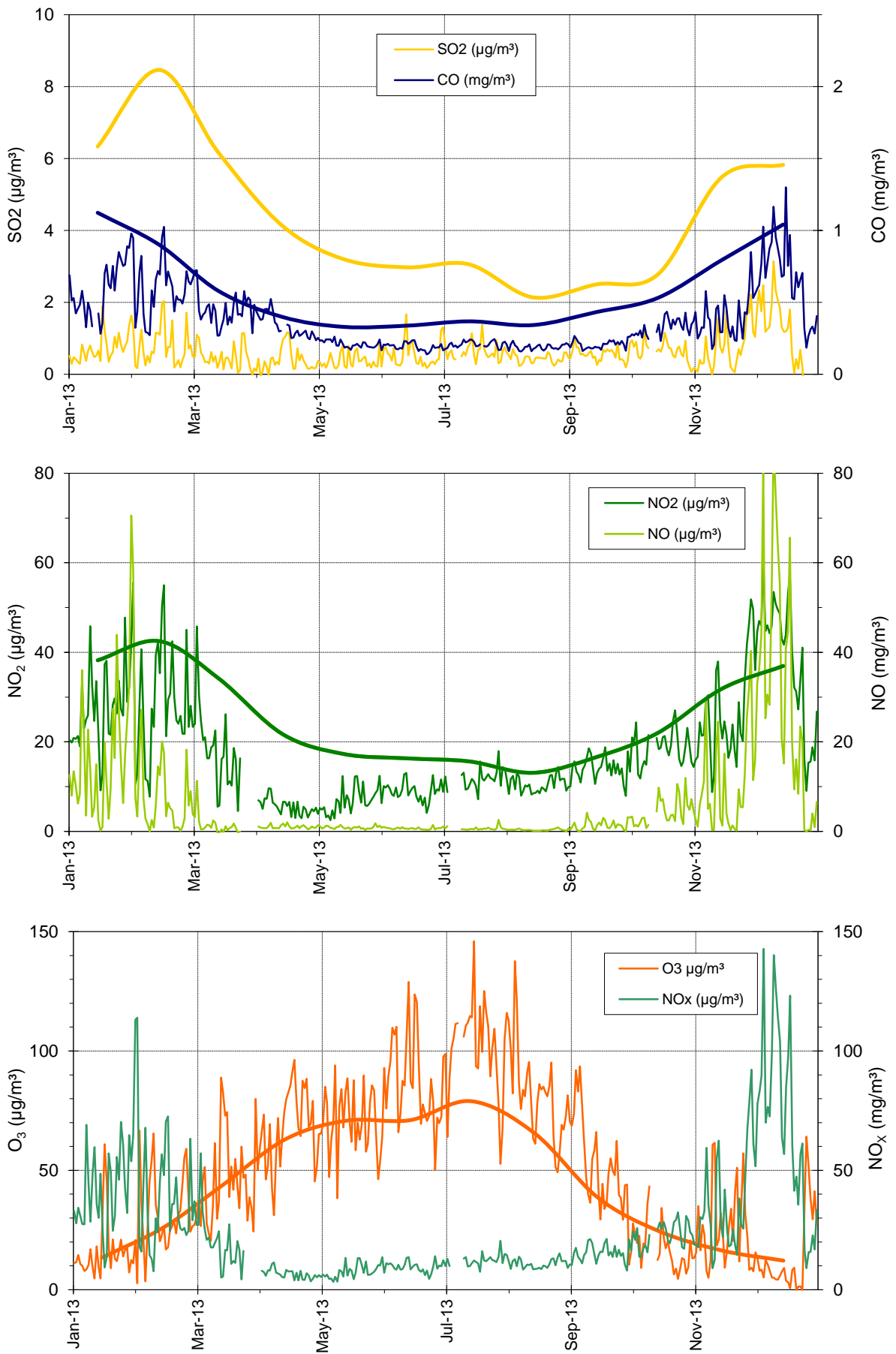
Fig. 20. *Seasonal variations of the 24 hr averaged concentrations of SO$_2$, CO, NO$_2$, NO, O$_3$ and NO$_x$ in 2013 (thin lines) and 1990-1999 monthly averages (thick lines: yellow=SO$_2$, blue=CO, green=NO$_2$, orange=O$_3$).*

44

The mean O_3 concentration in *2013* (51 µg m^{-3}, 26 ppb) was 6% higher than in 2012, for which a 30% increase had already been observed compared to 2011. O_3 average concentrations are currently back to values observed during the period 1990-1999. Furthermore, several ozone indicators (Fig. 21) largely deteriorated compared to previous years, as further illustrated by Figure 46 on 68.

The vegetation exposure to above the ozone threshold of 40 ppb (AOT 40 = Accumulated dose of ozone Over a Threshold of 40 ppb, normally uses for "crops exposure to ozone") was 32300 ppb h in 2013 (with a data coverage for O_3 of 98 % for the whole year), i.e. + 30% compared to 2012, and 3 times as much as much as in 2011. AOT 40 in 2013 got close to the 34000 ppb h yr^{-1} observed over the 1990-1999 decade (Fig. 21).

For quantification of the health impacts (population exposure), the World Health Organisation uses the SOMO35 indicator (Sum of Ozone Means Over 35 ppb, where means stands for maximum 8-hour mean over day), i.e. the accumulated ozone concentrations dose over a threshold of 35 ppb (WHO, 2008). In 2013, SOMO35 was 4700 ppb day (Fig. 21), i.e. not significantly different from 2012 data, but twice as much as in 2011. Eighteen (18) extreme O_3 concentrations (>180 µg m^{-3} over 1 hour) were also observed in 2013, to be compared to 8 extreme events in 2012. The value 180 µg m^{-3} over 1 hour corresponds to the threshold above which authorities have to inform the public (European Directive 2008/50/EC on ambient air quality and cleaner air for Europe).
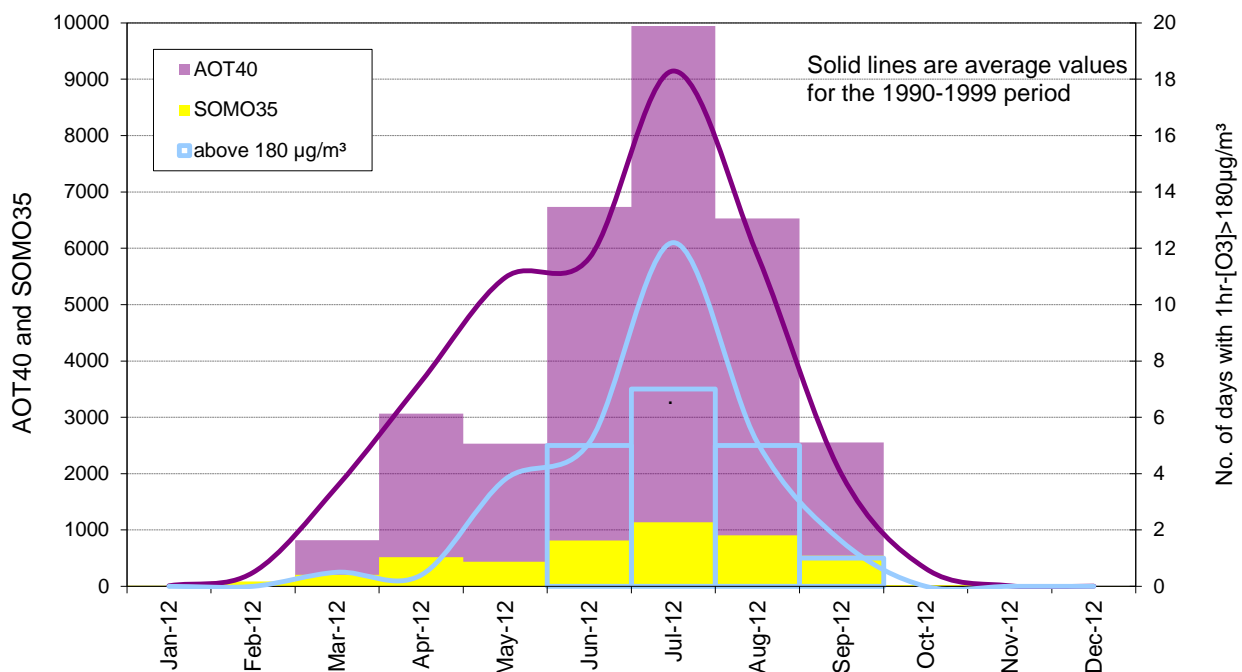

Fig. 21*: AOT 40 (ppb h), SOMO35 (ppb day) and number of exceedances of the 1-hour averaged 180 µg/m³ threshold values in 2013 (bars), and reference period values 1990-1999 (lines).*
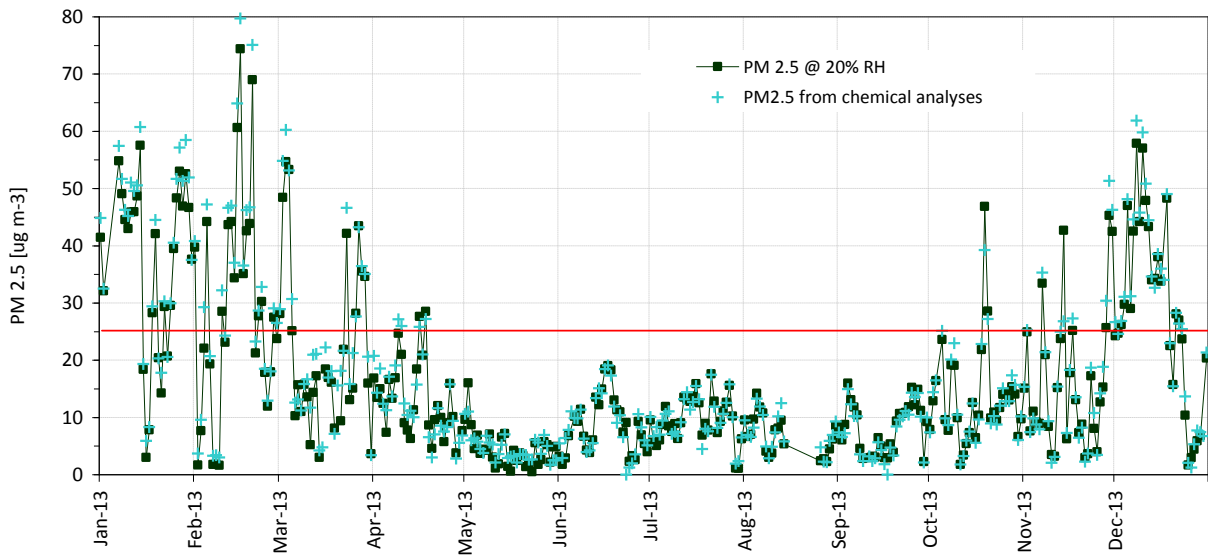
Fig. 22. *24hr-integrated PM2.5 mass concentrations from off-line gravimetric measurements at 20 % RH and chemical determination of main constituents in 2013.The red line indicates the annual limit value of 25 μg/m³ to be reached by 2015 (European directive 2008/50/EC)*
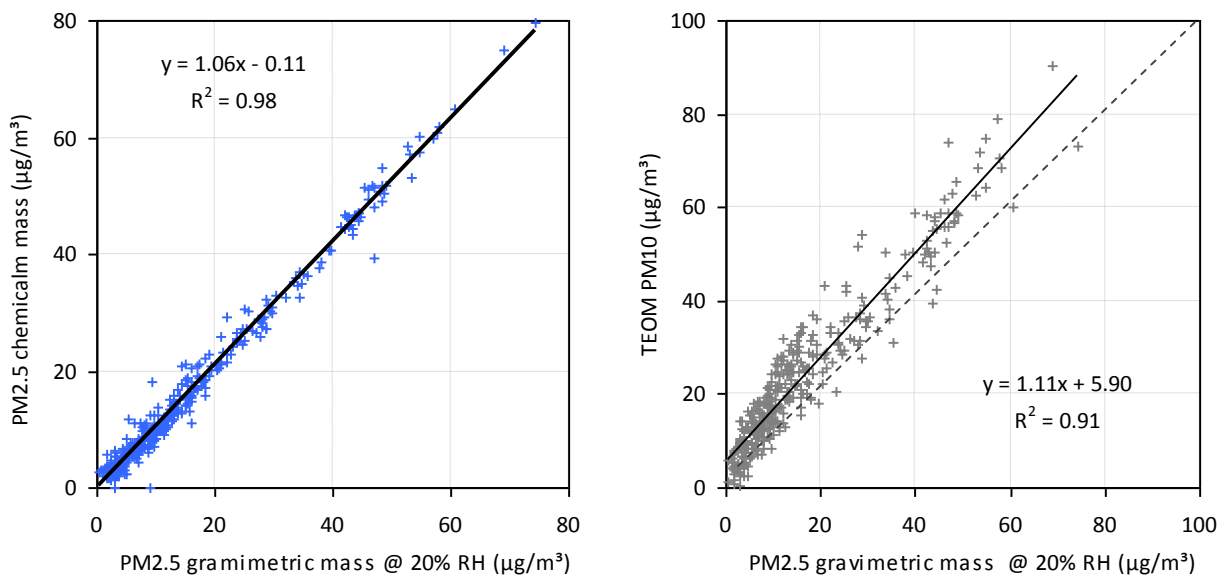

Fig. 23. *Regressions between gravimetric PM2.5 measurements at 20 % RH and sum of the PM2.5 chemical constituents (left), and between FDMS-TEOM PM10 and gravimetric PM2.5 measurements at 20 % RH (right) in 2013.*

46

During the reference period 1990-1999, the information level of 180 µg m^{-3} has been exceeded 29 times per year on average. The other "protection of human health factor" mentioned by the European Directive 2008/50/EC (120 µg m^{-3} as maximum daily 8-hour average) was exceeded 65 times in 2012, i.e. well above the threshold of 25 exceedances per year (averaged over three years).

Particulate phase

Particulate matter mass concentrations

PM$_{2.5}$ concentrations (Fig. 22) measured gravimetrically at 20 % relative humidity (RH) averaged 16.1 µg m^{-3} over 2013 (data coverage = 93%, including 11 measurements discarded for inconsistency with others). This was the lowest value observed since this measurement was started in 2002 (second lowest value = 17.5 µg m^{-3} in 2010), well below the European annual limit value of 25 µg m^{-3} that has to be reached by 2015 (European directive 2008/50/EC). Gravimetric measurements of PM$_{2.5}$ mass at 20% RH (11 outliers discarded) and the sum of PM$_{2.5}$ mass constituents determined from chemical analyses (see p. 49) are well correlated (Fig.23).

FDMS-TEOM_A (s/n 233870012) was used to measure PM$_{10}$ in 2013, except for the 06 May - 29 July, and 09 - 23 Nov. periods during which FDMS-TEOM_B (s/n 253620409) was used. 38 exceedances of the 24-hr limit value for PM$_{10}$ (50 µg/m³) were observed in 2013 (99% annual data coverage), to be compared to the 51 exceedances observed in 2012. The annual PM$_{10}$ average (23.6 µg m^{-3}) was far below the 40 µg m^{-3} annual average limit value though.

The correlation between gravimetric PM$_{2.5}$ and PM$_{10}$ concentrations measured with a TEOM-FDMS (Fig. 23, right hand) was marginal (R²=0.86) in 2013, and suggests an offset of close to 6 µg m^{-3} from the TEOM. PM$_{10}$ was about 30 % higher than PM$_{2.5}$ on average. The difference was much larger for lower concentrations (< 20 µg m^{-3} PM$_{2.5}$) and reached a factor of 2 (offset corrected).
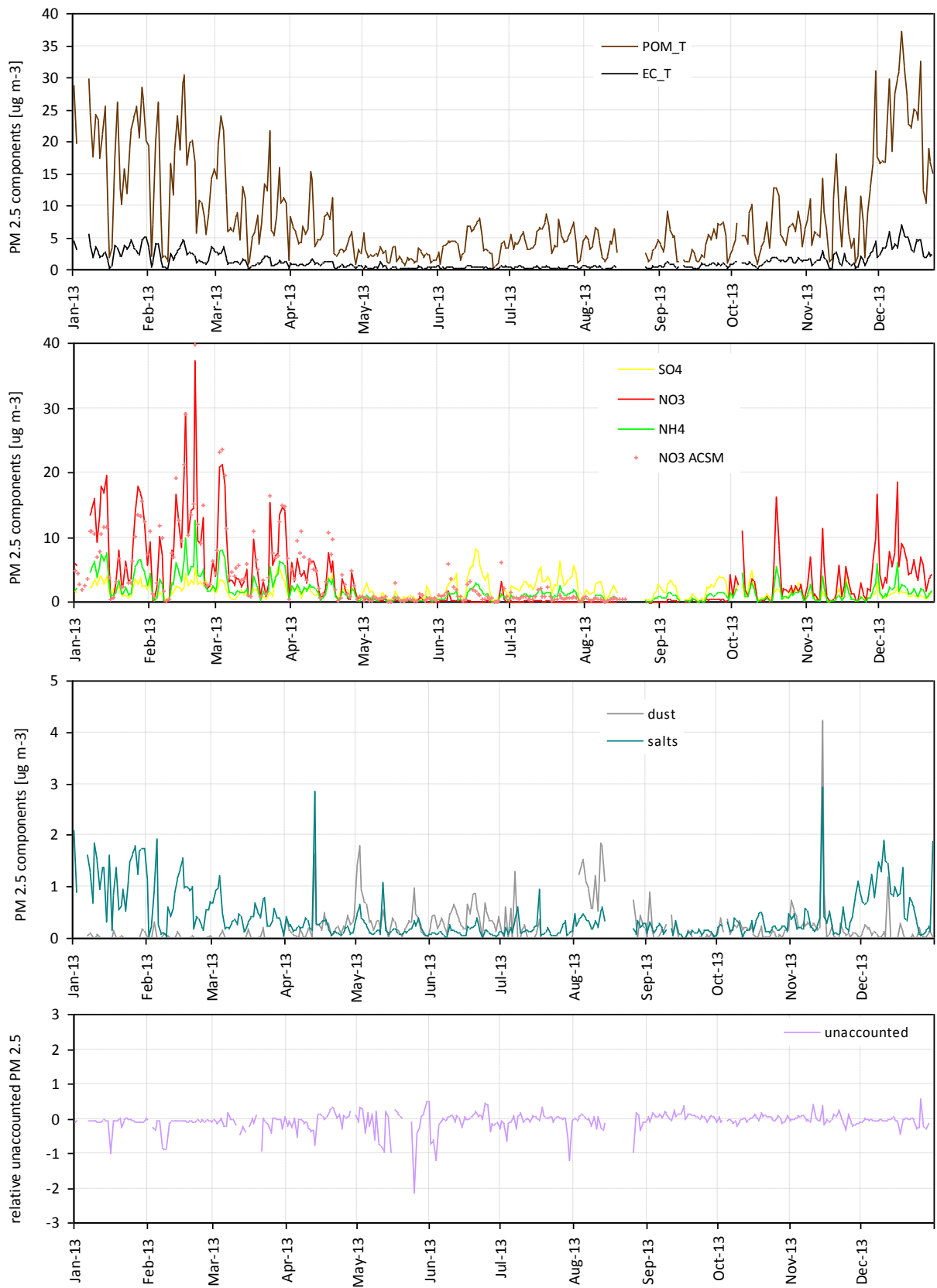
Fig. 24. 24-hr integrated concentrations of the main aerosol constituents of PM2.5 during 2013.

<u>PM2.5 chemistry:</u>

Main ions (Cl^-, NO_3^-, SO_4^{2-}, $C_2O_4^{2-}$, Na^+, NH_4^+, K^+, Mg^{2+}, and Ca^{2+}), OC and EC were determined from the quartz fibre filters (for the whole year) collected for PM mass concentration measurements.

Fig. 24 shows the temporal variations in the PM2.5 main components derived from these measurements. Particulate organic matter (POM) is calculated by multiplying OC (organic carbon) values by the 1.4 conversion factor to account for non-C atoms contained in POM (Russell et al., 2003). "Salts" include Na^+, K^+, Mg^{2+}, and Ca^{2+}. Dust is calculated from Ca^{2+} concentrations and the regression (slope = 4.5) found between ash and Ca^{2+} in the analyses of ash-less cellulose filters (Whatman 40) in previous years. Most components show seasonal variations with higher concentrations in winter and fall, and lower concentrations in summer, like $PM_{2.5}$ mass concentrations. This is mainly due to changes in pollutant horizontal and vertical dispersion, related to seasonal variations in meteorology (e.g. lower boundary layer in winter). The amplitude of the POM, NH_4^+ and NO_3^- seasonal cycles may be enhanced due to equilibrium shifts towards the gas phase, and/or to enhanced losses (negative artefact) from quartz fibre filters during warmer months. Indeed the concentration of NH_4NO_3 in $PM_{2.5}$ during May – Sept. 2013 (0.2 µg / m³) was 80% than in submicron aerosol (1.0 µg / m³) as measured with the ACSM (see next page).

NH_4^+ follows NO_3^- + SO_4^{2-} very well as indicated by the regression shown in Fig. 25. This correlation results from the atmospheric reaction between NH_3 and the secondary pollutants H_2SO_4 and HNO_3 produced from SO_2 and NO_x, respectively. The slope of this regression is very close to 1, which means that NH_3 was sufficiently available in the atmosphere to neutralise both H_2SO_4 and HNO_3. This furthermore indicates that PM2.5 aerosol was generally not acidic in 2013.
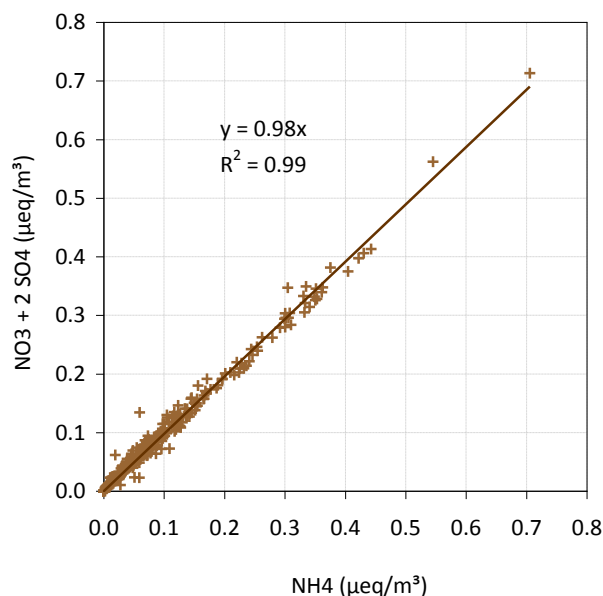

Fig. 25. SO_4^{2-} + NO_3^- vs. NH_4^+ (µeq/m³) in $PM_{2.5}$ for 2013

Table 4: *annual mean concentrations and contributions of major PM$_{2.5}$ constituents in 2013*

constituent	salts Cl$^-$, Na$^+$, K$^+$, Mg^{2+}, and Ca^{2+}	NH$_4^+$	NO$_3^-$	SO$_4^{2-}$	POM	EC	dust	unaccounted
Mean conc. (µg m^{-3})	0.40	1.57	3.22	1.70	8.02	1.23	0.21	- 0.10
Mean cont. (%)	3.1	10.2	14.6	16.0	52.1	7.8	2.9	-6.6
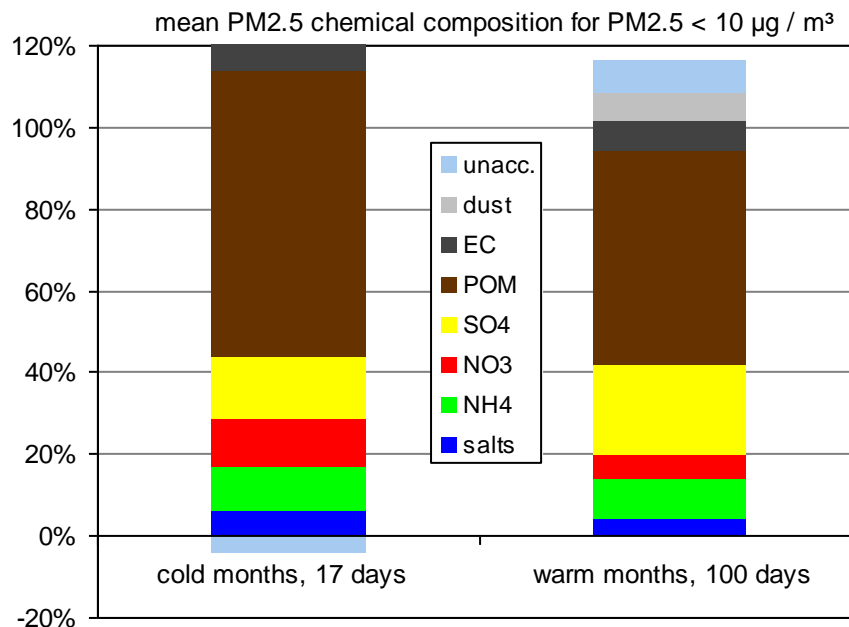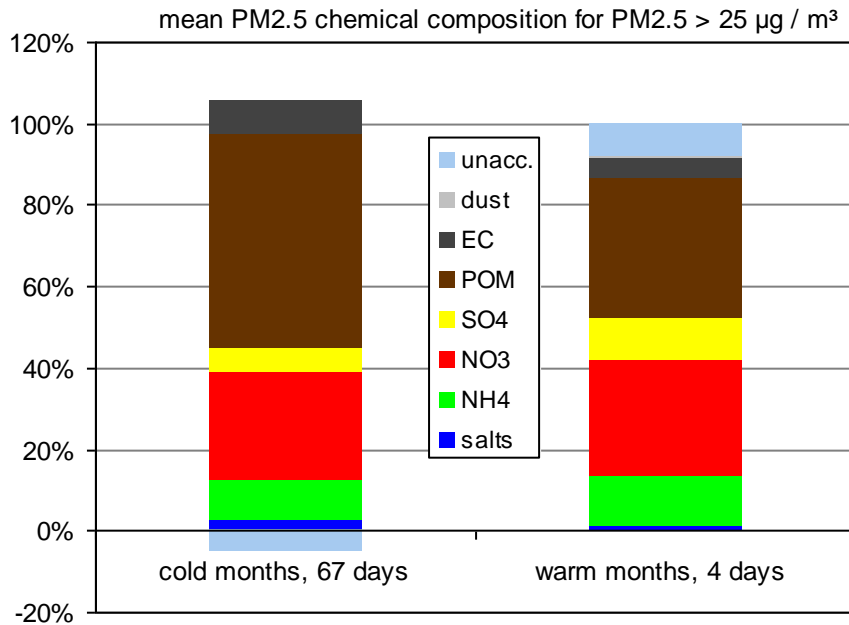
Fig. 26. *Average composition of PM2.5 in 2013 for days on which PM2.5 > 25 µg/m³(top) and PM2.5 < 10 µg/m³(bottom), over cold (Jan., Feb. ,Mar., Nov., Dec.) and warm (Apr. – Oct.) months*

50

Contribution of the main aerosol constituents to PM2.5

The contributions of the main aerosol components to PM2.5 are presented in Table 4 (annual averages) and in Fig. 26 (a) for days on which the "24-hr limit value for PM2.5 of >25 µg/m³ was exceeded" during cold months (Jan., Feb., March, Nov. and Dec., 67 cases) and the warm months (Apr. to Oct, 4 cases) and (b) for days on which 24-hr integrated $PM_{2.5}$ concentration was below 10 µg / m³ during cold (17 cases) and warm months (100 cases).

These $PM_{2.5}$ compositions may not always represent accurately the actual composition of particulate matter in the atmosphere (mainly due to possible negative sampling artefacts), but are suitable to assess which components contributed to the PM2.5 mass collected by a quartz fiber filter downstream of a 20 cm-long carbon monolith denuder.

Over the whole year 2013, carbonaceous species accounted for 60% of $PM_{2.5}$ (EC:8%, POM: 52%), and secondary inorganics for 31% (NH_4: 10 %, NO_3: 15%, and SO_4:16%). In both the cold and the warm seasons, particulate air pollution days are characterised by a strong increase in NO_3 contribution. Considering low $PM_{2.5}$ concentration days, summertime is characterised by higher SO_4^{2-} concentrations (faster SO_2 photochemical conversion) and lower NO_3^- concentrations ($HNO_3 + NH_3 \leftrightarrows NH_4NO_3$ equilibrium shifted towards the gas phase, on the left hand side, as temperature increases). Dust and salts do not contribute significantly to the $PM_{2.5}$ mass (about 3 % each.). Their contribution is larger on cleanest days compared to most polluted days.
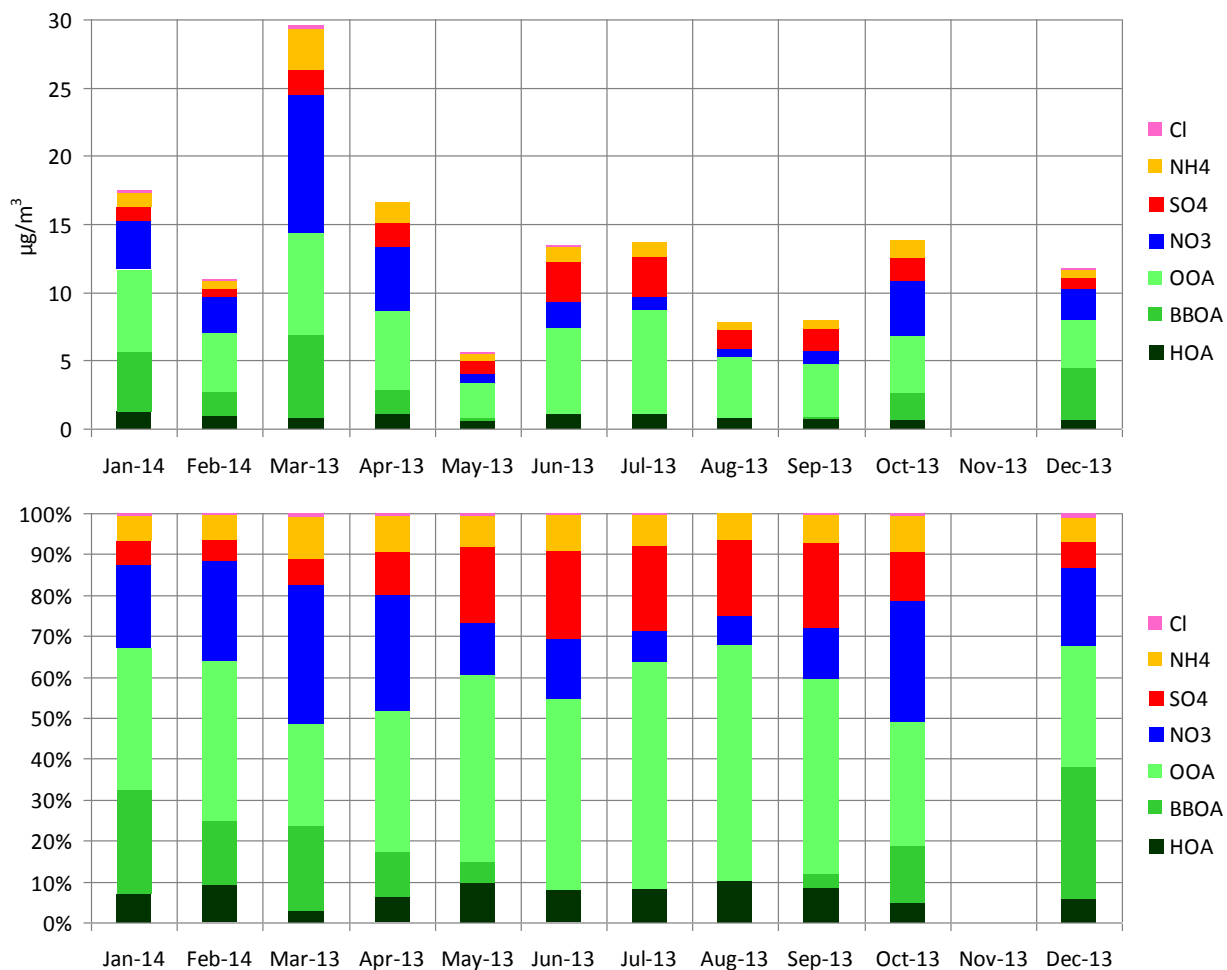
Fig. 27. *Monthly absolute (top) and relative (bottom) chemical composition of NR-PM$_1$ determined with the ACSM from March 2013 to February 2014. Organic aerosol (OA) was apportioned into HOA, BBOA and OOA (see text for definitions).*

<u>Contribution of the main aerosol constituents to the submicron aerosol</u>

The monthly chemical composition of non-refractory submicron aerosols (NR-PM$_1$) between March 2013 and Feb 2014 is shown in Fig. 27. Organic aerosol (OA) has been apportioned using the Multilinear-Engine 2 algorithm (Paatero, 2000) into three main components that are: i) hydrocarbon-like OA (HOA) which is a surrogate for fossil fuel emissions, ii) primary biomass burning OA (BBOA) associated with residential wood burning emissions here and iii) oxygenated OA (OOA) which can be regarded as secondary, oxidized and aged OA (Zhang et al., 2011). Clear seasonal variations are observed for both NR-PM$_1$ levels and chemical composition. Secondary inorganic compounds follow patterns similar to those already described in the PM$_{2.5}$ size fraction (see p. 48). Organic aerosols are primarily made of OOA (44 to 87% of OA) indicating that OA is mostly of secondary nature in Ispra. The highest OOA contributions are found during summer (>85% of OA), which likely reflects enhanced photochemical production due to increased solar irradiation (Fig. 19). BBOA is a substantial component of OA during cold months and can contribute up to 25-48% of its mass, consistent with previous studies conducted in the Alpine region (Herich et al., 2014). Residential wood burning emission reductions would thus likely help decreasing NR-PM$_1$ levels at our site during winter. Finally HOA is a minor component of OA throughout the year (5-16%) implying that fossil fuel emissions are not a notable source of primary OA in Ispra, in agreement with what has been reported at rural sites worldwide (Zhang et al., 2011).
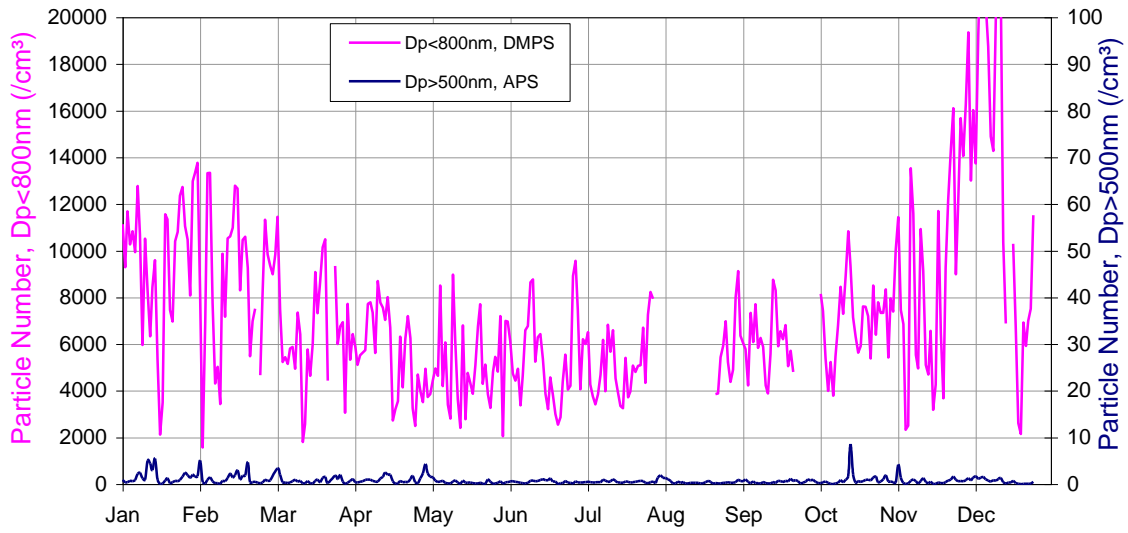
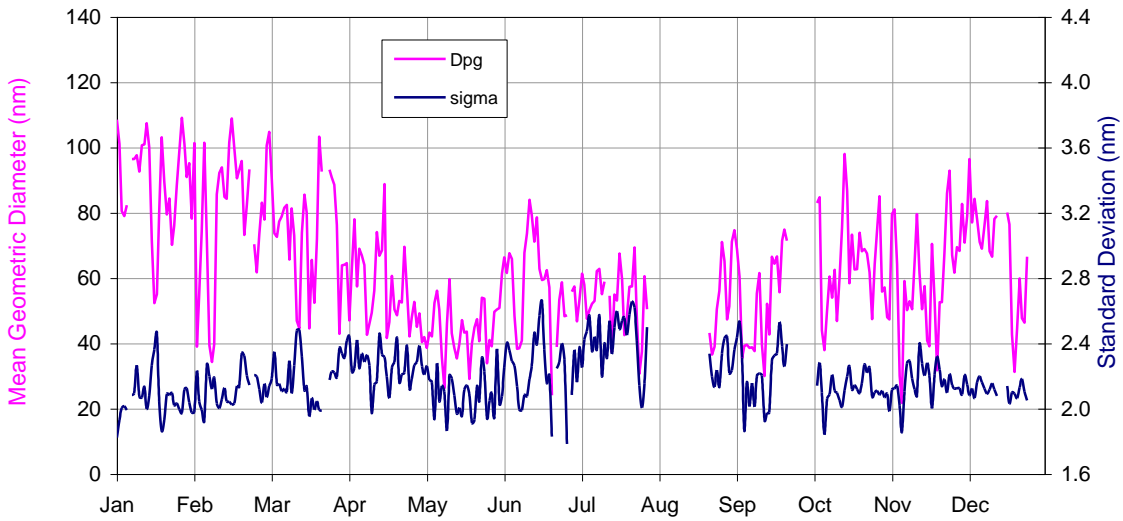Fig. 28. *24 hr – mean particle number concentrations for Dp > 500 nm and Dp< 600 nm.*

Fig. 29*. 24 hr - averaged particle geometric mean diameter (measured with DMPS) and standard deviation*
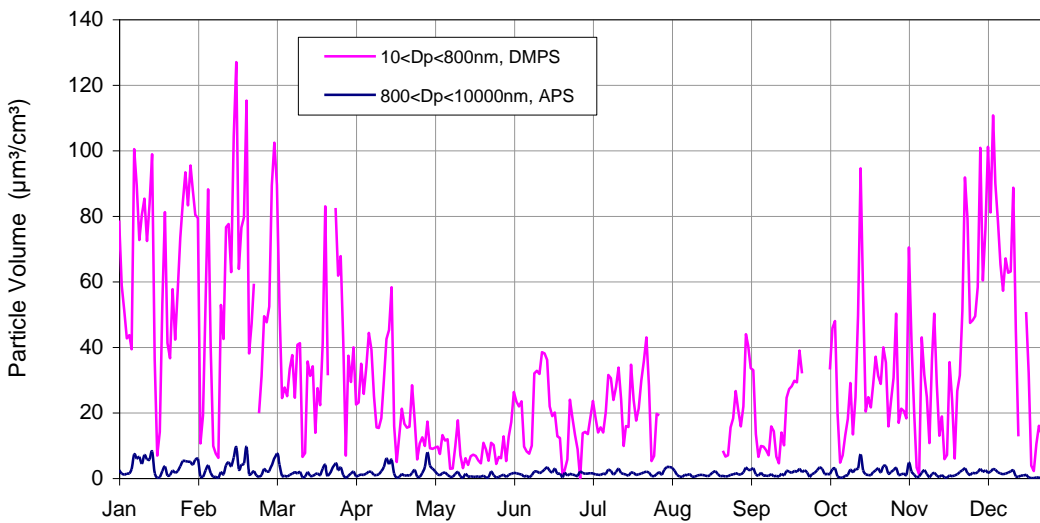

Fig. 30*. 24 hr - averaged particle volume concentrations for Dp< 800 nm and Dp > 800 nm.*

54

<u>Aerosol physical properties</u>

Measurements of the particle number size distributions smaller than 800 nm diameter were carried out using a Differential Mobility Particle Sizer almost continuously in 2013, except during the inter-laboratory comparison at the WRCAP in Leipzig. DMPS were discarded for the period 2-25 Aug. due to leaks at the inlet of the instrument. These two breaks resulted in a data coverage of 89%.

Particle number concentrations averaged over 24 hr (from 08:00 to 08:00 UTC) ranged from 2100 to 25200 cm^{-3} (average: 8220 cm^{-3}) and followed a seasonal cycle similar to that of PM mass concentrations, with maxima in winter and minima in summer (Fig. 28). It should be mentioned, that the DMPS data presented here have not been corrected for inlet diffusion losses and CPC efficiency, but those normally account for only a few percent on particle number and have no impact on the other variables. The vicinity of internal and external roads led to numerous episodes of local contamination, which were flagged during the data analysis process. Excluding the data points affected by local contamination, the mean particle number was 7290 cm^{-3}.

The mean mode diameter at RH < 30 % ranged 22 – 109 nm (average = 64 nm) in 2013. The variations in particle size distributions parameters (Fig. 29) show seasonal patterns as well: the mean geometric diameter is generally larger in winter (about 60-100 nm) than in summer (about 40- 60 nm), whereas the standard deviation of the distribution follows an opposite trend (larger in summer than in winter).

The size distribution of particles larger than 500 nm was measured using an Aerodynamic Particle Sizer almost continuously over 2013 (data coverage: 98%). Aerodynamic diameters were converted to geometric diameter assuming a particle density of 1.50. As previously observed, particles larger that 500 nm generally (90th percentile) accounted for <<0.1% of the total particle number only (Fig. 28), but for about 7 % of the total particle volume on average (Fig. 30). The seasonal variations in particle volume concentration reflect the changes in particle number and mean geometric diameter, with larger volumes in winter than in summer.
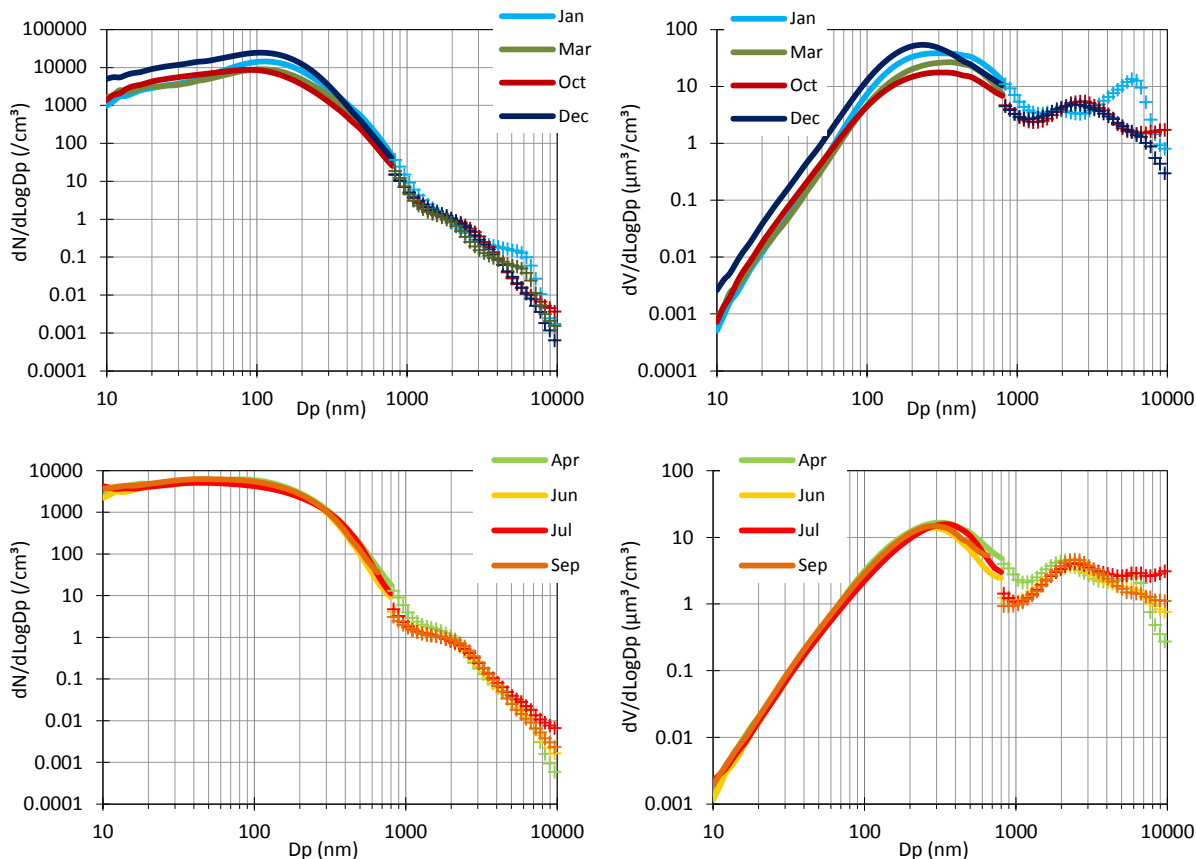
Fig. 32. *Monthly mean particle number (left) and volume (right) size distributions measured in 2013 with a DMPS (10-800 nm, solid lines) and an APS (0.85-10 µm, crosses). A density of* **1.0 g cm**$^{-3}$ *was used to convert aerodynamic to geometric diameters.*
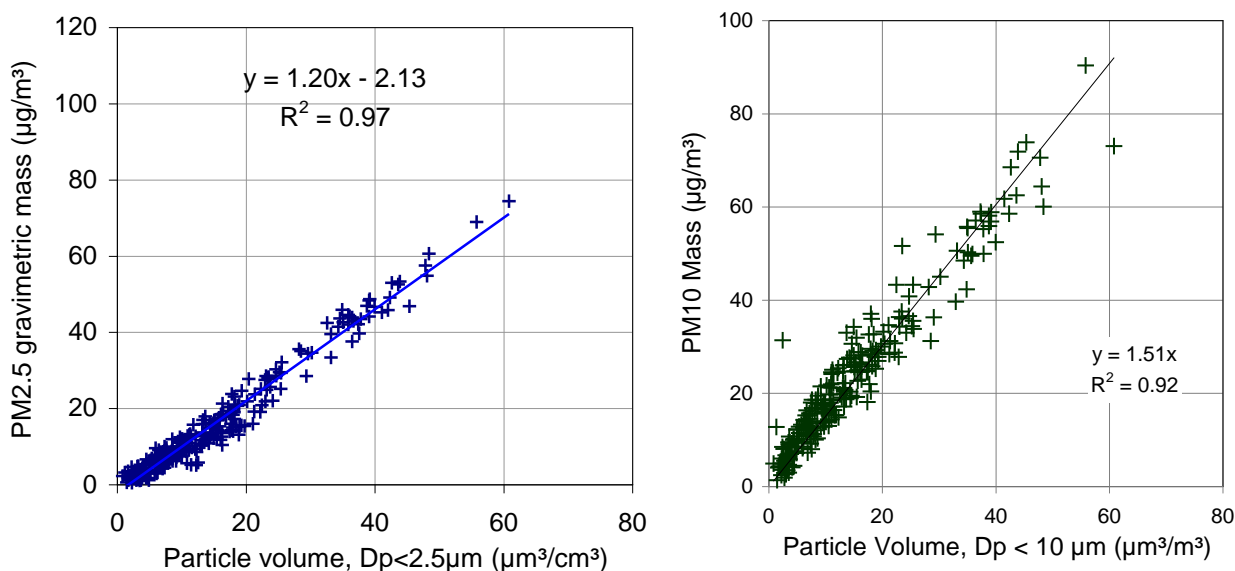

Fig. 33. *2013 regressions between (right) PM2.5 mass concentrations determined from gravimetric measurements at 20 % RH and particle volume (Dp < 2.5 µm) calculated from DMPS and APS measurements, and (left) between PM10 mass concentrations with the FDMS at 30 % RH and particle volume (Dp < 10 µm)*

The apparent good agreement between particle number size distributions (Fig. 32) measured with the DMPS and the APS actually reveals a significant inconsistency between these two instruments, since the aerosol density (1.0 g cm^{-3}) used to convert aerodynamic diameters (measured by the APS) to mobility diameters (measured by the DMPS) is out of the range (1.6 ± 0.1 g cm^{-3}) expected for atmospheric particles (McMurry et al., 2002). This was already observed in December 2012, and may be due to over-counting by the DMPS of particles larger than 300 nm, as also suggested by the 2013 DMPS intercomparison at the WCCAP in Leipzig.

The comparisons between PM mass and aerosol volume concentrations show both a good correlation (Fig. 33). The slope of the regression between PM$_{2.5}$ at 20 % RH and particle volume suggests an aerosol density of 1.20 (to be compared to 1.31, 1.38 and 1.37 in 2012, 2011 and 2010, respectively), while the regression between PM$_{10}$ mass and aerosol volume concentration (for Dp < 10 µm) suggests a density of 1.5, equal to the nominal value of 1.5 g cm^{-3} assumed to convert aerodynamic diameters to mobility diameters for particle volume calculation. This (together with the comparison between PM$_{2.5}$ mass and chemistry) might indicate that PM$_{2.5}$ gravimetric measurements are underestimated.
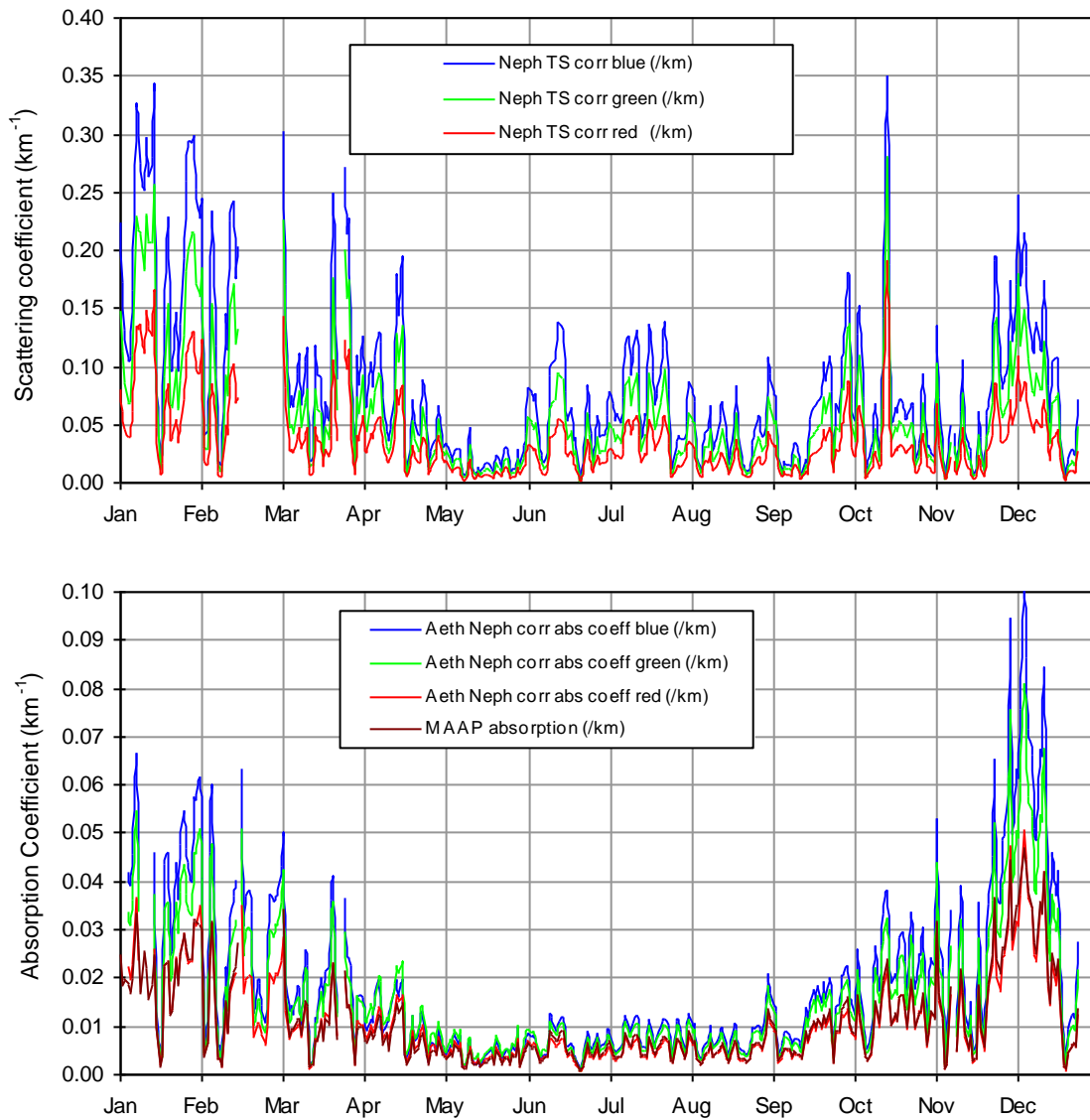
Fig. 34 *Daily mean atmospheric particle scattering (top) and absorption (bottom) coefficients at three wavelengths, derived from Nephelometer, Aethalometer and MAAP measurements (not corrected for RH) performed in 2013.*

Aerosol optical properties

Aerosol optical properties have been monitored continuously during 2013 (data coverage = 95-97%). Data from the Nephelometer (Fig. 34a) have been corrected for angular non idealities (truncation to 7 – 170°, slightly not cosine-weighted distribution of illumination) according to Anderson and Ogren (1998), but not for RH effects. Although a Nafion dryer is implemented to dry the air entering the nephelometer, RH > 40% commonly occurred between June 15th and Sep. 30th, 2013. At 40% RH, aerosol scattering is on average increased by 20% compared to 0% RH in Ispra (Adam et al., 2012).

Atmospheric particle absorption coefficients at 7 wavelengths (Fig. 34b) were derived from the Aethalometer AE-31 data corrected for the shadowing and multiple scattering effects when Nephelometer data were available, according to Weingartner et al (2003), making use of coefficients derived from Schmid et al. (2006), i.e. 3.60, 3.65 and 3.95 at 470, 520, and 660 nm, respectively.

Both scattering and absorption coefficients follow seasonal variations (Fig. 34) in line with PM mass variations, mainly controlled by pollutant dispersion rates.

The uncertainty of the multiple scattering correction factor may introduce a quite large uncertainty in the aerosol absorption coefficient values, since correction factors ranging from 2 to 4 have been proposed (Weingartner et al., 2003; Arnott et al., 2005). However, the use of the correction factors listed above leads to an aerosol absorption coefficient at 660 nm in good agreement with the absorption coefficient obtained from the Multi Angle Absorption Photometer (MAAP) for 670 nm (Fig. 35, R^2 = 0.99, slope = 0.95). Deviations from the 1:1 line are mainly observed for absorption coefficient values > 0.04 km^{-1}. This behavior strictly depends on the aerosol absorption coefficient and not on instrumental parameters such as the filter loading.
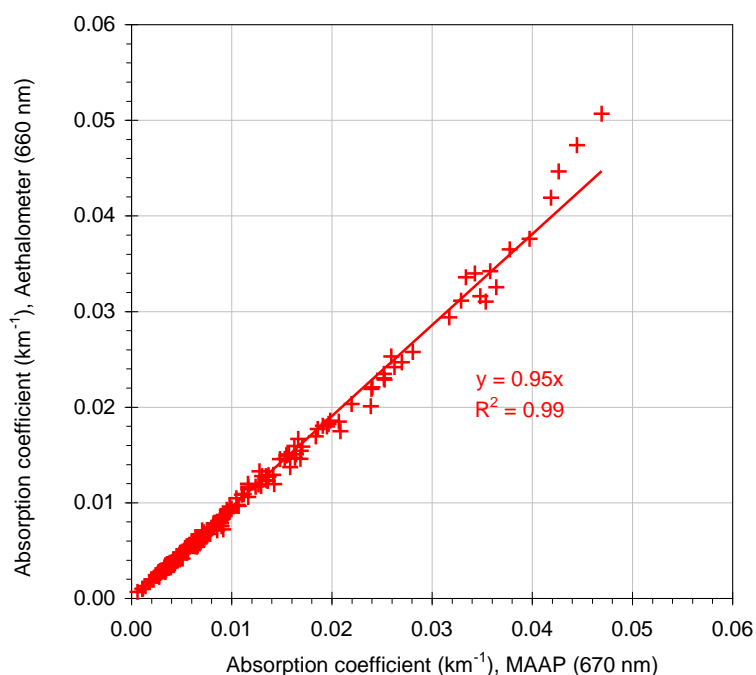

Fig. 35. *Comparison of Aethalometer and MAAP derived absorption coefficients at 660 and 670 nm, respectively. Data points are daily averages (2013).*
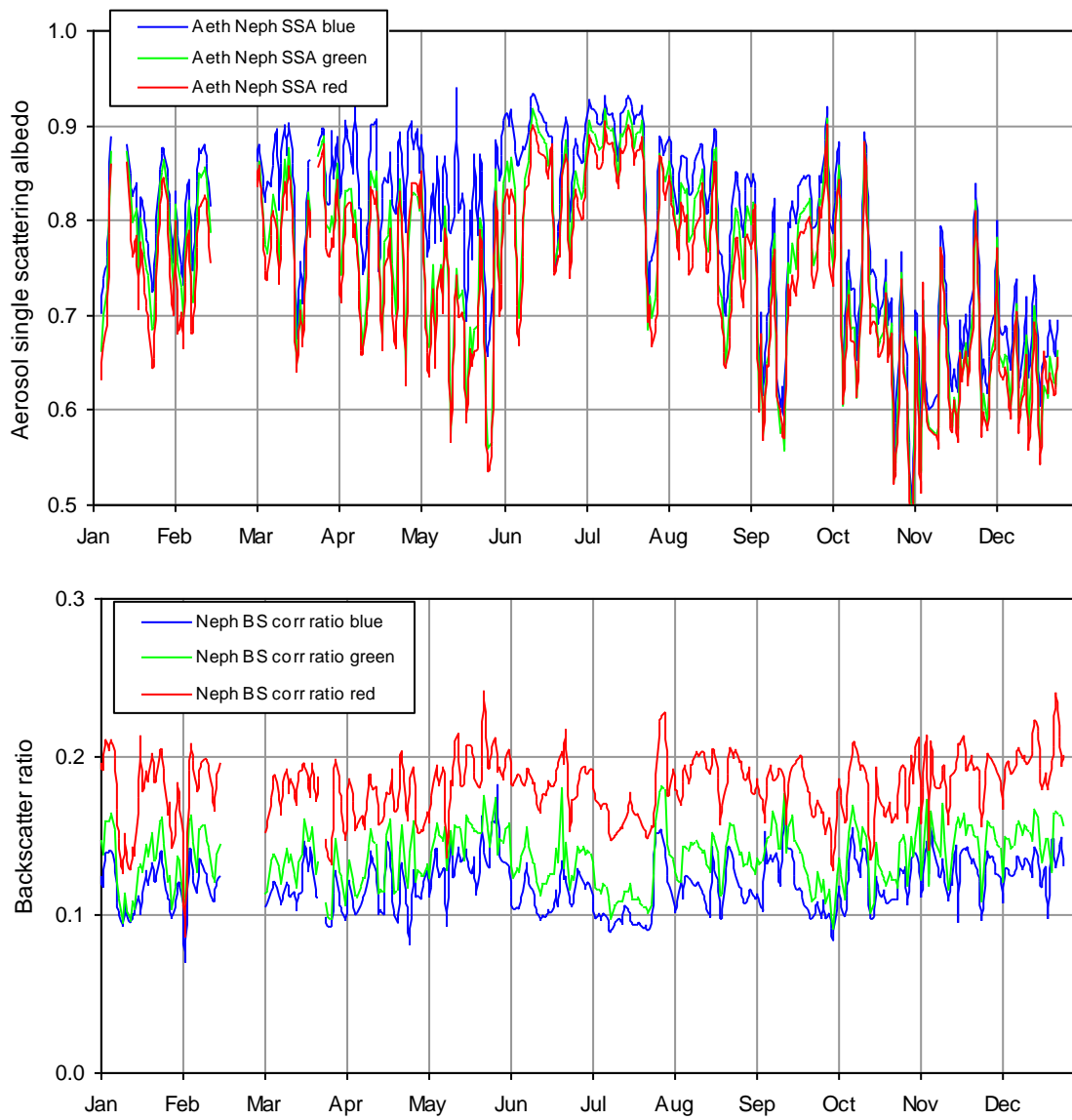
Fig. 36. Aerosol 24-hr average single scattering albedo and backscatter to total scatter ratio at three wavelengths corresponding to blue, green and red calculated for 2013 (RH generally < 40%).

The 24 hr averaged aerosol single scattering albedo (SSA) at λ = 550 nm (at RH generally < 40 %) ranged from 0.45 to 0.92 (annual average 0.76), with generally higher values in summer compared to winter (Fig. 36a). In 2013, the lowest aerosol single scattering albedo values were affected by the proximity of the provisional measurement site from the internal and external roads of the JRC. As a consequence, the mean SSA was lower than in 2012 (0.79), but still comparable to 2010 (0.75) and 2011 (0.77). The absorption coefficient values clearly affected by local influences were flagged before submission to the WDCA data bank (EBAS). The backscatter / total scatter ratio at 550 nm (Fig. 36b) ranged from 0.09 to 0.18 (average 0.14), with no significant change compared to previous years.

The aerosol extinction coefficient and particle mass or volume concentrations are rather well correlated (Fig. 37). The slope of the regression between extinction and mass shows that the extinction mass efficiency is on average 3.4 m^2 g^{-1} (like in 2012), i.e. low compared with 4.5 m^2 g^{-1}, the value calculated based on the aerosol mean chemical composition during 2013, and mass cross section coefficients for the various constituents found in the literature (see Table 7). The agreement between these two estimates of the aerosol extinction cross section deteriorated compared to 2010 - 2012.
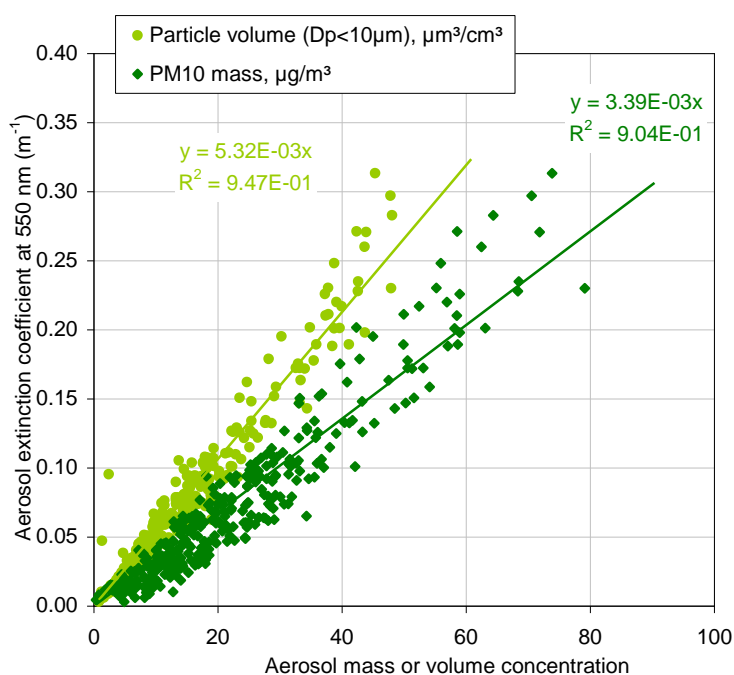

Fig. 37. *Regression between the aerosol extinction coefficient and PM10 mass (FDMS-TEOM) and volume (DMPS + APS) concentrations in 2013.*

Table 7. *Mean aerosol chemical composition (PM2.5) in 2013 and extinction efficiency.*

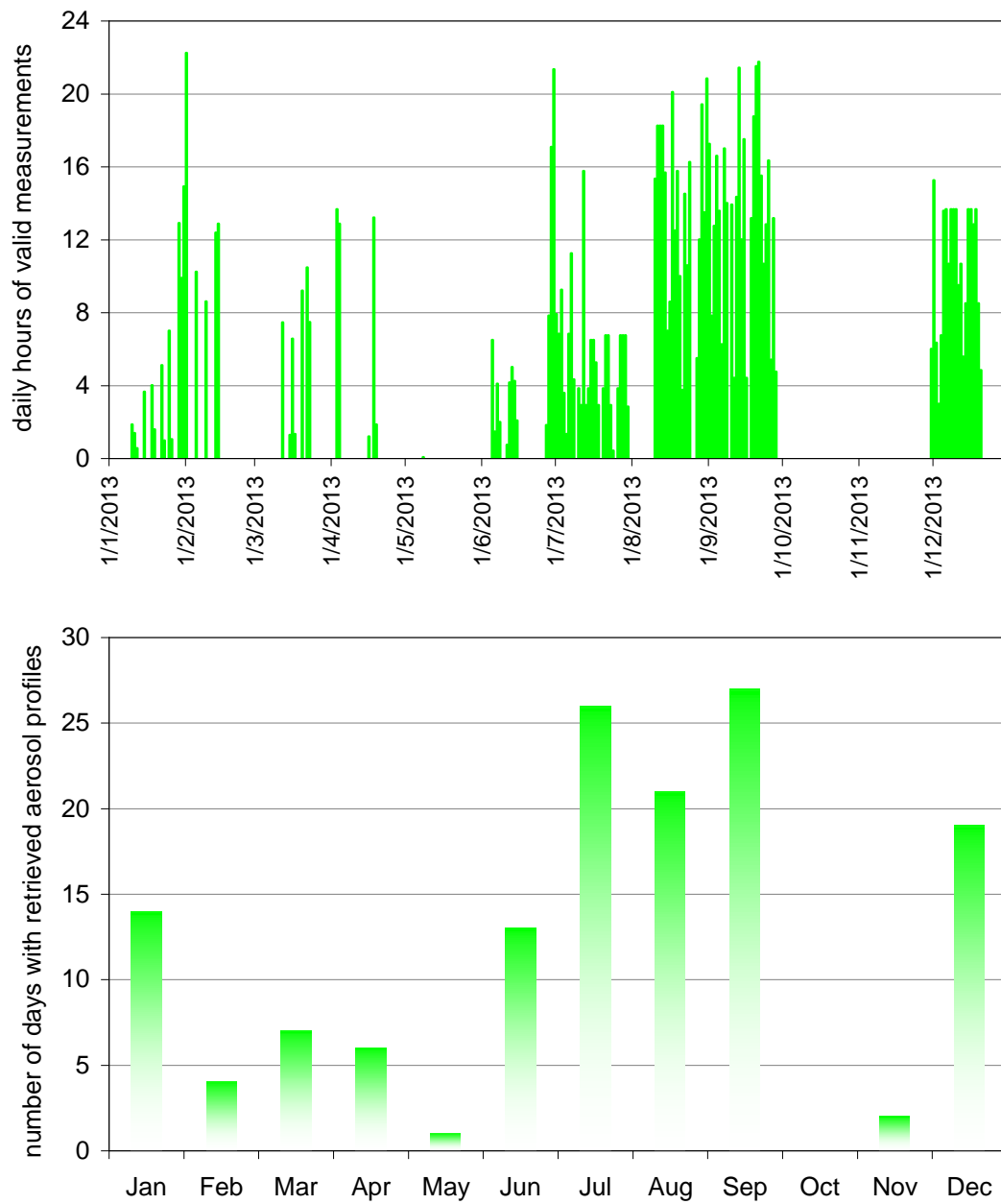|	2013 PM2.5 comp. (%)	σ_{ext} (m²/g)	Reference (for σ_{ext})
"sea salt"	3	1.3	Hess et al., 1998
NH_4^+, NO_3^- and SO_4^{2-}	38	5.0	Kiehl et al., 2000
organic matter	49	3.6	Cooke et al., 1999
elemental carbon	7	11	Cooke et al., 1999
Dust	3	0.6	Hess et al., 1998
Total	**100**	**4.5**	

61

Fig. 38. *Aerosol vertical profile measurements performed with the Raymetrics Raman lidar in 2013 on daily (top) and monthly (bottom) bases.*

<u>Aerosol *vertical* profiles</u>

The backscatter LIDAR (CAML) from CIMEL was operated almost continuously, weather permitting (no rainfall/snow, storm etc.) until May 2013. From May 28th, the signal became very low, although the laser power was OK (53 mW on June 3rd, 2013, 2012, compared to 52 mW on Sep. 25th, 2012) but coupling into the fiber insufficient (36%). The acousto-optic modulator was substituted in July, but this did not have any noticeable effect on the signal received. Due to the difficulties to get accurate data with this instrument (mainly due to the variability of the overlap function), no further effort to fix it was attempted. The data acquired for this year were inverted but did not lead to satisfactory results. Results derived from CAML measurements performed in Ispra the past can be found in Barnaba et al., 2010.

The Raman Lidar from Raymetrics (ADAM) started to be operated for measuring aerosol vertical profiles from January 10th, 2013.

Fig. 39 shows an example of range corrected backscatter signal at 532 nm (no data inversion applied) recorded on July 11th, 2013, from 05:45 to 15:05 00:00 (cloud free day). The "low value" area at the bottom of the chart is due to the overlap function dropping to 0 at the ground. Pollution particles are observed up to 2km in the morning, and up to 3 km in the afternoon. Above the pollution aerosol in the mixed boundary layer, various layers of particles can be observed, which were identified as smoke particles coming from forest fires in Canada.
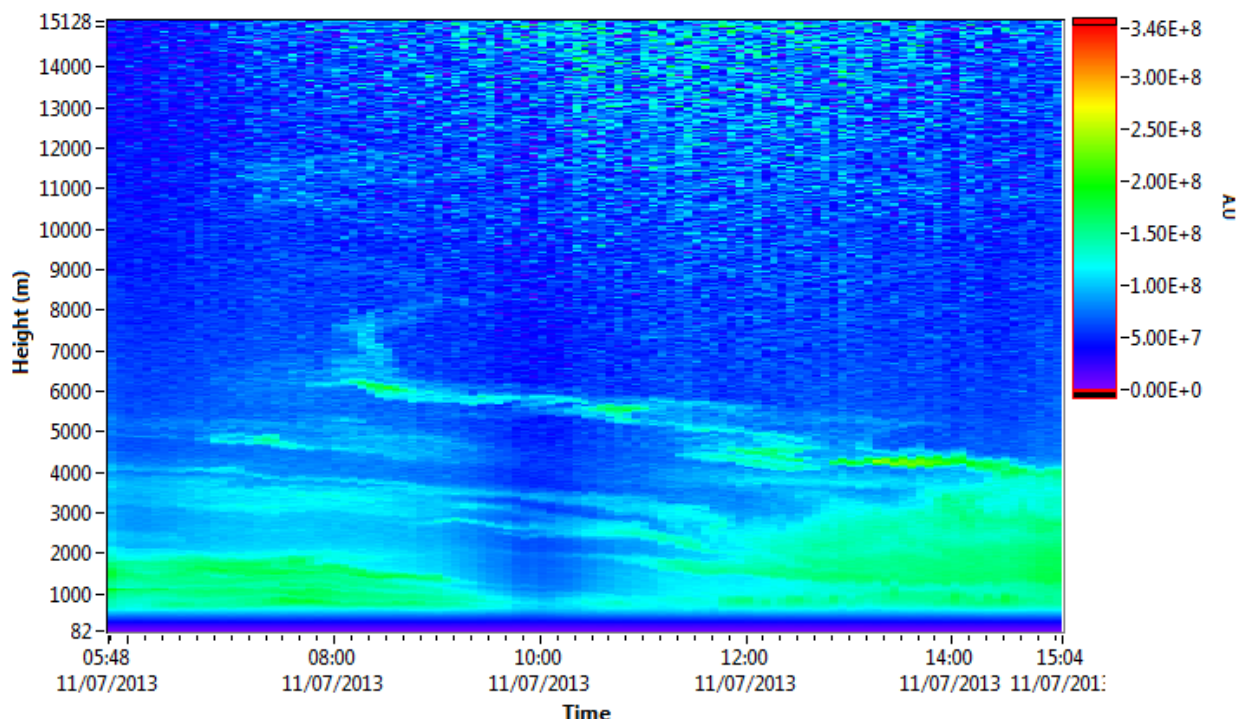

Fig 39: *Lidar signal obtained at ABC-IS on July 11th, 2013, illustrating the detection of long range transported smoke from Canada.*
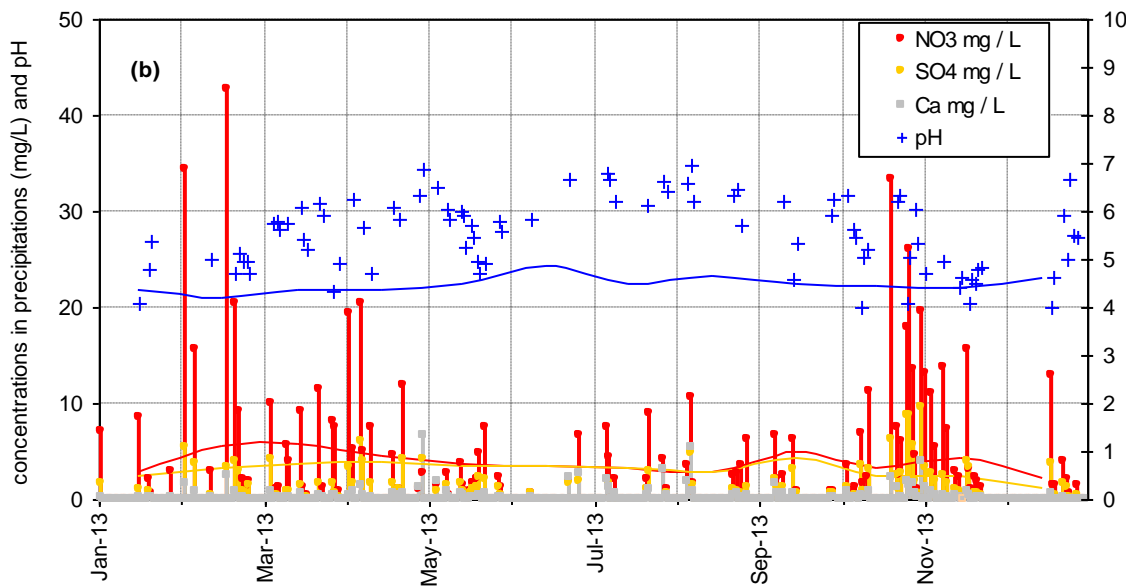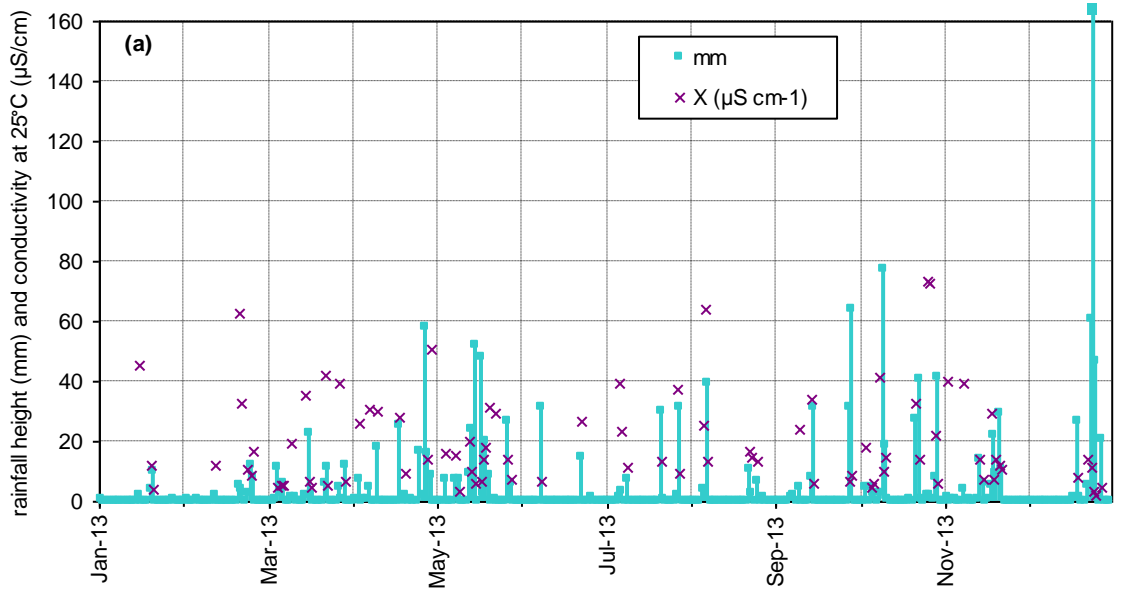
Fig. 40. *(a) Precipitation amount, conductivity and (b) concentrations of 3 major ions in precipitation (bars) and pH (crosses) in 2013, and during the 1990-99 period (lines)*
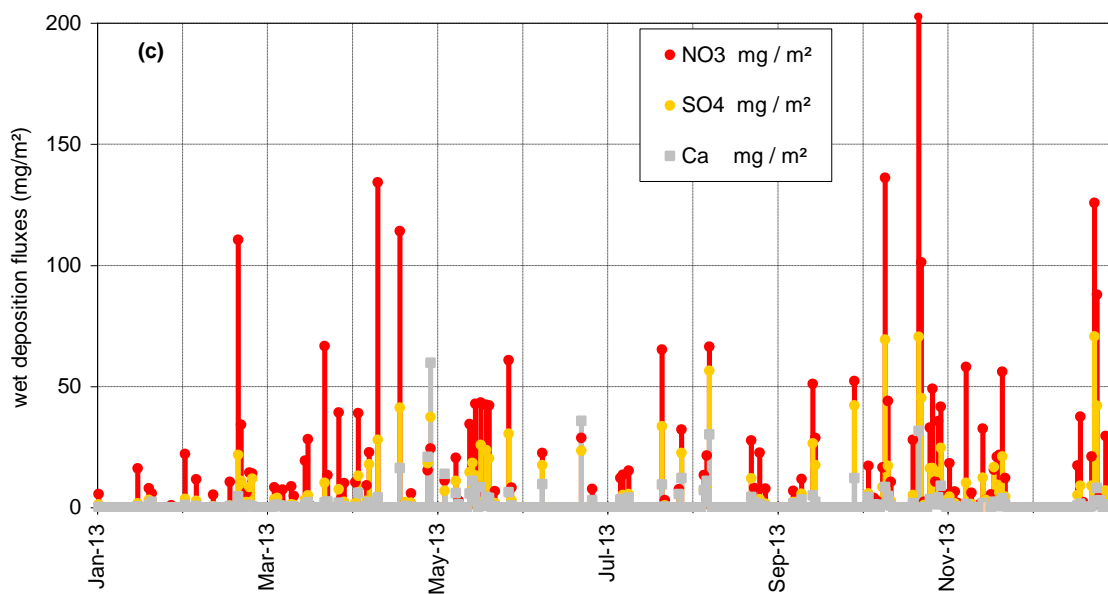

Fig. 40c. *Wet deposition fluxes of 3 main components in rain water in* 2013.

Precipitation chemistry

In 2013, 116 precipitation samples were collected and their ion content determined. Acidity (pH) and conductivity were also measured in 87 of those samples (insufficient water volume was available for the remaining samples). The precipitation height of the collected events ranged from 0.2 to 162 mm (Fig. 40a) for a total of 1514 mm *vs.* 1724 mm detected by the rain sensor at the ABC-IS forest flux tower. Three major rain events (> 2mm) in April were not sampled.

The ranges of concentrations measured in these samples are indicated in Table 8. Volume weighted mean concentrations of all species but Na^+ were in 2013 smaller than the 1990-1999 averages. All precipitation samples collected in 2013 were acidic (pH < 7.0). However, pH<5.6 (equilibrium with atmospheric CO_2) was measured in 43 samples (compared to 28 in 2012 and 17 in 2011) and pH < 4.6 in 9 samples only.

Wet deposition occurred mainly in March-April and October - November (Fig. 40c). The annual wet deposition flux of the main acidifying and eutrophying species was 1.3, 3.1, and 1.3 g m^{-2} for SO_4^{2-}, NO_3^-, and NH_4^+, respectively. These fluxes were slightly larger than in 2012 (1.2, 2.9, 1.3 g m^{-2}, respectively), and significantly larger than in 2011 (0.9, 1.9, 0.8 g m^{-2}, respectively).

Table 8. *Statistics relative to the precipitation samples collected in 2013 (averages are volume weighted)*

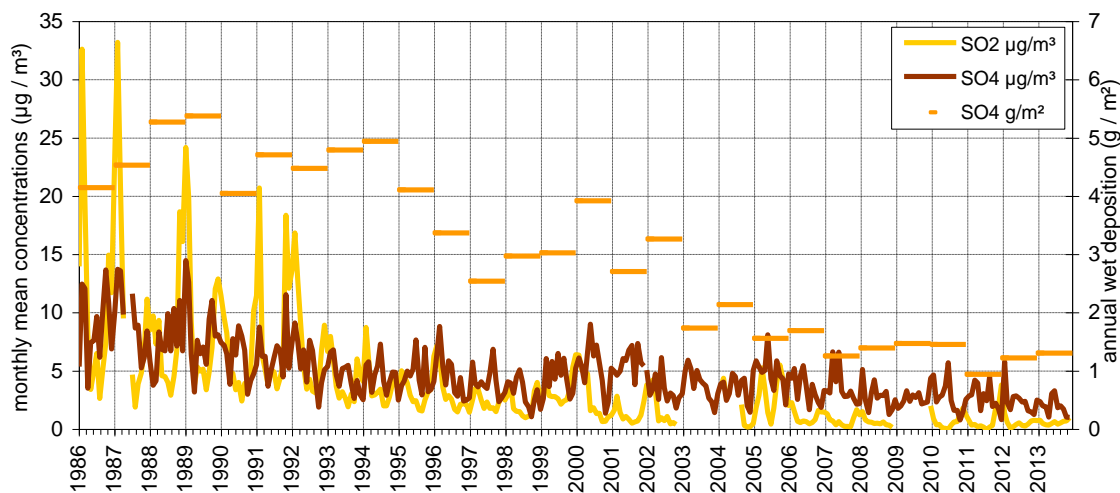|	pH	cond.	Cl^-	NO_3^-	SO_4^{2-}	Na^+	NH_4^+	K^+	Mg^{2+}	Ca^{2+}
		$\mu S\ cm^{-1}$	mg l^{-1}	mg l^{-1}	mg l^{-1}	mg l^{-1}	mg l^{-1}	mg l^{-1}	mg l^{-1}	mg l^{-1}
Average	5.16	12.6	0.26	2.4	0.93	0.23	0.95	0.04	0.05	0.40
Min	3.98	1.8	0.02	0.1	0.04	0.01	0.04	<0.01	0.01	0.04
Max	6.94	73	8.5	43	9.5	6.1	8.2	0.6	0.67	6.7
1990-1999 average	4.40	25	0.44	3.9	3.1	0.23	1.3	0.09	0.06	0.45

Fig. 41. Oxidized sulfur species monthly mean concentrations and yearly wet deposition.
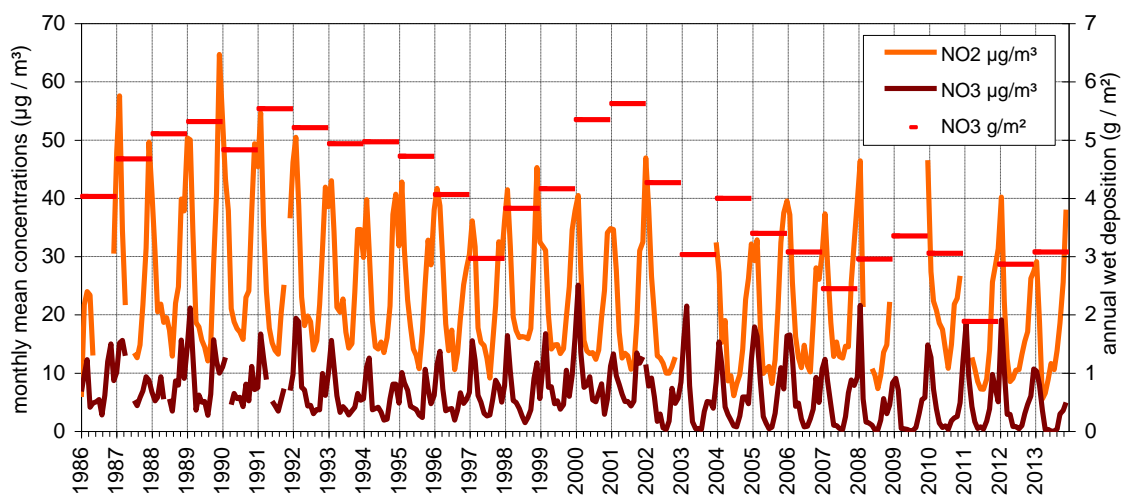

Fig. 42. Oxidized nitrogen species monthly mean concentrations and yearly wet deposition.
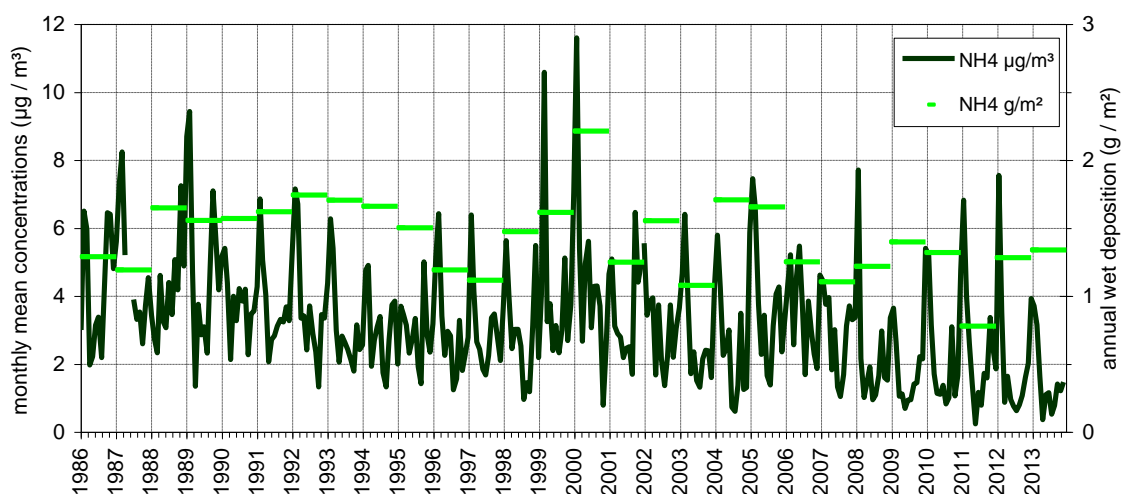

Fig. 43. Reduced nitrogen species monthly mean concentration and yearly wet deposition.

Results of year 2013 in relation to > 25 years of monitoring activities

Sulfur and nitrogen compounds

2013 annual averages for particulate SO_4^{2-}, NO_3^-, and NH_4^+ in PM_{10} (estimated from $PM_{2.5}$ data) were 25, 19 and 21% less than averages calculated over the past 5 years (2.7, 4.6 and 2.2 µg/m³, respectively).

Annual mean particulate concentration SO_4^{2-} reached a new historical minimum in 2013, after a 3-fold decrease from 1986 to 1998, followed by a stagnation around the mean 90's value (see Fig. 41). In contrast, both winter maxima and summer minima monthly mean concentrations of sulfur dioxide (SO_2) decreased by a factor of more than 10 over the past 20-25 years (Fig. 41) but remained roughly constant during the past 3 years. These data show that locally produced SO_2 decreased much more than possibly long-range transported SO_4^{2-} over the past 20-25 years, but no more for the past 3 years. It should be kept in mind that SO_4^{2-} concentrations were measured in PM_{10} or in $PM_{2.5}$ from 2002 onwards, whereas it was measured in TSP (Total Suspended Particulate) from 1986 to 2001. However, simultaneous sampling of PM10 and TSP over 14 months showed that SO_4^{2-} in PM_{10} is generally less than 5 % lower than in TSP. It should also be mentioned that SO_4^{2-} is mainly present in the $PM_{2.5}$ fraction (see Fig. 24 of the ABC-IS annual report 2010). From 2005 onwards the calculations were as follows:

$$SO_4^{2-}(PM_{10}) = SO_4^{2-}(PM_{2.5}) \times <SO_4^{2-}(PM_{10})/ SO_4^{2-}(PM_{2.5})>$$

the average $<SO_4^{2-}(PM10)/ SO_4^{2-}(PM2.5)>$ being calculated based on the 4-6 simultaneous PM_{10} and $PM_{2.5}$ samples collected each month). SO_4^{2-} wet deposition in 2013 was the fourth lowest value (after 2011, 2012 and 2007) recorded at the station.

Monthly mean concentrations of nitrogen dioxide (NO_2) do not show such a pronounced decreasing trend as seen for SO_2 over the past 27 years (Fig. 42). Wintertime NO_2 maxima indeed have remained quite constant since 1992, which does not reflect the 30 % abatement in NO_x emissions expected from emission inventories. Particulate NO_3^- wintertime concentrations observed in 2003 - 2013 are comparable to values observed earlier too. It should be reminded that since October 2000, NH_4^+ and NO_3^- have been measured mostly from quartz fibre filters, which are known to lose NH_4NO_3 at temperatures > 20 °C, as demonstrated e.g. by the comparison with the ACSM measurements we performed in Ispra in 2013. This might contribute significantly to the fact that NO_3^- summertime minima are particularly low since 2002. Furthermore, NO_3^- was measured from PM_{10} or in PM 2.5 from 2002, and no more from TSP, as over the 1986 to 2001 period. However, simultaneous sampling of PM10 and TSP over 14 months showed that NO_3^- in PM10 is generally less than 5 % lower than in TSP, like SO_4^{2-}. From 2005 and onwards the calculations were as follows

$$NO_3^-(PM_{10}) = NO_3^-(PM_{2.5}) \times < NO_3^-(PM_{10})/ NO_3^- (PM_{2.5})>$$
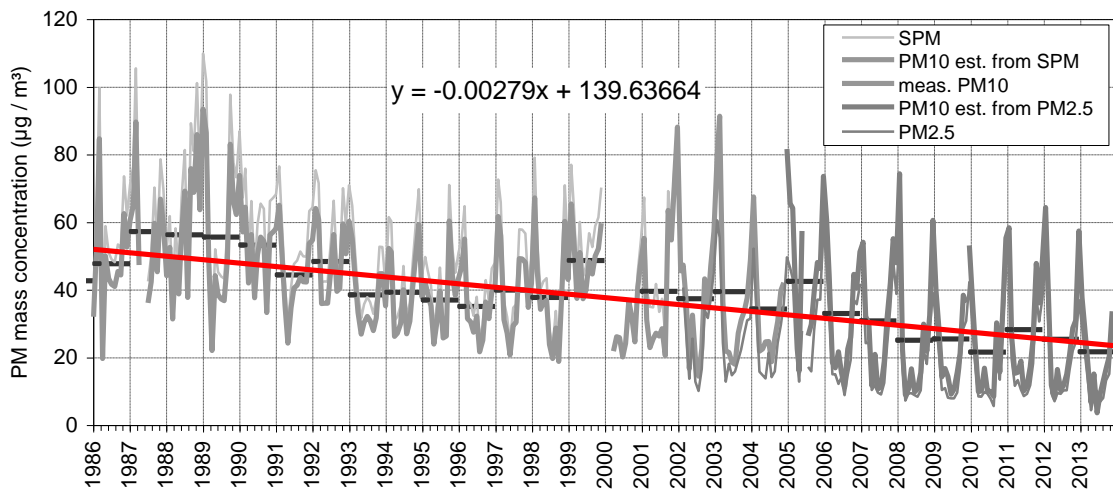
Fig. 44. Particulate matter mass concentration monthly (grey) and annual (black) averages. The red line is the long term trend over annual averages. All values in the figure are from gravimetric measurements or estimated from gravimetric measurements.
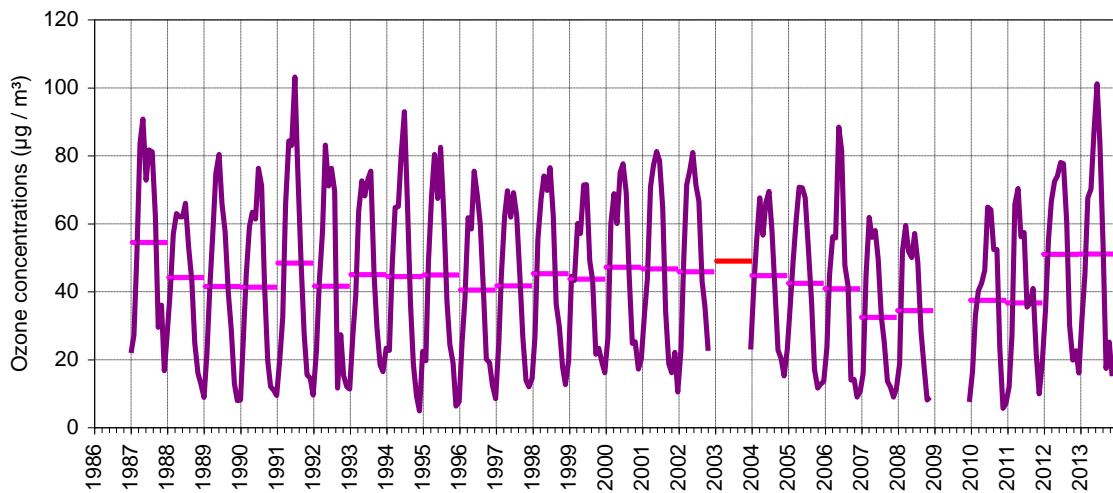
Fig. 45. Ozone yearly and monthly mean concentrations at JRC-Ispra.

Fig. 46. AOT40, SOMO35 values, and number of days on which O_3 limit values were reached. The 3 red spots are data points from Malpensa.

the average < $NO_3^-(PM_{10})$/ $NO_3^-(PM_{2.5})$> being calculated based on the 4-6 simultaneous PM_{10} and $PM_{2.5}$ samples collected each month. NO_3^- wet deposition annual flux observed in 2013 was among the 10 lowest ever recorded since 1986 in Ispra, but very close to the average over la last decade.
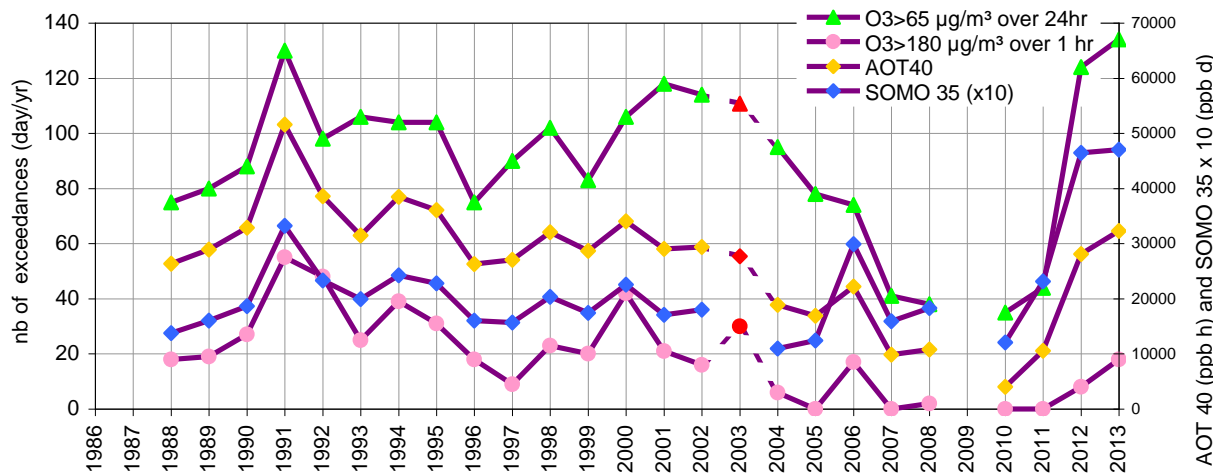
Monthly mean concentrations of NH_4^+ in the particulate phase seem to have decreased slightly since 1986 (Fig. 43), especially because summertime minima decreased. Because winter-time maxima increased much since 2009, there is no significant long-term trend regarding NH_4^+.

It should be reminded that from the year 2002, NH_4^+ was measured in the PM_{10} or in the $PM_{2.5}$ fraction. From 2005 and onwards, NH_4^+ concentrations in PM_{10} were calculated as follows:

$NH_4^+(PM_{10}) = NH_4^+(PM_{2.5})$ x <$NH_4^+(PM_{10})$/ $NH_4^+(PM_{2.5})$>

where the average <$NH_4^+(PM_{10})$/ $NH_4^+(PM_{2.5})$> is calculated based on the 4-6 simultaneous PM_{10} and $PM_{2.5}$ samples collected each month). On average, NH_4^+ can neutralize close to 100% of the acidity associated with NO_3^- and SO_4^{2-} in the particulate phase (see Fig. 21). NH_4^+ is also quite well correlated with $NO_3^- + SO_4^{2-}$ in rainwater. NH_4^+ annual wet deposition in 2013 was very close to the average recorded in Ispra over the last decade.

Particulate matter mass

PM mass concentrations observed in 2013 confirm the general decreasing trend in wintertime maxima observed over the last decade (Fig. 44), while summer time minima remain more or less constant. The 2013 annual average PM_{10} concentration (estimated from $PM_{2.5}$ measurements) reached 21.8 µg/m³, i.e. less than in 2011 and 2012, and very close to the historic minimum of 21.6 µg/m³ observed in 2010. A linear fit indicates that PM_{10} has been decreasing by 1.0 µg m^{-3} yr^{-1} between 1986 and 2013. It should however be kept in mind that PM_{10} concentrations were estimated from TSP mass concentration measurements (carried out by weighing at 60 % RH and 20 °C cellulose acetate filters sampled without any particle size cut-off and "dried" at 60 °C before and after sampling) over 1986-2000, based on a comparison between TSP and PM_{10} over the Oct. 2000 - Dec. 2001 period (R^2 = 0.93, slope = 0.85), and based on measured $PM_{2.5}$ values for years 2005-2013.

Ozone

Figure 45 shows monthly and yearly mean O_3 concentrations observed since 1987. Ozone was not measured in 2009 and there was a major data acquisition breakdown in 2003. The decreasing trends in wintertime minimums and summertime maximums observed over 2001 - 2009 (2006 mini-heat wave peak excluded) are no more observed from 2010. On the contrary wintertime, summertime, and annual averages are all increasing again, getting back to values observed 2 decades ago.

As a consequence, all ozone indicators (Figure 46) have much deteriorated. The frequency of extreme O_3 concentrations (days on which the limit of 180 µg/m³ over 1hr was exceeded) is back to the values of 10- 15 years ago. Both indicators for the vegetation

protection increased back to the highest values observed in the 1990's: the number of days with a 24-hour mean O_3 concentration > 65 µg/m³ (vegetation protection limit) reached a historical record (134), and AOT40 (Accumulated Ozone exposure over a Threshold of 40 ppb), the vegetation exposure to above the O_3 threshold of 40 ppb (about 80 µg/m³), got back to values observed in the 90's. The population exposure indicator SOMO 35 (Sum of Ozone Means Over 35 ppb, where means stands for maximum 8-hour mean over day) also reached a historical highest record, not significantly higher than in 2012, but well above (x 3) the mean value observed over the last decade.

Conclusions

In 2013, solar radiation and temperature were generally within the standard deviation of the average over 1990-1999, except for June and July, which were significantly sunnier and warmer than usual. In contrast, 2013 was more watered than average, especially in April, May, and above all December, which is usually quite dry.

Dry and warm weather conditions may at least partly explain that various indicators for O_3 pollution were very bad in 2013 compared to the past decade. In contrast, the annual mean concentrations of SO_2, NOx and CO were not especially high compared to the recent years. Indeed SO_2 annual average reached the lowest record ever observed at the EMEP-GAW station of Ispra.

Aerosol sampling on quartz fibre filter, and subsequent gravimetric and chemical analyses were limited to the $PM_{2.5}$ fraction (daily) in 2013, using a Partisol samplers equipped with a carbon monolith denuder. With the assumption used to estimate POM and dust from organic carbon (OC) and Ca^{2+}, respectively, $PM_{2.5}$ mass concentration was generally over-explained (107%) in 2013. $PM_{2.5}$ average chemical composition was dominated by carbonaceous species (POM: 50%, EC: 8%), followed by secondary inorganics (NH_4^+:9%, NO_3^-: 14%, SO_4^{2-}: 15%). The contribution of sea-salt ions and mineral dust were about 3 % each. However, there is a clear increase of NO_3^- contribution to $PM_{2.5}$ when shifting from cleaner ($PM_{2.5}$ < 10 µg/m³) to more polluted periods ($PM_{2.5}$ > 25 µg/m³). Both $PM_{2.5}$ and PM_{10} annual mean concentrations (16 and 24 µg/m³respectively) were below the EU annual limit value (25 and 40 µg/m³, respectively), but 38 exceedances (derived from FDMS-TEOM measurements) of the 24-hr limit value (50 µg/m³) were observed. The long term time series still suggests a PM_{10} mass concentration decreasing trend of 1.0 µg m^{-3} yr^{-1} over the last 28 years of records. It should be noticed that the annual mean PM_{10} level in 2013 was the 2nd lowest values recorded since 1986, after 2010 (see Figure 44).

The average particle number in 2013 (average:8220 cm^{-3}, range 2100 – 25200 cm^{-3}) was larger than to the 2010, 2011 ($\sim$ 6900 cm^{-3}) and 2013 (7540 cm^{-3}) values. This might at least partially derive from the frequent local contaminations due to the vicinity of the provisional measurement site to internal and external roads. Particle number size distributions were as usual generally broadly bimodal, with a submicron mode at ca. 100 nm (dry) and a less pronounced coarse mode around 2 µm. Atmospheric aerosol scattering and

absorption coefficients at various wavelengths were derived from Nephelometer and Aethalometer measurements in dried atmosphere (generally lower than 40%). The mean single scattering albedo at λ = 550 nm (not corrected for hygroscopic growth) was 0.76 in 2013 (vs 0.77 in 2011 and 0.79 in 2012). Here the impact of local traffic can also be part of the explanation.

The aerosol extensive variables measured at JRC-Ispra (at ground level) all follow comparable seasonal variations with minima in summer. These variables are generally well correlated and lead to reasonable degrees of chemical, physical, and optical closures. However, the average sub-2.5 µm aerosol density of 1.20 g/cm^3 derived from the gravimetric mass and DMPS + APS volume was too low compared to 2010 - 2012 (1.32 – 1.38 g/cm^3), while the ratio between PM_{10} mass concentration measured with the FDMS-TEOM and the aerosol volume DMPS + APS volume leads to a density of 1.50 g/cm^3. This might indicate that $PM_{2.5}$ gravimetric measurements were underestimated in 2013. However, the extinction-to-mass ratio of 3.4 m^2 g^{-1} (close to the 2012 value but lower than the value of 3.9 m^2 g^{-1} observed in 2011), is also low compared to the value that can be calculated from the mean PM2.5 chemical composition, which averages to 4.5 m^2 g^{-1} in 2013 (see Table 7), which could suggest that the aerosol volume and PM_{10} concentrations were overestimated.

Aerosol backscatter profiles were obtained with the Raymetrics Raman LIDAR across the whole seasons during 2013. Due mainly to unsuitable meteorological conditions, 138 out of the 188 profiles scheduled by EARLINET could be measured. Aerosol backscatter profiles were retrieved for 61 of these measurements and submitted to the EARLINET data base using the Single Calculus Chain.

The concentrations of all rainwater components (Cl$^-$, NO$_3^-$, SO$_4^{2-}$, NH$_4^+$, K$^+$, Mg^{2+}, and Ca^{2+}), but Na$^+$ were lower in 2013 compared to the 1990-1999 average. The annual wet deposition flux of the main acidifying and eutrophying species (1.3, 3.1, and 1.3 g m^{-2} for SO$_4^{2-}$, NO$_3^-$, and NH$_4^+$, respectively) were larger than the 2011 and 2012 values, and close to the values observed at the EMEP-GAW station in Ispra over the last decade. Rain pH<4.6 (10 times more acidic than due to the equilibrium with atmospheric CO$_2$) was measured in 9 samples (compared to 3 in 2012), partly resulting from our collecting more minor rain events this year.

2013' data listed by EMEP and ACTRIS as core variables have been all reported to EBAS in 2014, as requested by these programs.

Fig. 48: The 36 high self-standing tower at the ABC-IS Forest Flux Station

Atmosphere – Biosphere flux monitoring at the forest flux station in Ispra

Location and site description

The ABC-IS Forest Flux Station is part of the large ABC-IS infrastructure focussing on the measurement and monitoring of exchange processes of a forest ecosystem with the atmosphere, predominantly relying on the use of the eddy covariance technique for flux measurements. The measurement site (45°48'45.68"N, 8°38'2.09"E) is placed inside a small forest of approximately 10 ha that is part of the JRC Ispra premises. Situated in an almost flat area, this forest is unmanaged since the foundation of the JRC Ispra in the late 1950's and therefore now characterized as a mixed, almost natural forest ecosystem. The tree species composition consists of ~80% Quercus robus, ~10% Alnus glutinosa, ~5% Popolus alba and ~3% Carpinus betulus, the predominant soil type is Regosol.

The ABC-IS Forest Flux Station comprises a 36 m high self-standing tower (Fig. 48) as a platform to hold instruments, an air-conditioned container for instrumentation and IT infrastructure plus the surrounding forest where above and below ground sensors are installed. A detailed project documentation can be found in Gruening et al. (2011). A report of the performance of the instruments at the site also in comparison with measurements from the EMEP station is given in Gruening et al. (2012).

Since 2013, the ABC-IS Forest Flux Station takes part in the European Fluxes Cluster and the measurement data have been submitted under the station name IT-Isp to the Fluxnet database at http://www.europe-fluxdata.eu.

Tab. 10: ICOS level 2 Ecosystem Station core parameters.

Core variables continuous	Core variables daily to monthly	Core variables yearly
CO_2, H_2O and energy fluxes	leaf area index	biomass (above ground)
wind speed and direction		soil carbon
CO_2 concentration vertical profile, normal precision		stem diameter
net radiation: • incoming/reflected global radiation • incoming/outgoing longwave radiation • Albedo		above-ground Net Primary Production (NPP)
diffuse global radiation		litter fall
incoming / reflected under canopy Photosynthetic Active Radiation (PAR)		land-use history
temperature and relative humidity vertical profile		managements and natural disturbances
air pressure		C and N import and export on managed sites
precipitation, through-fall, snow depth		
soil heat flux		
ground water level		
soil temperature profile		
water content profile		

Core variables continuous	Core variables daily to monthly	Core variables yearly

Measurement program

The ABC-IS Forest Flux Station has been originally projected as a platform to perform long-term monitoring activities with the additional possibility to engage in short-term research projects, mainly in the frame of international collaborations. The scientific activities are embedded at the moment into two major European programs: the ICOS initiative and the FP7 project ECLAIRE.

ICOS

ICOS (Integrated Carbon Observation System, www.icos-infrastructure.eu) is one of the pan-European research infrastructure projects identified by the European Strategy Forum on Research Infrastructures (ESFRI) for implementation. After its preparatory phase planned for 2008 until 2013, during which monitoring infrastructure and technical procedures were developed, its operational phase will run for 20 years from 2014 / 2015 onwards.

Once in operational mode, greenhouse gas concentrations and fluxes will be monitored on a routine basis following a very strict quality controlled protocol, both in terms of measurement instrumentations required to be used and procedures to be followed. The JRC plans to contribute with a class 2 Atmospheric Station (AS) for the high precision monitoring of greenhouse gas concentrations and two level 2 Ecosystem Stations (ES), the ABC-IS forest flux tower and the second installation in the Parco San Rossore near Pisa, for the monitoring of ecosystem fluxes. Level 2 stations provide data for less parameters compared to level 1 stations and thus require less investment for instrumentation and have lower running costs in terms of instruments and staff. The mandatory variables to be monitored at the level 2 Ecosystem Station ABC-IS forest flux tower are shown in Tab. 1.

ÉCLAIRE

ÉCLAIRE (Effects of Climate Change on Air Pollution and Response Strategies for European Ecosystems, www.eclaire.ceh.ac.uk) is a four year (Oct 2011 - 2015) large scale integrating project funded by the EU's Seventh Framework Programme for Research and Technological Development (FP7) involving 39 partner institutions across Europe. It investigates the ways in which climate change alters the threat of air pollution on European land ecosystems including soils. Based on field observations, experimental data and models, it establishes new flux, concentration and dose-response relationships, as a basis to inform future European policies.

The ABC-IS flux tower was one of three forest ecosystem sites with a continuous measurement program from summer 2012 until the end of 2013, and several intensive periods in 2013 requiring more sophisticated instrumentation. In addition to the ICOS core parameters (see Tab. 1) the following measurements were performed continuously in 2013:

- atmospheric O_3 fluxes using eddy covariance technique
- soil NO / NO_2 fluxes with an automated dynamic chamber system

Measurements in 2013

Fluxes of CO_2, H_2O, sensible heat and ozone were measured with eddy covariance techniques using EddyMeas (Olaf Kolle, www.bgc-jena.mpg.de) for data acquisition and evaluated with the EdiRe software package from the University of Edinburgh (www.geos.ed.ac.uk/abs/research/micromet). For soil NO / NO_2 fluxes, an automated dynamic chamber system was developed and deployed in the forest. The ancillary parameters (meteorology, radiation and soil) were obtained with respective sensors and the data quality checked for instrument malfunctioning, obvious outliers and consistency. In the following chapters, first the instruments used are described and then daily averages of the different parameters measured during the course of 2013 are presented.

Table 10: Variables measured during 2013

FLUXES	CO_2, latent heat, sensible heat, ozone
METEOROLOGY	3D wind speed, temperature, relative humidity, pressure, precipitation
RADIATION	short & long wave incoming & outgoing, direct, diffuse & reflected above canopy photosynthetic active radiation (PAR) incoming and ground reflected PAR below canopy
SOIL	temperature profile, water content profile, heat flux, water table height, respiration, NO / NO_2 fluxes
BIOLOGICAL	litter fall

Description of Instruments:

Infrastructural:

Sensor location

The instruments for the eddy covariance flux system, i.e. sonic anemometer and fast gas analysers, radiation and meteorological sensors plus gas inlets are mounted on the 36 m high self-standing tower. Soil parameters including NO / NO_2 fluxes are measured on the forest ground approximately 35 m north-east of the tower.

Data acquisition

Eddy covariance flux data are acquired and stored with high frequency, i.e. 10 Hz, as chunks of 30 minutes on a local laptop connected to the sonic anemometer. Data from most other sensors are read every 10 s by a respective CR3000 data logger from Campbell Scientific (www.campbellsci.co.uk) which saves 30 minute averages of the acquired data.

For eddy covariance flux data, the start time of every 30 minutes measurement period is saved as the reference time, whereas for all other data, the end of the 30 minutes measuring period is used. The time reference for all measurements is UTC.

Sonic Anemometer for 3D wind direction Gill HS-50

Sonic anemometers determine the three dimensional wind vectors at high frequency using the speed of sound. The Gill HS-50 (www.gill.co.uk) emits ultrasonic pulses between its pairs of transducers, measures the flight time of the pulses to the paired transducer and calculates the wind speed in the direction of the transducer pair (see Fig. 49). Combining the results from the three transducer pairs, the 3 dimensional wind speed is calculated at a frequency of 10 Hz. After a rotation of the coordinate system during the data processing to align it with the north direction, horizontal and vertical wind speeds and the wind direction are calculated besides their use for flux calculations. As the speed of sound measured with the anemometer depends on the temperature, the so-called sonic temperature is reported by the instrument as well.

Due to the absence of moving parts and the fact that no calibration is required, the instrument is very robust and reliable. Instrument servicing is done at the manufacturer's.
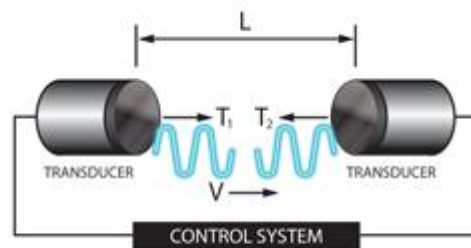
$$T_2 = \frac{L}{C-V} \quad \text{and} \quad T_1 = \frac{L}{C+V}$$

therefore

$$V = \frac{L}{2}\left\{\frac{1}{T_1} - \frac{1}{T_2}\right\} \quad C = \frac{L}{2}\left\{\frac{1}{T_1} + \frac{1}{T_2}\right\}$$

Fig. 49: Measurement principle of sonic anemometers, T: travelling time of sound pulses, L: distance between transducers, C: speed of sound, V: wind speed in direction of transducers (sketch from www.gill.co.uk)

Fast infrared gas analyser (IRGA) for CO_2 & H_2O concentration LI-7200 FM from Licor

For the determination of CO_2 and H_2O fluxes with the eddy covariance technique, fast analysers (10 to 20 Hz) for concentration measurements of the gases of interest are obligatory. At the ABC-IS forest flux tower in Ispra, a LI-7200 FM system from LI-COR (www.licor.com) has been installed, consisting of the LI-7200 enclosed CO_2/ H_2O analyser, the LI-7550 analyser interface unit and the LI-7200-101 flow module.

The LI-7200 is a high performance, non-dispersive, enclosed open path infrared CO_2/H_2O analyser based on the infrared absorption of CO_2 and H_2O at ambient conditions that provides concentration measurements at a frequency of up to 20 Hz. With the flow module, ambient air is drawn into to analyser through the sample inlet at a set flow rate of 15 l/min. In the sample volume of 16.09 cm^3 (see Fig. 50), light from the infrared source is absorbed at characteristic wavelengths for CO_2 and H_2O. This specific absorption is a function of the gas concentration in the sample volume. Using the absorption measurements at the CO_2 & H_2O wavelengths, at a non-absorbing wavelength plus calibration factors and measured temperature and pressure, the LI-7200 provides molar densities, mass densities or mole fraction of the two gases.

Zero and span checks and calibrations are done about 3 times a year using zero gas from a cylinder plus a dew point generator (LI-COR 610) and a CO_2 standard from a cylinder.
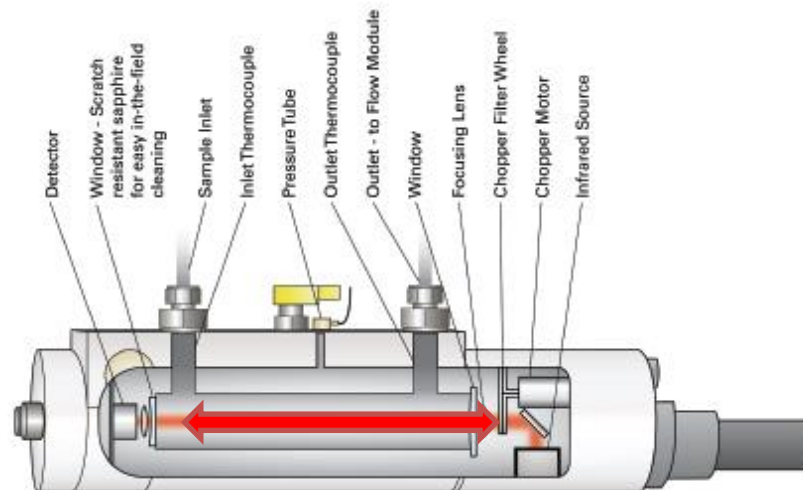

Fig. 50: LI-7200 analyser head (from www.licor.com), arrow indicates sampling volume

Fast ozone sensor - Sextant FOS

The measurement principle of the Fast Ozone Sensor (FOS), manufactured by Sextant Technology Ltd. (www.s-t.co.nz), is based on chemiluminescence. In a measurement chamber, ambient air containing ozone passes above a 25 mm diameter disc coated with coumarin. The dye coumarin reacts with ozone under the emission of light. This emission is proportional to the ozone concentration in the air and the reaction and the air exchange in the reaction chamber is sufficiently fast to allow 10 Hz measurements of ozone concentrations.

The sensitivity of the coumarin discs unfortunately changes within hours. Therefore an independent measurement of the absolute value of the ozone concentration is mandatory and realized with a Thermo Scientific 49C Ozone Analyser (see p. 26 for instrument description) sampling air at vicinity of the FOS. A linear calibration of the FOS is automatically done in data post-processing using the 30 minute mean values of the FOS signal and the 49C concentration plus zero as offset.

The lifetime of the coumarin-coated discs depends on the total ozone exposure and is limited to two to three weeks.

CO_2 and H_2O vertical profile system from ACU

The profile of CO_2 and H_2O within and above the canopy space is sampled with a manifold hosting 8 lines sampling air from different heights (0.5, 1, 2, 4, 8, 16, 29, 37 m above ground). In order to avoid leaching, each line is equipped with a membrane pump that keeps the air pressure within the system slightly above ambient pressure.

The array of valves is controlled by two units:

* Data logger and control unit: Campbell CR1000
* Relay Controller: Campbell SDM-CD16AC AC/DC

Atmospheric mixing ratios of CO_2 and H_2O are monitored with a close-path InfraRed Gas Analyzer (IRGA) LiCOR 7000. A measurement cycle per sampling line consists of 8 s flushing and 7 s of data acquisition.

Calibration is performed about 3 times a year using zero gas from a cylinder plus a dew point generator (LI-COR 610) and a CO_2 standard from a cylinder.

Radiation instruments

Net radiometer Kipp & Zonen CNR1

The net radiometer CNR1 from Kipp & Zonen (www.kippzonen.com) measures the energy balance between incoming and reflected radiation in the short (305 – 2800 nm) and long (5-50 μm) wavelength range to obtain the net radiation at the earth's surface. The short wavelength range is measured with two CM3 pyranometers, one facing upwards and one downwards. For the long range, two CG3 pyrgeometers facing opposite directions are used. The design of the instrument ensures a field of view of 180° upwards and downwards for the respective sensors.

The energy E_{short} of the short wave or so-called global (solar) radiation is calculated from the voltages provided by the CM3's using their sensitivity C_{CM3}: $E_{short} = V/C_{CM3}$.

To calculate the energy E_{long} of the long wave radiation from the reported voltages, besides the sensitivities of the CG3's C_{CG3}, also the sensor temperature T measured with a PT-100 is needed: $E_{long} = V/C_{CG3} + 5.67 \cdot 10^{-8} \cdot T^4$ .The net radiation over all wavelengths is then easily calculated by adding the respective energies: $E_{net} = E_{short}^{up} + E_{long}^{up} - E_{short}^{down} - E_{long}^{down}$. In addition, the Albedo of the earth's surface defined as the ratio of outgoing to incoming solar radiation can be obtained with the instrument as well: $Albedo = E_{short}^{downt} / E_{short}^{up}$.

Calibration and instrument checks at the factory are recommended every two years according to the manufacturer.

Photosynthetic active radiation Delta-T BF3 & BF5

With the Sunshine Sensor BF3 and the newer model BF5 from Delta-T (www.delta-t.co.uk), total (in the sense of direct plus diffuse) solar radiation, diffuse radiation and the sunshine state is measured as photosynthetic active radiation (PAR) of the solar spectrum, i.e. from 400-700 nm. To distinguish between direct and diffuse radiation, a set of seven photodiodes (PD) is arranged under a patterned hemispherical dome with 50% black bands such that at any position of the sun in the sky at least one photodiode is completely in the shade and at least one is fully exposed to direct sunlight. This design eliminates the necessity of frequent alignment of the shading parts to the position of the sun. The diffuse radiation is then given by $PAR_{diffuse} = 2 \cdot PD_{min}$ and the direct by $PAR_{direct} = PD_{max} - PD_{min}$. The instrument reports $PAR_{diffuse}$, $PAR_{total} = PAR_{diffuse} + PAR_{direct}$ and sunshine state. The latter one indicates sunshine if

$PAR_{total} / PAR_{diffuse} > 1.25$ and $PAR_{total} > 50 \, \mu mol \cdot m^{-2} \cdot s^{-1}$.

Fraction of absorbed PAR – Apogee SQ110-L-10 sensor array

SQ110-L-10 quantum sensors from Apogee (www.apogeeinstruments.co.uk) are used to measure PAR originating from different directions. The Fraction of Absorbed Photosynthetic Active Radiation (FAPAR) can be calculated from the measurements of these four distinct PAR fluxes: above canopy incident (*PARi*) and reflected (*PARr*), below canopy transmitted (*PARgi*) and ground reflected (*PARgr*):

$$FAPAR = 1 - \frac{PAR_r + PAR_{gi} - PAR_{gr}}{PAR_i}$$

As a trade-off between complexity of the setup and the inhomogeneity of the forest canopy and changing incoming solar radiation conditions, the setup consists of one sensor each for PAR_i and PAR_r, mounted on the top of the flux tower. On the forest ground, 5 sensors are mounted on ~2 m high poles facing downwards for PAR_{gr} and 15 sensors on ~1.5 m high poles facing upwards for PAR_{gi} measurements. Data for

all sensors are stored as 1 minute averages instead of 30 minutes to account for transients in incoming radiation.

Meteorological sensors

Weather transmitter WXT 510 from Vaisala

A WXT510 weather transmitter from Vaisala (www.vaisala.com) records simultaneously the six weather parameters temperature, pressure, relative humidity, precipitation and horizontal wind speed and direction.

The wind data measurements utilise three equally spaced ultrasonic transducers that determine the wind speed and direction from the time it takes for ultrasound to travel from one transducer to the two others. The precipitation is measured with a piezoelectrical sensor that detects the impact of individual raindrops and thus infers the accumulated rainfall. For the pressure, temperature and humidity measurements, separate sensors employing high precision RC oscillators are used.

Soil instruments

Soil heat flux sensors HFP01 from Hukseflux

Two thermal sensors HFP01 from Hukseflux (www.hukseflux.com) have been buried ten centimetres underground in the undisturbed soil around the tower to obtain a good spatial averaging of the soil heat flux. The determination of the heat flux is based on measuring the temperature difference of two sides of a plate that is exposed to a heat flow using a number of thermocouples connected in series (see Fig. 31). Ignoring possible errors, the temperature difference between the hot and cold side of the sensor is proportional to the heat flow. As the thermocouples provide a voltage proportional to the temperature, the voltage output of the sensor is proportional to the heat flow across the sensor.
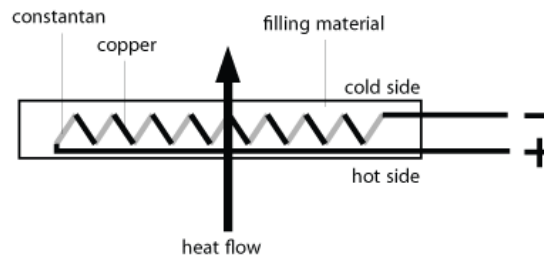

Fig. 31: Sketch of a soil heat flux sensor (drawing from www.wikipedia.org)

Soil water content vertical profile with TRIME-TDR from IMKO

Profile measurements of the soil water content are performed using the TRIME-TDR (Time domain Reflectometry with Intelligent MicroElements) from IMKO (www.imko.de). Based on Time-Domain-Reflectometry, the sensor generates high frequency electromagnetic pulses that propagate along a wave guide and reflected back into the sensor. Depending on the dielectric constant of the material surrounding the waveguide, the round trip time of the hf-pulses varies between some tens and thousand picoseconds. As the dielectric constant of soil and thus the round trip time strongly depends on the soil moisture content, measuring this time gives the water content of the soil surrounding the sensor. Burying several sensors at depths of 10, 30, 50, 100 cm below ground provides the soil humidity profile.

Soil temperature profile with Th3-v probe from UMS

For the measurement of soil temperatures at different depths, a Th3-v probe from UMS (www.ums-muc.de) is used. This probe features a convenient set of 6

temperature probes in a profile system buried at 5, 10, 20, 30, 50 and 100 cm below ground.

Ground water level Diver PR26W/10mH20 from Keller Druckmesstechnik

The ground water level is monitored with a Diver from Keller Druckmesstechnik (www.keller-druck.com). The device is placed in a water filled hole, 2.6 m below ground, and logs autonomously the pressure. Combining the measurement with the barometric pressure at the site gives the height of the water column above the sensor. Together with the known sensor depth below ground, the water table height can be easily calculated (see also Fig. 52):

$$WL = TOC - CL - WC \quad \text{with} \quad WC = 9806.65 \cdot \left(p_{Diver} - p_{baro} \right) \Big/ \rho \cdot g \; ; \; g = 9.81 \text{ m/s}^2, \rho = 1000 \text{ kg/m}^3$$
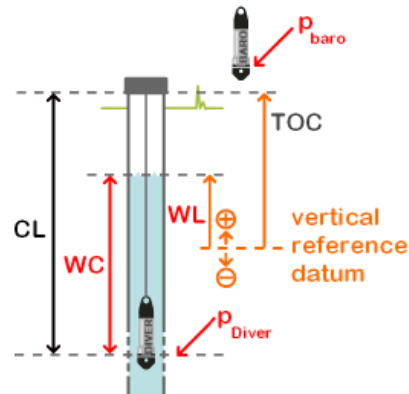

Fig. 52: Principle of water level calculation using the Diver (sketch from www.swstechnology.com). CL: cable length, TOC: top of container, WC: water column, WL: water level relative to a reference, p: pressure.

An automated dynamic chamber system for soil NO & NO$_2$ fluxes from ACU

During 2013, an automated dynamic chamber system to measure NO & NO$_2$ fluxes from the soil, based on Butterbach-Bahl et al. (1997) was constructed at the JRC and subsequently deployed at the ABC-IS forest flux site in Ispra (see Fig. 53). The setup consists of 5 replicate chambers measuring soil fluxes and one chamber that is closed to the ground and thus serves as a measurement blank. The analysers, pumps, control and data acquisition systems were installed in a small, air-conditioned trailer. The description of the system in a nutshell is the following: During a measurement cycle, the lids of one chamber are closed and that chamber is flushed with approx. 55 l/min for 6 minutes. At the same time, the concentrations of NO, NO$_2$ are measured with a Thermo Scientific 42C analyser at the outflowing air of chamber. The values of the first 3 minutes of each 6 minutes cycle are always discarded to allow for flushing and stabilization of the system. To account for concentration changes due to the reaction NO + O$_3$ = NO$_2$ + O$_2$ in the chamber and sampling lines, the concentration of O$_3$ is measured as well with a Thermo Scientific 49C analyser. In addition, the temperature and relative humidity in the chamber are recorded. Combining the measured concentrations, temperature, air flow and chamber size, raw soil fluxes of NO and NO$_2$ are calculated. In order to take chamber and sampling artefacts into account, the blank chamber, whose bottom part is closed to the ground, is measured in the same way before and after each soil chamber and the flux values calculated from that blank chamber are subtracted from the raw soil fluxes.

Fig. 53: Chamber system to measure NO & NO₂ fluxes from soil at the ABC-IS forest flux site.

The description of the system in a nutshell is the following: During a measurement cycle, the lids of one chamber are closed and that chamber is flushed with approx. 55 l/min for 6 minutes. At the same time, the concentrations of NO, NO_2 are measured with a Thermo Scientific 42C analyser at the outflowing air of chamber. The values of the first 3 minutes of each 6 minutes cycle are always discarded to allow for flushing and stabilization of the system. To account for concentration changes due to the reaction $NO + O_3 \rightarrow NO_2 + O_2$ in the chamber and sampling lines, the concentration of O_3 is measured as well with a Thermo Scientific 49C analyser. In addition, the temperature and relative humidity in the chamber are recorded. Combining the measured concentrations, temperature, air flow and chamber size, raw soil fluxes of NO and NO_2 are calculated. In order to take chamber and sampling artefacts into account, the blank chamber, whose bottom part is closed to the ground, is measured in the same way before and after each soil chamber and the flux values calculated from that blank chamber are subtracted from the raw soil fluxes.

Flux data processing

Data evaluation for flux data is done using the free EdiRe software package developed at the micrometeorology group from the University of Edinburgh. (www.geos.ed.ac.uk/abs/research/micromet/EdiRe/). As input data, EdiRe uses the 30 min raw flux data files in the binary ∗.slt format plus 30 minute averaged pressure, temperature and relative humidity data in ASCII format. As time convention, the start of the measurement period has to be assigned to the input data, the middle of the measurement period is assigned to the output data.

The main processing steps used within EdiRe to arrive at final, 30 minute averaged flux data that are corrected for various effects are listed in Table 11.

In order to obtain budgets from e.g. annual datasets that unavoidably contain gaps in the data, a gap filling procedure must be established to calculate the missing values based on drivers for the respective parameter. In addition, partitioning of the measured CO_2 flux (that is the Net Ecosystem Exchange, NEE), into Gross Primary Production (GPP, the gross carbon uptake) and respiration of the Ecosystem (Reco) enables a better understanding of the underlying ecosystem exchange processes. Gap-filling and partitioning of the data measured at the ABC-IS station is done with the online tool at www.bgc-jena.mpg.de/bgi/index.php/Services/REddyProcWeb.

Table 11: Processing steps for flux calculations using the EdiRe Software package.

| EdiRe Process	brief description
Preprocessed Files	data from input file, gas concentrations as molar densities
Extract	all high speed data
Despike	all high speed data
Linear	conversion of raw data from voltages into physical variables
1 chn statistics	averages of 3D wind, sonic temperature and gas concentration
Gas conversion	conversion of molar densities to molar fraction
Filter – detrend	linear detrending of gas concentrations
Wind direction	align with geographic direction
Rotation coefficients	perform 3D coordinate rotation
Cross Correlate	gas concentrations with vertical wind speed
Remove Lag	remove time lag between anemometer and gas analyser
Friction Velocity	calculate u*
Sensible heat flux coefficient	
Latent heat of evaporation	
2 chn statistics	calculate covariances, i.e. uncorrected fluxes
Sonic T - heat flux correction	
Stability - Monin Obhukov	calculate z/L stability parameter
Frequency response	calculate high frequency correction for all fluxes
Webb correction	calculate water density fluctuation correction for all fluxes
Stationarity	perform stationarity test
Integral Turbulence	calculate integral turbulence
Cospectra	calculate co-spectra for all fluxes
Storage	calculate storage term
User defined	determine quality flag (0,1,2) for all flux data according to Carboeurope methodology
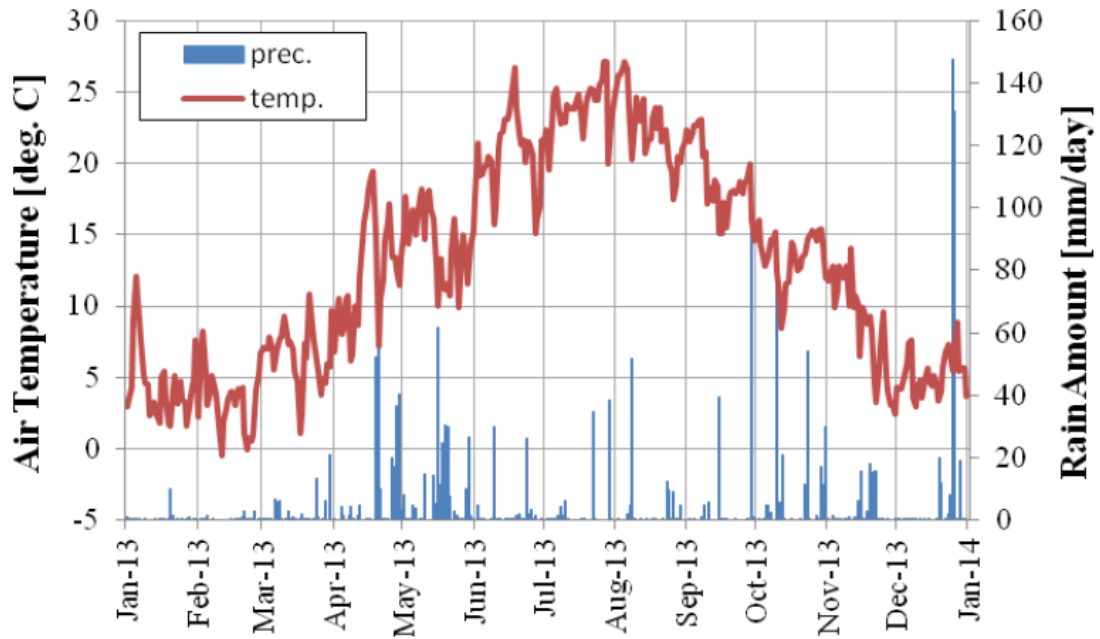
Fig. 54: *Daily average of the air temperature (red) and daily sum of the precipitation (blue) measured at the tower top.*
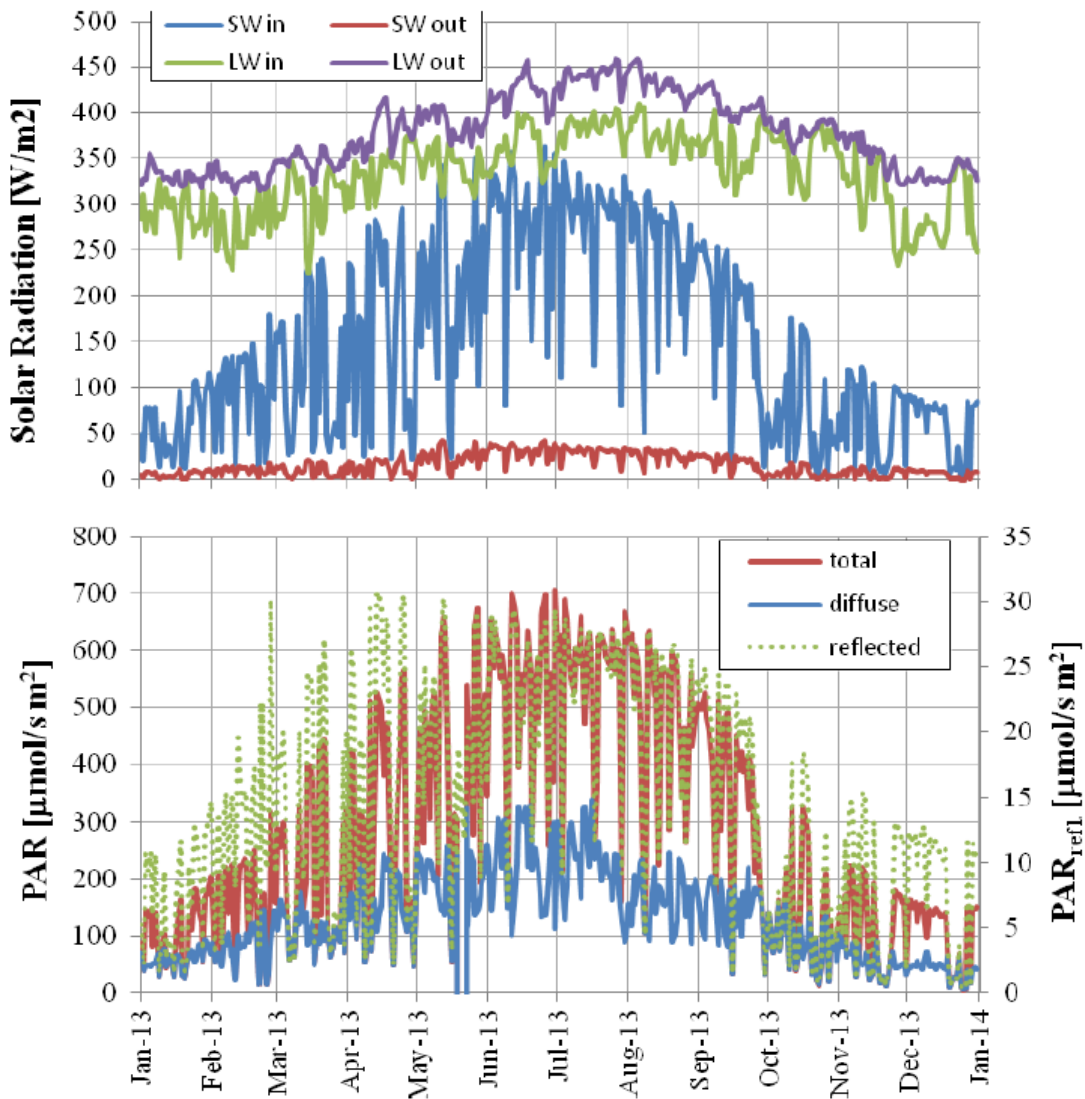

Fig. 56: *Solar radiation parameters measured with the net radiometer (top) and the sensor for Photosynthetic Active Radiation (bottom).*

Results of the year 2013

The ABC-IS Forest Flux Station is still on its way to be set-up as a long-term monitoring station following ICOS procedures, so measurements with some sensors have only started during the course of 2013. Also, the specific ICOS measurement protocols for all variables to be followed by every ICOS measurement station are still under preparation and scheduled to be finalized at the end of 2014.

Meteorology

Daily averages of the air temperature and daily sums of the precipitation measured at the top of the ABC-IS Forest Flux Tower are shown in Fig. 54: Daily average of the air temperature (red) and daily sum of the precipitation (blue) measured at the tower top.

The annual mean temperature above the forest canopy at 37 m was 12.9 °C and the total amount of rainfall summed up to 1724 mm.

The wind measurements obtained with the 3D sonic anemometer indicate that north north-west is the predominant wind direction. Fig. 55 shows in red the frequency distribution of the wind directions for wind speeds > 0.5 m/s; the blue line indicates the average wind speeds per directional bin. Wind speeds with a value larger than 0.5 m/s occurred during 80 % of the measurements intervals. Time periods with air coming from either east or west occur only during very few occasions and wind from the south is rather infrequent as well.
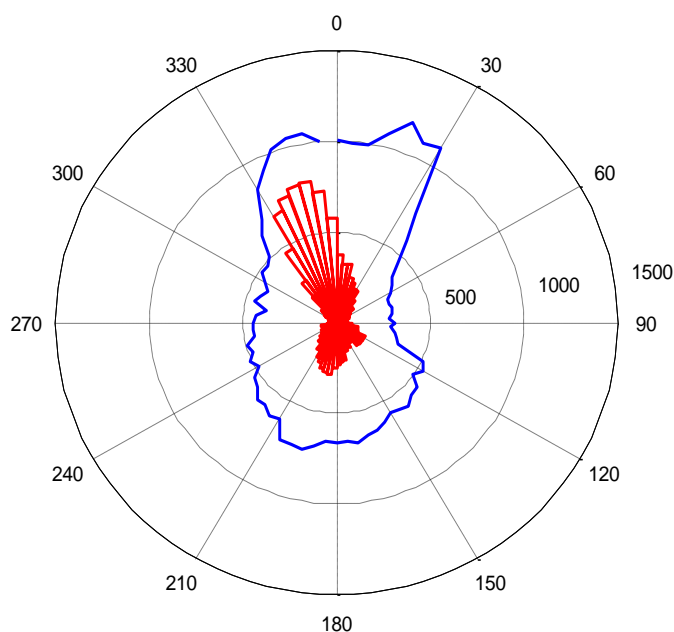

Fig. 55: *Wind rose for 30 min. averages of wind measurements with wind speeds >0.5 m/s. Red: wind directions, blue: average wind speeds per direction interval in a.u.*
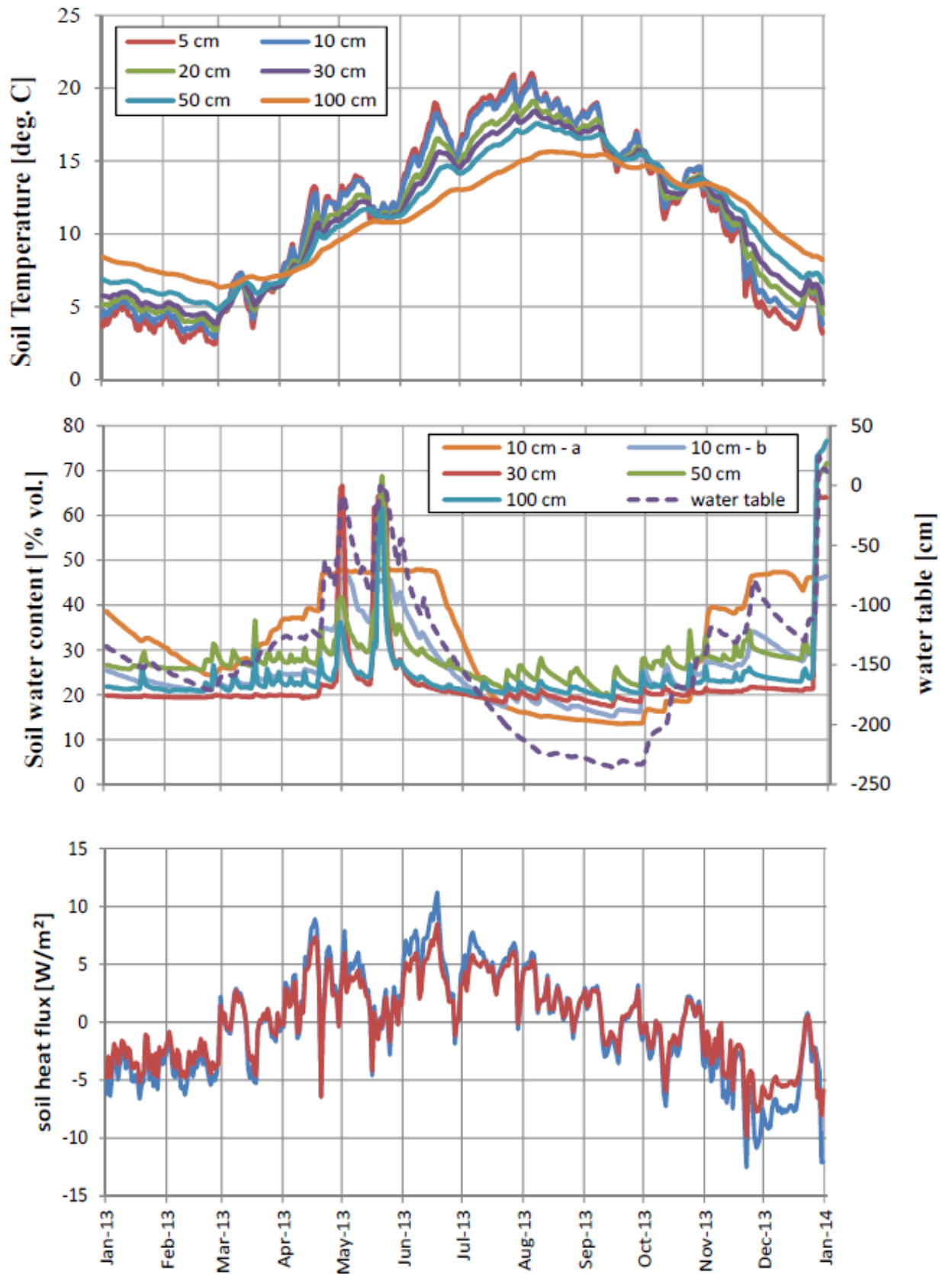
Fig. 57: *Timeline of daily averages of soil parameters measured at the ABC-IS forest flux site from top to bottom: soil temperature profile, soil water content profile plus water table below surface and soil heat flux at two replicates (10 cm below surface).*

Radiation

Different parameters regarding solar radiation are plotted in Fig. . On top, the daily averages of short & long wavelength incoming & outgoing radiation are plotted as measured with the CNR1 net radiometer above the forest canopy at 36 m. The surface albedo, i.e. the ratio between SWout and SWin (305 – 2800 nm) averages to approximately 0.11 for the summer period and 0.12 for the winter period of the measurement. On the bottom part of Fig. , the photosynthetic active radiation (PAR) part of the solar spectrum (approx. 400 – 700 nm) is shown as total & diffuse incoming (left axis) and reflected radiation (right axis). During the vegetative period, i.e. late spring, summer and early autumn, the surface albedo at this part of the solar spectrum is approximately 0.04. The albedo increases in winter up to 0.08 as the deciduous trees in the forest lose their leaves.

Measurements for the FAPAR calculations have started at the end of May 2013. Averaging the 15 ground PAR sensors facing upwards, the 5 ground PAR sensors facing downwards and calculating FAPAR every minute during daytime according to

$$FAPAR = 1 - \frac{PAR_r + PAR_{gi} - PAR_{gr}}{PAR_i}$$

results in an FAPAR value of 0.92 (+/- 0.01) during the vegetative period when the leafs of the deciduous trees and thus the canopy is fully developed.

Soil parameters

The soil parameters measured at the ABC-IS Forest Flux Station are shown in the three plots of Fig. 57. In the top one, daily temperature averages at 6 different depths are plotted. As expected, soil temperature decreases with measurement depth during summer and increases during winter. The tipping points when the temperature profile is reversed occurred in early April and in October.

The plot in the middle depicts the soil water content (SWC) at different depths (left axis) and the water table (right). Jumps in the daily averages of the SWC occur during precipitation events and thereafter the soil starts to dry again. The differences seen at the surface replicates at 10 cm give a glimpse on the heterogeneity of the soil and the forest environment. Due to rather little rainfall during summer 2013, the water table went down to almost 240 cm below the forest surface. On the other hand, in late December the measurement area was flooded with a maximum water level of 24 cm above ground because of exceptionally heavy rainfall.

In the bottom plot of Fig. 57, the soil heat flux measured at two locations is presented. Obviously during summer time the soil heats up due to solar irradiation and in winter time it cools down. Again, the differences of the heat fluxes at the two sensor positions are due to different environmental situations at the two locations, i.e. different irradiance by the sunlight and to a lesser extend soil variation.
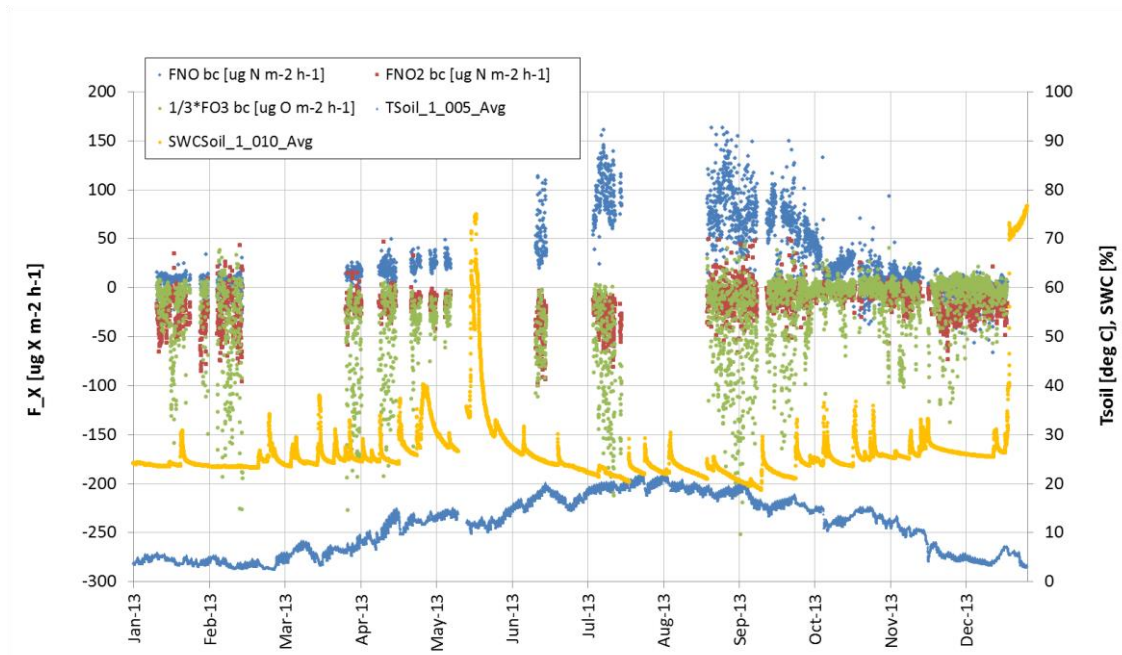
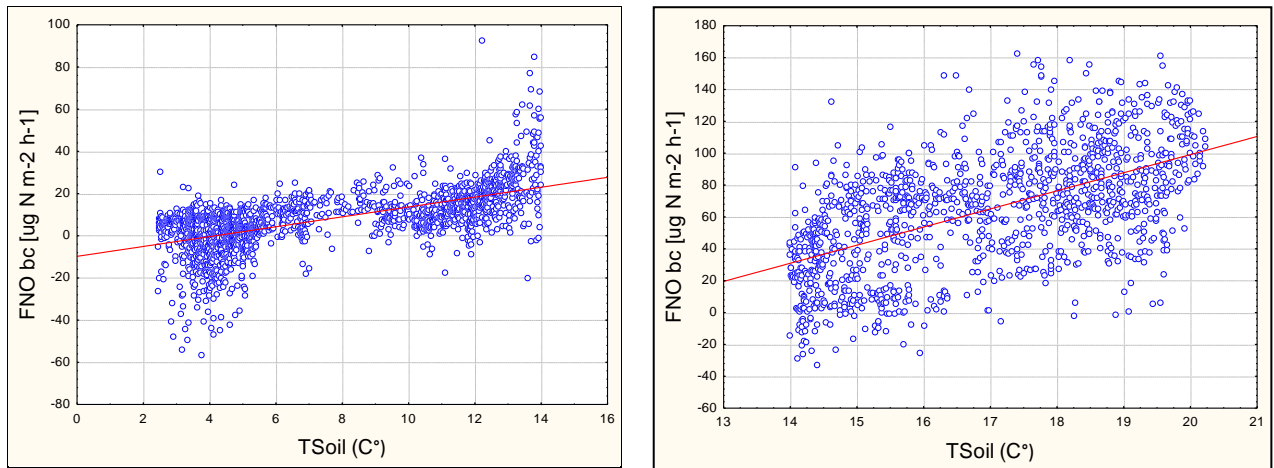Fig. 58a*: Hourly averages of soil fluxes measured with the 5 dynamic soil chambers.*

Fig. 58b: measured NO fluxes vs. soil temperature below and above a threshold of 14 C°.*

Tab. 12: Averages over all sampling points for soil respiration measurements plus standard variation.

measurement date	soil respiration CO_2 [g / m^2 / h]	variability (std deviation) CO_2 [g / m^2 / h]
17/01/2013	0.11	0.07
31/01/2013	0.22	0.23
15/02/2015	0.18	0.32
01/03/2013	0.14	0.09
03/05/2013	0.39	0.25
24/05/2013	0.33	0.22
07/06/2013	0.53	0.40
21/06/2013	0.62	0.46
25/07/2013	0.93	0.61
31/07/2013	0.89	0.55
23/08/2013	0.56	0.42
30/08/2013	0.83	0.51
16/09/2013	0.65	0.54
19/09/2013	0.49	0.35

Results of NO, NO_2 and O_3 flux measurements from soil as measured with the automated dynamic chamber system are summarized in Fig. 58a. For fluxes, on the left axis hourly averages from the 5 replicate chambers (blank corrected) are plotted. Especially the NO fluxes show a pronounced seasonal cycle with high emissions during the warm summer time and low emissions in winter.

Regarding the replicate chambers used, measurements from each chamber showed some differences indicating certain inhomogeneity of the soil in this forest (data not shown), whereas their daily and seasonal cycles were quite similar.

Our results can be compared to those collect at several European forest sites (Butterbach-Bahl et al, 1997, William et al., 2001, Horváth et al., 2006), both for dry and wet soils, during middle and long term (1 year or more) measuring campaigns. Comparing literature describing short term continuous measurements (few weeks) it is possible to note that some different (lower NO in this case) average soil flux are recorded (see Table 12)

Tab. 12: NO flux ranges measured during short term campaigns.

References	NO fluxes range ($\mu g\ N\ m^{-2}\ h^{-1}$)
Johansson, 1984	0.3-2.9
Skiba et al.,1994	1.0- 3.5
Papen et al., 1993	15-33
Williams and Fehsenfel, 1991	0.2-4
our measurements	0-150

In particular, in our experiment fluxes were measured from the beginning of January to end of December except during rain events and some weeks in August due to instrumental problems. Soil NO fluxes ranged from small negative fluxes in winter to high emissions of up to 150 $\mu g\ N\ m^{-2}\ h^{-1}$ during warm summer times from July to early September. This confirms that summer and early autumn seasons are the periods of the year with highest production of NO in the soil (Butterbach-Bahl et al, 1997).

On the contrary, during the winter NO emissions are usually much lower and sometimes the soil behaves like a sink. During the entire measurement period for NO_2 and O_3 (red and green, respectively) forest soil acts is a sink except for very brief periods.

In the same figure, in yellow, the soil water content (SWC) and in light blue the soil temperature (Tsoil) are included as potential drivers for the release of NO and uptake of NO_2 by the soil. Soil NO emission clearly go down as soil temperature decreases and the pattern changes as well significantly during and after rain events, indicated by a steep increase of the SWC. During rain events, the system was not measuring soil fluxes in order not to dry the soil covered by the chambers. Correlation values among several parameters measured in our experiments are reported in Table 13.

Table 13. Correlations among several parameters measured at the forest site

Parameter 1	Parameter 2	Cor. Coef.
FNO bc [µg N m^{-2} h^{-1}]	TSoil_1_005_Avg	0.7764
FNO bc [µg N m^{-2} h^{-1}]	Air Temp. in the Chambers	0.7287
FNO bc [µg N m^{-2} h^{-1}]	SWCSoil_1_010_Avg	-0.5621
FNO bc [µg N m^{-2} h^{-1}]	SWCSoil_1_010b_Avg	-0.6127
FO3 bc [µg O m^{-2} h^{-1}]	O$_3$ corrected [ppbv]	-0.7188
FO3 bc [µg O m^{-2} h^{-1}]	Air RH in the Chambers	0.6686
FO3 bc [µg O m^{-2} h^{-1}]	TSoil_1_005_Avg	-0.1967
FNO2 bc [µg N m^{-2} h^{-1}]	TSoil_1_005_Avg	0.1878
NO$_2$ corrected [ppbv]	FNO2 bc [µg N m^{-2} h^{-1}]	-0.4864
NO$_2$ corrected [ppbv]	TSoil_1_005_Avg	-0.4239
NO$_2$ corrected [ppbv]	O$_3$ corrected [ppbv]	-0.3811
O$_3$ corrected [ppbv]	Air RH in the Chambers	-0.6801
O$_3$ corrected [ppbv]	Air Temp. in the Chambers	0.5825

Data on the soil temperature, soil moisture and NO fluxes from field experiments have been reported and compared in several papers. Often, like in our experiment, there is a positive correlation between NO fluxes and Tsoil. These results can be explained through several indicators of soil microbial activity, such as respiration, that are positively related to temperature (Chen et al.,2000; Curiel Yuste et al., 2004, Franzluebbers et al., 2002, Sulzman et al., 2005). In particular, we observed two different slopes according to Tsoil, a lower value until 14 C° and a higher one above 14 C° (Fig. 88b).

NO fluxes that increase with soil temperature in sufficiently wet condition (review by Williams et al., 1992) seems to be confirmed by our data. In our experiment we also found a negative correlation between NO fluxes and SWC (r_{corr} = -0.5621) during very wet soil conditions. Soil water content at our site ranged widely from dry soil to water saturated soil values, in particular after heavy rain fall episodes.

However in our experiments large emissions of NO from soil after rainfall, due to a sudden mineralization of nutrients accumulated during dry period as reported in the literature (Gut et al., 2002; Stark et al., 2002), are not so evident.

Most literature reported that soil moisture regulates N oxides fluxes from forest soil (Erickson et al., 2014, Davidson et al., 2000, Firestone et al., 1989, Stark et al., 2002, Venterea et al., 2003,

Schaufler et al., 2010) but optimal moisture for NO emission can be significantly different between soils (Schindlbacher, A. et al., 2004). These differences may be related to different reaction of microbial communities to soil conditions in terms of N availability, nitrification and denitrification processes, C/N ratios, pH, texture, structure and thickness of the humus layer, density and so on. While in our experiments we have found a rather strong seasonal pattern regarding NO fluxes from soil, the pattern of the SWC did not vary much during the year with subsequent rain episodes distributed along the experimental period. Only between May and June

the SWC reached very high values (> 70%) with respect to the recorded trend. This episode has been followed in the days after by higher NO fluxes.

This situation could be explained from others concomitant conditions like high Tsoil and high level of microbial communities present during this specific season.

During the course of 2013, 14 measurements of soil respiration have been done in the forest. To obtain a good spatial representation, at each measurement date soil respiration at 25-34 locations inside the ABC-IS forest was measured and averaged. The results are reported in Tab. 14 including the standard variation as an indication for the variability among the measurement locations. As expected, soil respiration is highest during the warm summer months and reduced during winter time.

Eddy covariance fluxes

The timelines of daily averages of the different fluxes calculated from measured data using EdiRe, following the Carboeurope methodology (no correction for storage), are shown in Fig. 59 and Fig. 60. Gap filling and flux partitioning of the dataset has been performed without u* filtering using the 'Eddy covariance gap-filling & flux-partitioning tool' for missing and quality class 2 data available online at: www.bgc-jena.mpg.de/bgi/index.php/Services/REddyProcWeb.

During the cold season when the deciduous trees in the Ispra forest are without leaves, the CO_2 flux of the forest is positive and ecosystem acts a source of CO_2 (see Fig. 60 on p. 92). During the growing season on the other hand, the flux is negative and the forest is a strong sink of CO_2 due to photosynthesis.
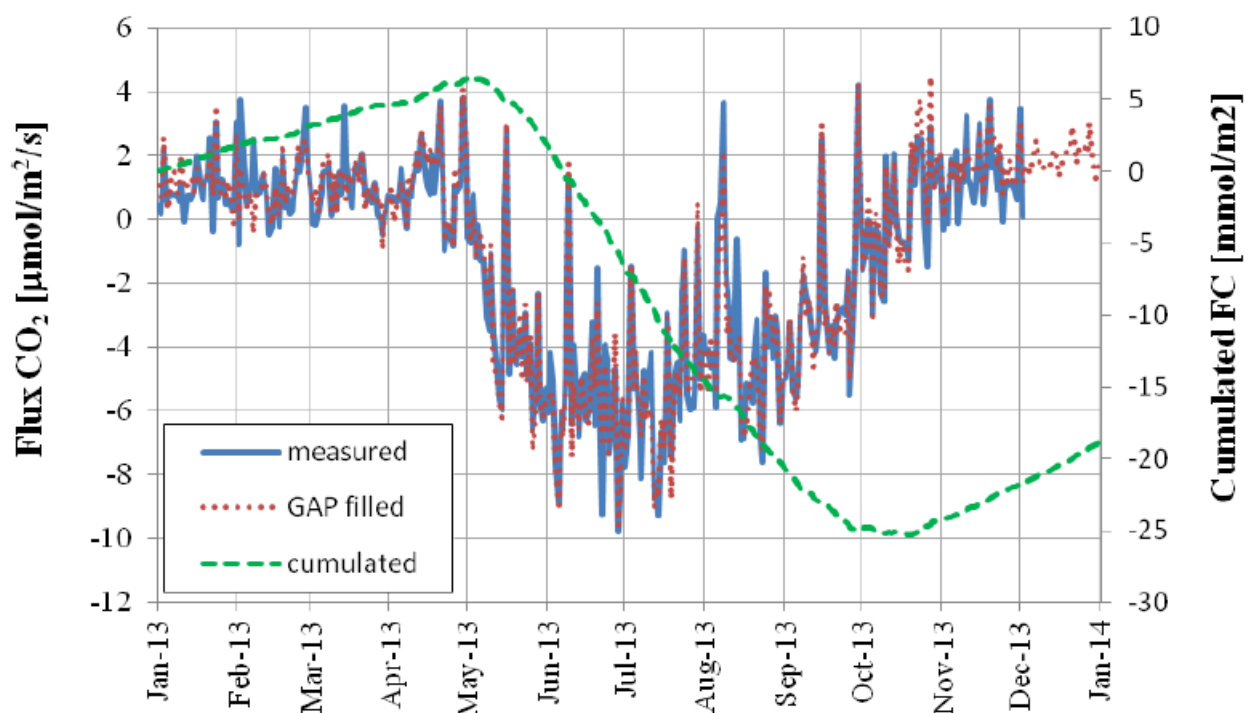

Fig. 59: Timelines of the daily averages of measured (blue), gap filled (red) and cumulated (green) CO_2 fluxes.
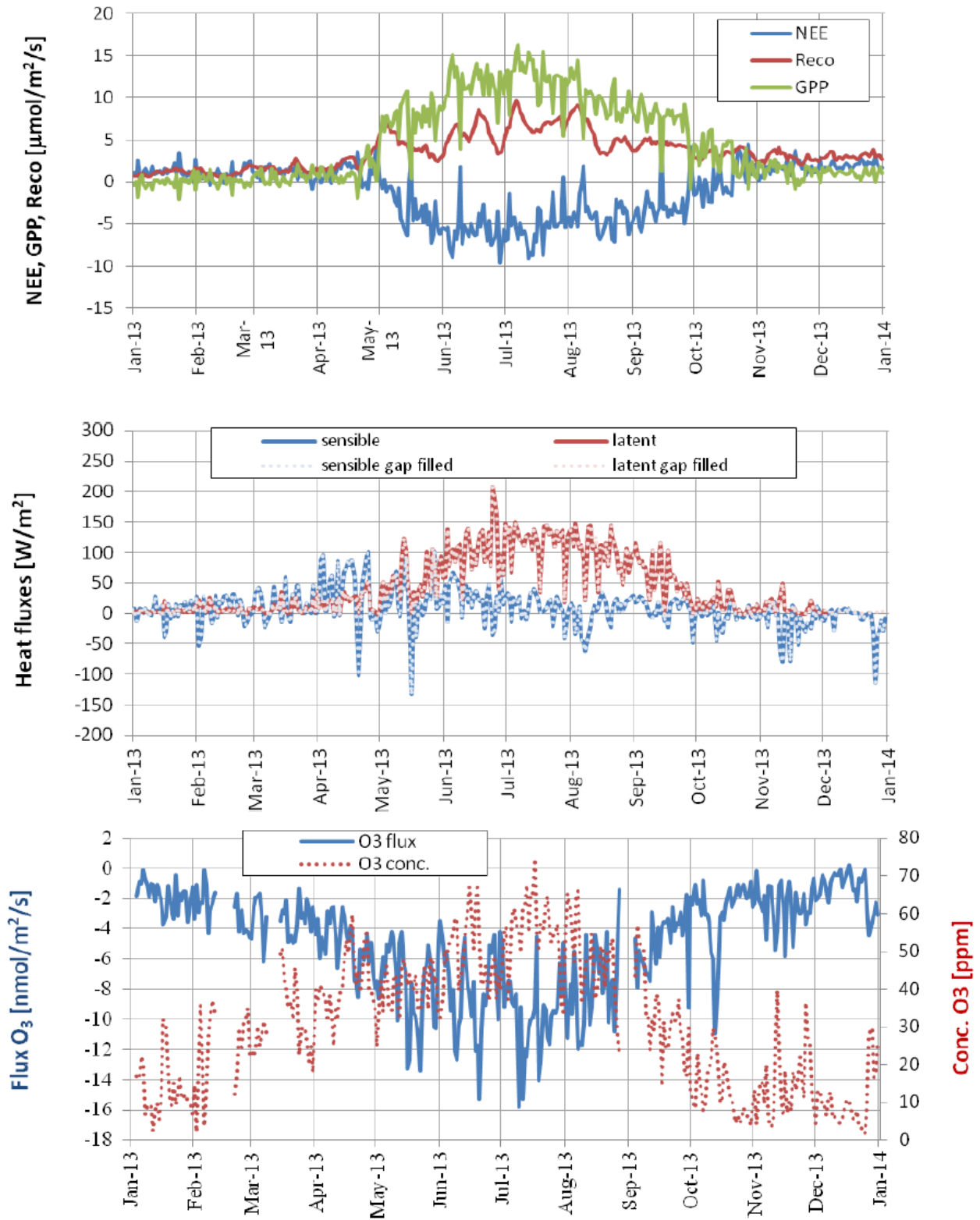
Fig.60: *Timelines of daily averages of fluxes calculated from data measured at the ABC-IS forest flux site, from top to bottom: CO$_2$ fluxes, i.e. NEE, GPP & Reco, sensible & latent heat flux plus ozone flux & concentration.*

Partitioning CO_2 flux data as *NEE = Reco - GPP* results in the daily averages plotted in Fig. 60 top panel. Despite the increased ecosystem respiration (Reco) during summer compared to winter, the photosynthetic activity of the plants results in an even higher Gross Primary Production (GPP) and thus leads to net uptake of CO_2 by the forest. Calculating the budgets for 2013, NEE sums up to -407 g C m^{-2} $year^{-1}$, GPP to -1765 g C m^{-2} $year^{-1}$ and Reco to 1358 g C m^{-2} $year^{-1}$.

Fig. 60 middle panel shows the latent (red) and sensible (blue) heat fluxes for 2013 as daily averages. The latent heat flux, i.e. water vapour flux, especially during the warm summer period, is much higher than the sensible heat flux. This is characteristic of rather humid ecosystems with high water availability also during warm periods as it is the case in Ispra.

O_3 fluxes were measured continuously in 2013 (Fig. 60 bottom panel) and indicate that the forest is a significant sink for ozone during the entire year. As both O_3 concentrations and the activity of the ecosystem increase in late spring, also ozone deposition into the ecosystem increases.

An assessment of the applicability of the eddy covariance (EC) method to measure fluxes at any time is given by the stationarity and integral turbulence tests. They are combined in the Carboeurope methodology into a quality flag (QF) for every data point. A value of 0 indicates strong turbulence and good stationarity, giving reliable EC flux values. A QF = 1 indicates acceptable quality and flux data with QF = 2 are unreliable and thus should not be used in further calculations. For the measurements at the ABC-IS station, the distribution of quality flags for all flux data are given in Tab. 14. The table shows that 60 – 67 % of the data depending on the flux type are usable for further data evaluation and interpretation.

Tab. 14: Total number of flux data points and percentage of data points with quality flags according to the Carboeurope methodology.

	H [%]	LE [%]	FC [%]	FO$_3$ [%]
data points	17576	16105	16103	16136
QF = 0	12	8	9	9
QF = 1	55	52	53	56
QF = 2	33	40	37	35

H: sensible heat flux
LE: latent heat flux
FC: CO_2 flux
FO$_3$: ozone flux

Fig. 61: Newly erected tower at the pinus pinea site that will hold the measurement equipment.

Atmosphere – Biosphere flux monitoring at San Rossore

Location and site description

The new measurement site 'San Rossore' (43°43.9205'N, 10°17.45817E, 12 m a.s.l.), operated by the Air and Climate Unit, is located in the Parco San Rossore (www.parcosanrossore.org), approximately 9 km west of Pisa and 1200 m east of the seashore in a Mediterranean forest ecosystem (see Fig. 61). The Climate Change and Air Quality Unit began to operate the predecessor site in the Parco San Rossore site in 1999.

The measurement site is situated in an almost flat area with a morphology characterized by the presence of sandy dunes. The vegetation in the direct vicinity is a pinewood established in 1921 following artificial seeding and it is dominated by the evergreen tree Pinus pinea with very sparse Quercus ilex. The average canopy height is approximately 19 m whereas the needles start at about 16.5 m. The understory vegetation is confined to the forest edges and canopy gaps and very sparse as well.

The area has a Mediterranean – type climate within the sub-humid zone, with a mean annual rainfall of 876 mm yr^{-1} and a range of 534 – 1270 mm for the period 1980 – 2005. The long term data were obtained from a meteorological station located at a distance of approximately 10 km and managed by the Regional Hydrologic Service of Tuscany. Rain falls mainly during autumn and winter with about 50% occurring between September and November, while the driest months are July and August. The average annual temperature is approximately 14.2 °C with the average temperature of the coldest month (January) being 7 °C and that one of the warmest month (August) being 25 °C. The wind regime is characterized by a sea – land breeze circulation, i.e. the air flows quite predictable from the west (sea) during day and from east (land) during night.

Starting in 2009, major clear cuts of the forest in the vicinity of the old measurement site, approximately 700 m south-west were initiated as a response of the park management to the infection of the Pinus pinaster with 'Matsucoccus feytaudi' (Fig. 62). As it is obvious from the satellite picture, the cuts destroy the homogeneity of the canopy around the measurement site (red circle). This inhomogeneity of the ecosystem in the fetch of the old flux tower rendered eddy covariance measurements of ecosystem fluxes meaningless. It has therefore been decided to move to a new location within the park that is not threatened by the 'Matsucoccus feytaudi' and has a homogeneous canopy suitable for micrometeorological measurements. The new site has been identified in 2011 (blue circle in Fig. 62) within a rather homogenous stand of Pinus pinea. The new tower (Fig. 61) for eddy covariance measurements of fluxes has been erected in autumn 2012 and equipped with instrumentation to study ecosystem exchange processes. Thus 2013 marks the first year of measurements at the Pinus pinea site.
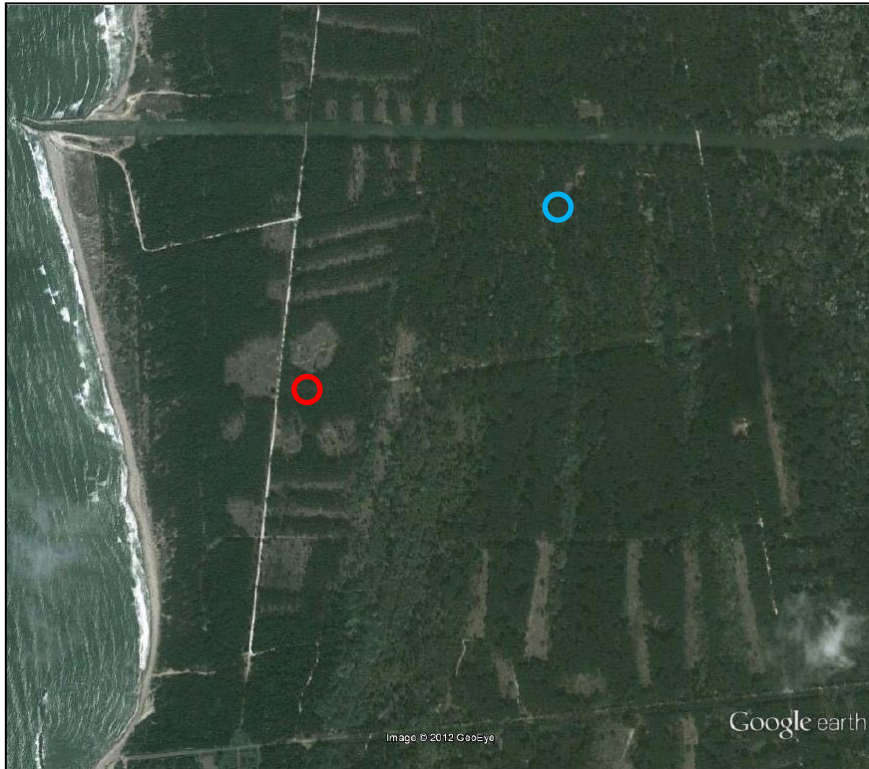
Fig. 62: The picture of the vicinity around the measurement site from Google Earth taken on 04.08.2011 visualizes the severe cutting of trees due to infection with 'Matsucoccus feytaudi'. The blue circle shows the location of the new tower at ~700m distance.

.

Dismantling of the old site has started in the first half of 2013 and finished in early 2014.

With regards to data reporting as in the previous years, quality checked data for 2013 have been submitted for the first time for the new measurement site under the new station name IT-SR2 to the Fluxnet database at the European Fluxes Database Cluster at www.europe-fluxdata.eu.

Monitoring program

The new measurement site in the Parco San Rossore will also be a level 2 Ecosystem Station within ICOS. For a brief description of ICOS and the obligatory parameters to be measured, please refer to the respective chapter in the description of the ABC-IS Forest Flux Station on page 73.

Despite being the year of setting up the measurement site, the monitoring program at the new Pinus pinea site started well and most parameters have been measured for the major part of 2013. The main variables measured are summarized in Table 5. In addition, ozone fluxes have been measured during three seasonal campaigns (23.4.2013 till 13.5.2013, 9.7.2013 till 29.7.2013 and 10.09.2013 till 30.09.2013).

Table 15: variables measured during 2013

FLUXES	CO_2, latent heat, sensible heat continuously, O_3 during campaigns
METEOROLOGY	3D wind speed, temperature, relative humidity, pressure, precipitation
RADIATION	short & long wave incoming & outgoing, direct & diffuse photosynthetic active radiation
SOIL	temperature profile, water content profile, heat flux, water table height
BIOLOGICAL	-

In the same way as it is done at the ABC-IS Forest Flux Station, fluxes of CO_2, H_2O and sensible heat were measured with eddy covariance technique and evaluated using the EdiRe software package (www.geos.ed.ac.uk/abs/research/micromet) from the University of Edinburgh. The ancillary parameters (meteorology, radiation and soil) were obtained with respective sensors and the data quality checked for instrument malfunctioning, obvious outliers and consistency. In the following section the site specific instrumental descriptions are presented. Daily averages of the different parameters measured during the course of 2013 are presented further down.

Description of the instruments

<u>Infrastructural:</u>

Sensor location

The instruments for eddy covariance flux system, i.e. sonic anemometer and fast gas analyser, solar radiation and meteorological parameters are mounted on the top of the guided wire tower at a height of 24 m above ground, 5 m above the canopy top at 19 m.

Soil parameters are measured at an undisturbed soil plot approximately 20 m west of the tower.

A wooden hut complements the installation hosting IT and communication equipment, a UPS system and is also used for storage.

Data acquisition

Eddy covariance flux data are stored with high frequency, i.e. 10 Hz, as chunks of 30 minutes on a local laptop connected to the sonic anemometer. Data from the sensors located on the tower top are read every 10 s and averaged and stored every 30 minutes by a CR3000 data logger from Campbell (www.campbellsci.co.uk) also installed on the tower top. Soil measurements are handled the very same way by a CR3000 installed on the ground.

For eddy covariance flux data, the start time of every 30 minutes measurement period is saved as the reference time, whereas for all other data, the end of the 30 minutes measuring period is used. The time reference used for all San Rossore measurements is UTC.

Power supply, IT & communication infrastructure

The fixed line power supply of 4 kW is locally backed up by an UPS system MSM 10 from Riello (www.riello-ups.de) to protect the system for transient power outages and provide an autonomous running time of approx. 19 hours for the installation. Computers and data loggers are connected via a local TCP/IP network. In addition, a cellular router TK704U from Welotec (www.welotec.com) provides internet access via the mobile 3G network. For safety reason at the remote site, a 3G repeater provides mobile phone coverage also on the forest ground in the vicinity of the site.

Measurement data is automatically transferred from San Rossore via ftp to a server (sanrosso@ftp-ccu.jrc.it) in Ispra at 6:00 UTC. Remote connection to a computer at the site can be established as well.

<u>Ecosystem fluxes:</u>

Sonic Anemometer for 3D wind direction Gill HS-50

Sonic anemometers determine the three dimensional wind vectors at high frequency using the speed of sound. As the Gill HS-50 (www.gill.co.uk) is an instrument almost identical to the Gill HS-100 used at the ABC-IS Forest Flux Station, please refer to the instrument description on page 76.

Fast infrared gas analyser for CO_2 & H_2O concentration (IRGA) LI-7200 FM

As the IRGA is identical to the one operated at the ABC-IS Forest Flux Station, please refer to page 77 for the instrument description.

Radiation instruments

Net radiometer Kipp & Zonen CNR1

See page 78 for instrument description

Photosynthetic active radiation Delta-T BF3

Refer to page 78 for instrument details.

Soil instruments

Soil heat flux sensors Hukseflux HFP01

A group of 3 thermal sensors HFP01 from Hukseflux (www.hukseflux.com) have been buried 10 centimetres underground in the undisturbed soil in the vicinity of the tower to obtain a good spatial averaging of the soil heat flux (see page 79 for description).

Soil water content vertical profile with TRIME-TDR from IMKO

Profile measurements of soil water content are performed using the TRIME-TDR (Time domain Reflectometry with Intelligent MicroElements) from IMKO (www.imko.de). Please refer to the instrument description for ABC-IS on page 79 for details. In San Rossore the sensors are buried at depths of 5, 30, 50, 100 cm below ground to provide the soil humidity profile.

Soil temperature profile with Th3-v probe from UMS

For the measurement of soil temperatures at different depths a Th3-v probe from UMS (www.ums-muc.de) is used. This probe features a convenient set of 6 temperature probes in a profile system buried at 5, 10, 20, 30, 50 and 100 cm below ground.

Ground water level with Diver CS456 from Campbell

The ground water level is monitored with Diver from Campbell (www.campbellsci.co.uk). As the device is very similar to the one used at the ABC-IS in Ispra, please refer to page 80 for details.

Flux data processing

The evaluation of flux data is performed in the very same way as at the ABC-IS Forest Flux Station in Ispra. Therefore please refer to page 83 for a detailed description.
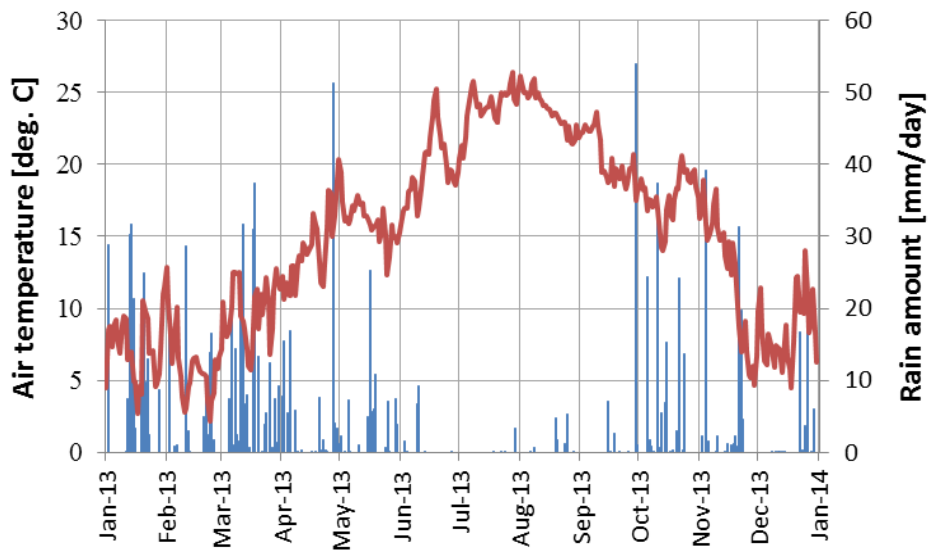
Fig. 64: Daily averages of air temperature (red) and daily sum of precipitation (blue) as measured in the Parco San Rossore. Gaps in the temperature curve show periods with missing data.
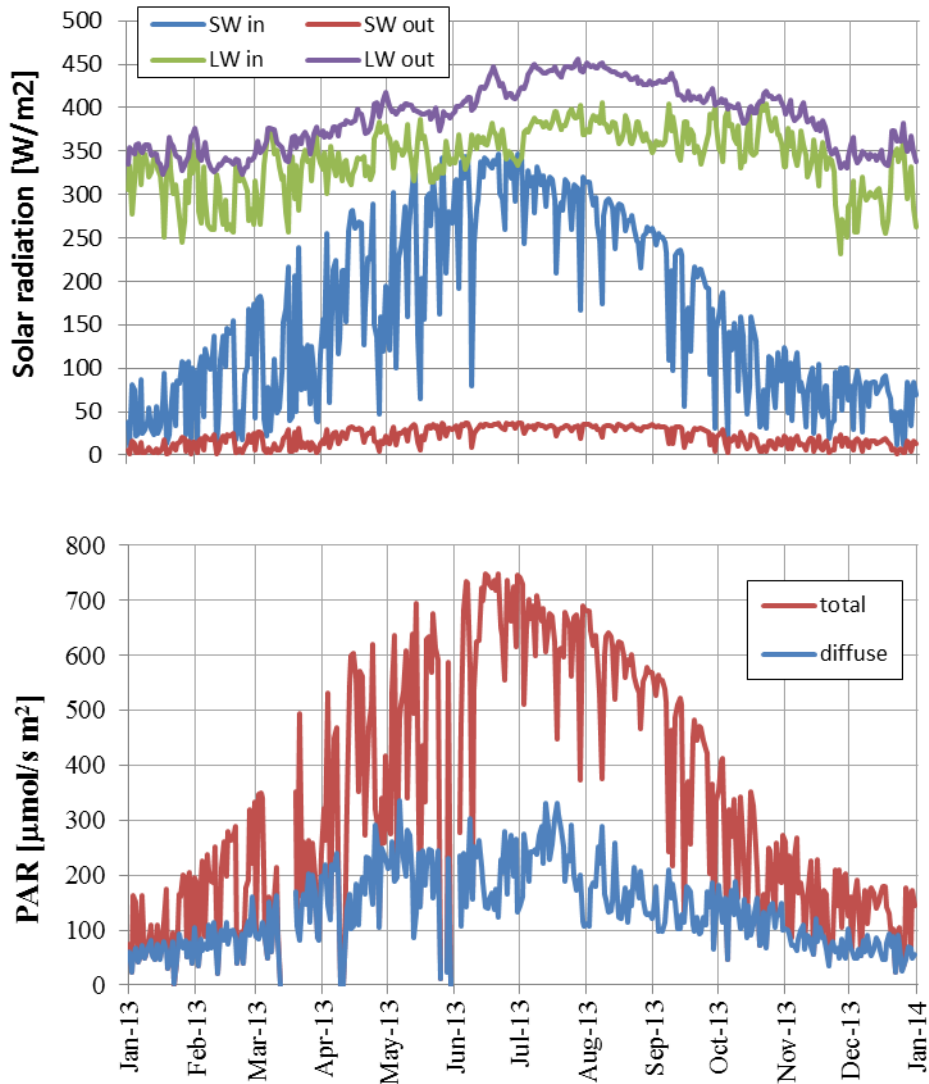

Fig. 66: *Daily averages of short wave incoming radiation (top) and incoming photosynthetic active radiation (bottom).*

Results of the year 2013

Meteorology

Daily averages for the annual cycle of air temperature and precipitation are shown in Fig. 64. The annual mean temperature for 2013 was 15.0° C, slightly above the long term average of 14.2° C. The total measured rainfall was 1132 mm, well above the mean annual rainfall for San Rossore of 876 mm yr^{-1}. With a dry summer experiencing only 47 mm of rain, 2013 was an average year regarding rainfall patterns. Most precipitation occurred during spring and autumn.

The predominant sea – land breeze wind circulation can be seen from the statistical evaluation of the 3D wind direction measurements and is shown in Fig. 65. The red plot shows the frequency distribution of the wind for winds speed > 0.5 m/s in terms of its origins; the blue line indicates the average wind speed per directional bin. In previous years, the direction of the wind vector has been plotted for San Rossore, resulting in a visual 180 deg. rotation of the wind rose. The average annual wind speed was 1.5 m/s. No change in wind patterns was observed compared to the old Pinus pinaster measurement site.

Fig. 65: Wind rose for 30 min. averages of wind measurements with wind speed >0.5 m/s. Red: directions of the wind origin, blue: average wind speeds per direction interval in a.u.
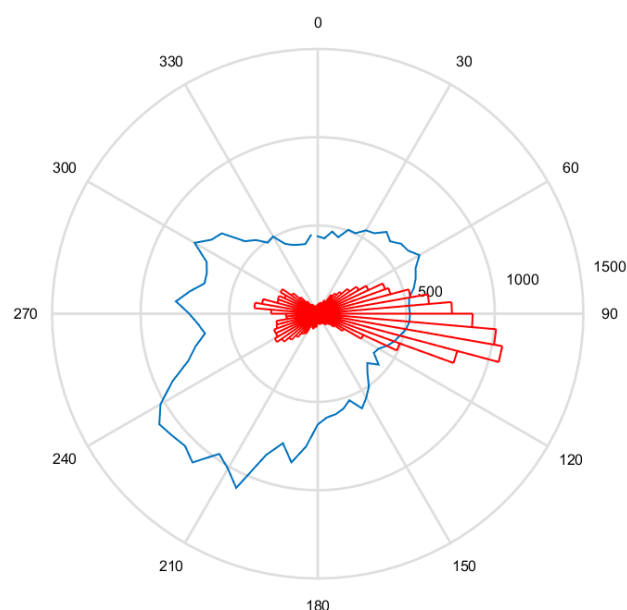
Radiation

In Fig 66, the annual cycle of short & long wavelength incoming & outgoing radiation are plotted as measured with the CNR1 net radiometer above the forest canopy at 24 m.

The surface albedo, i.e. the ratio between SWout and SWin (305 – 2800 nm) averages to approximately 0.12 for the summer period and 0.17 for the winter period of the measurement. On the bottom part of, the photosynthetic active radiation (PAR) part of the solar spectrum (approx. 400 – 700 nm) is shown as total and diffuse incoming radiation.
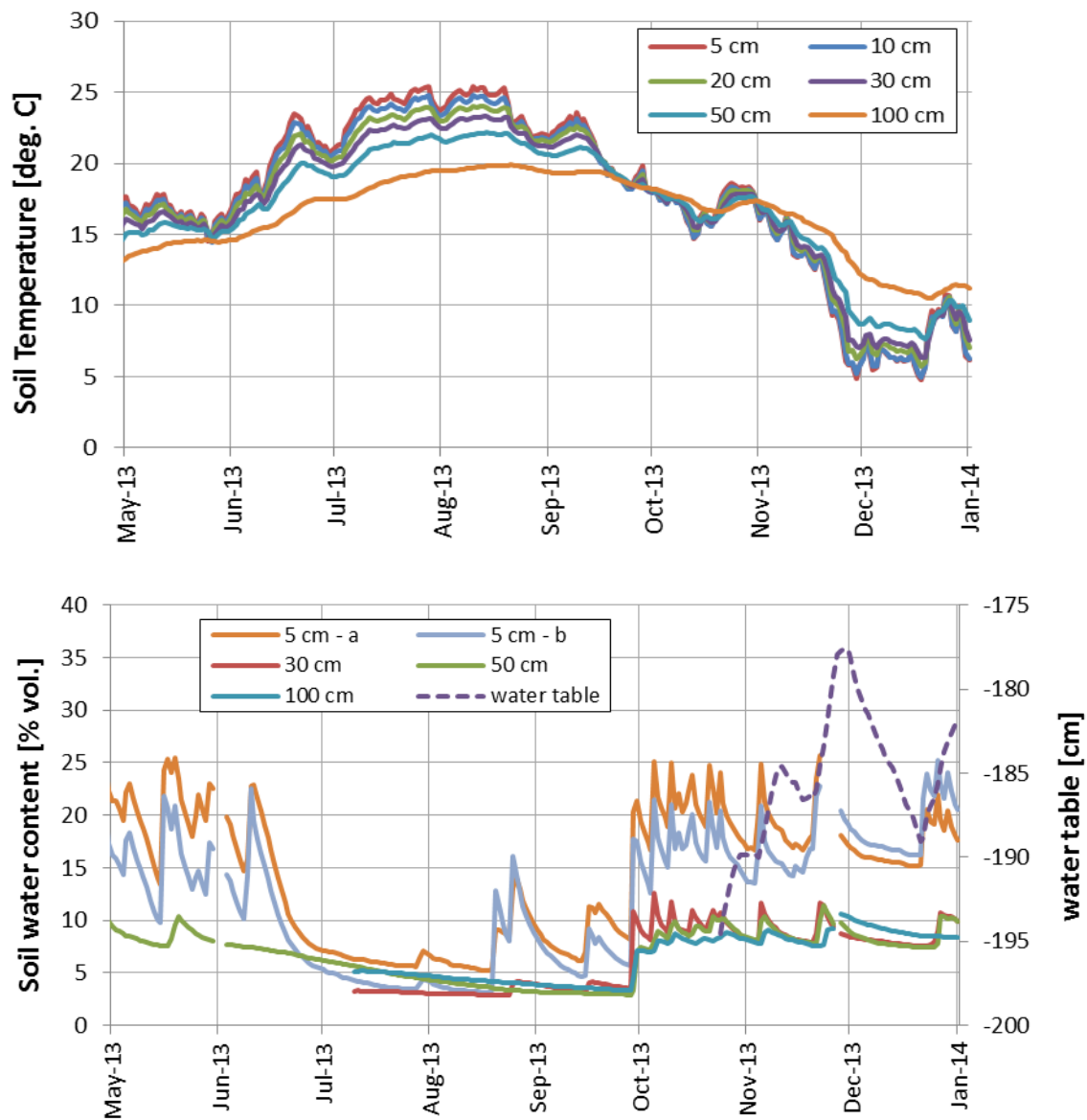
Fig. 67: Profiles of soil temperature (top) and soil water content plus water table (bottom) measured as daily averages.
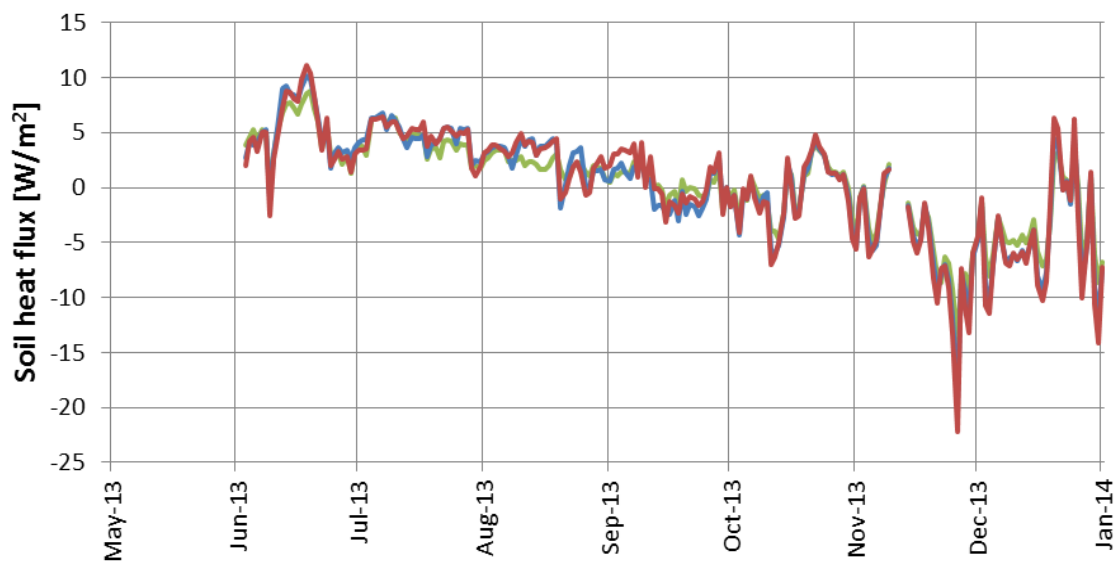

Fig. 68: Soil heat fluxes measured with two identical sensors located some meters apart.

Soil parameters

The soil parameters monitored in 2013 were the temperature at six different depths (5, 10, 20, 30, 50 and 100 cm), soil water content profile (2 replicates at 5 cm, 30, 50 and 100 cm), soil heat flux (3 replicates at 5 cm, a few meters apart) plus water table depths measured with a well requiring a minimum water level of 195 cm below ground. Monitoring of soil parameters started in the course of the year, therefore we do not have a full annual cycle in 2013. The daily averages of these measurements are illustrated in Fig. 67.

The soil heat flux measured with three identical sensors located a few meters apart in the forest soil is shown in Fig. 68, using the convention that positive values indicate a heat flux into the soil, negative values out of the soil. The slight differences between the three sensors originate from the different light intercept by the canopy at the different locations, and the soil inhomogeneity.

Flux measurements

The daily averages of CO_2 and heat fluxes measured during 2013 are shown in Fig. 70 and 71 (next page), respectively. To obtain the eddy covariance flux data for the 30 minute measurement periods, the high frequency data from the LiCor 7200 infrared gas analyser for CO_2 and H_2O have been evaluated together with the anemometer data using the EdiRe software package from the University of Edinburgh. Using the Carboeurope quality classification for the 17568 flux data points for 2013, only 12% of the CO_2 fluxes are of good quality (class 0), 55% middle quality (class 1), 26% low quality (class 2) and 7% are missing due to instrument maintenance or malfunctioning. For the ABC-IS forest site, 8% of the CO_2 fluxes were missing due to instrument maintenance or malfunctioning, 7% were of class 0, 48% of class 1 and 37% of class 2. This indicates - from a micrometeorological point of view – that the site in San Rossore is better suited to perform measurements of turbulent exchange processes between forest and atmosphere than Ispra.
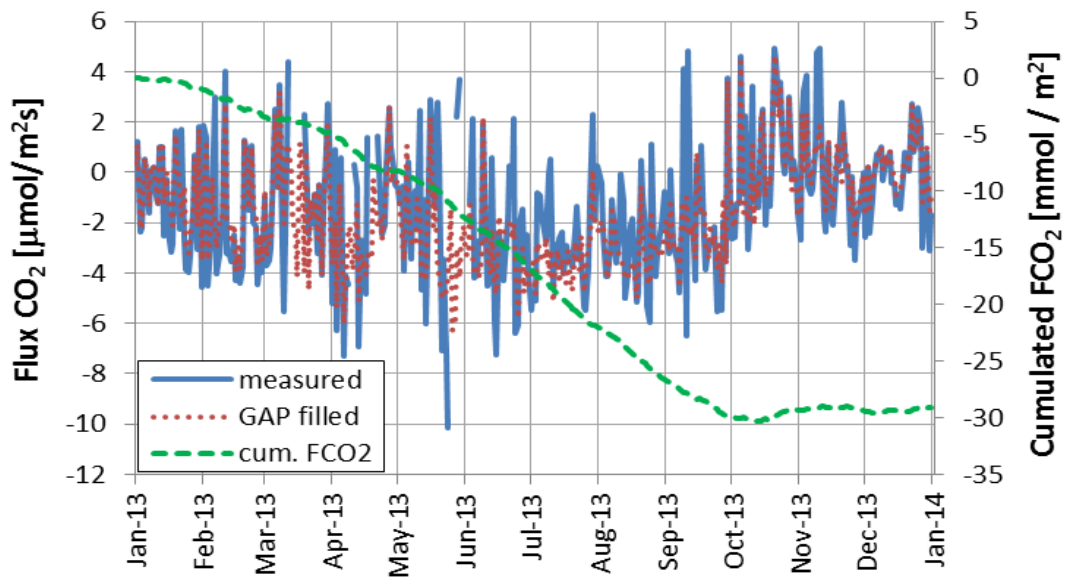
Fig. 70: Daily averages of measured (blue), gap filled (red) and cumulated (green) CO_2 fluxes.
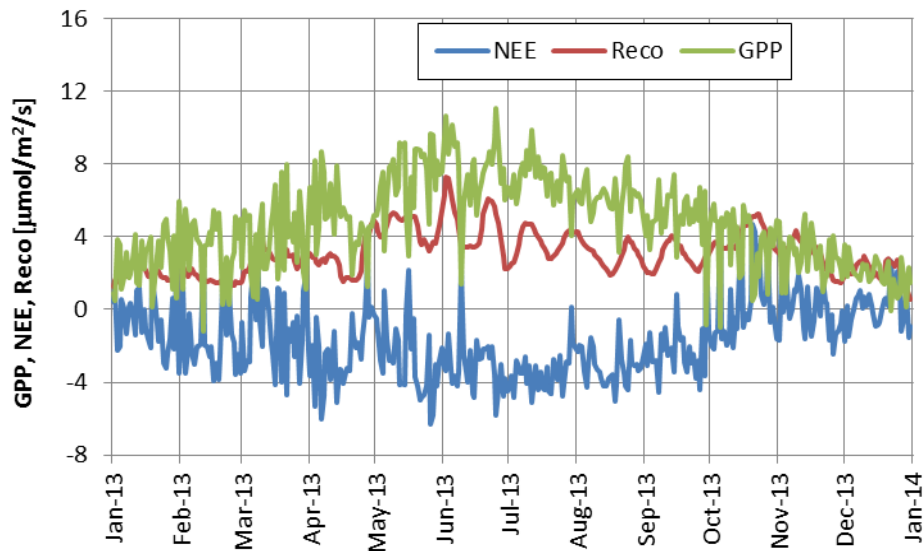

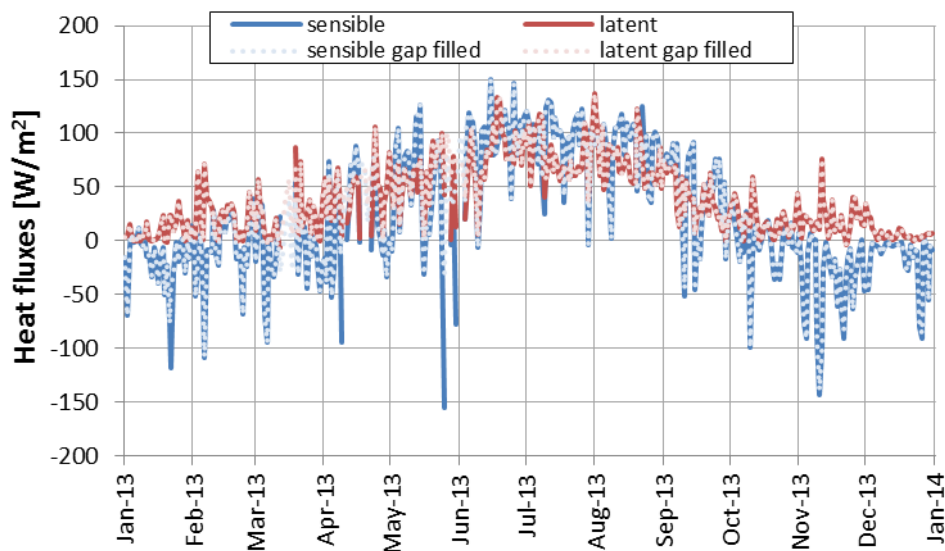*Fig. 71: Daily averages of NEE, GPP and Reco during 2013.*

Fig. 72: Daily averages of latent (red) and sensible (blue) heat fluxes.

Gap filling of the dataset has been performed without filtering for friction velocities (u*) below a threshold (that would indicate how turbulent the wind is) using the 'Eddy covariance gap-filling & flux-partitioning tool' online available at: www.bgc-jena.mpg.de/~MDIwork/eddyproc/ for missing and quality class 2 data. The cumulated sum of the gap filled 30 min CO_2 fluxes is shown in Fig. 70. The plot shows that in 2013 the Pinus pinea stand is a clear sink for CO_2 until October. Then ecosystem respiration and CO_2 uptake balance for the rest of the year. Using the flux partitioning module of the above mentioned online tool, the Net Ecosystem Exchange (NEE), i.e. the CO_2 flux measured, has been partitioned into Gross Primary Production (GPP) and Ecosystem Respiration (Reco) according to the equation:

$$NEE = Reco - GPP$$

and plotted as daily averages in Fig. 71. Calculating the budgets for 2013, NEE sums up to -630 g C m^{-2} year^{-1}, GPP to 1804 g C m^{-2} year^{-1} and Reco to 1174 g C m^{-2} year^{-1}. For the ABC-IS forest station in Ispra, the budgets sum up in 2013 for NEE to -407 g C m^{-2} year^{-1}, GPP to -1765 g C m^{-2} year-1 and Reco to 1358 g C m^{-2} year^{-1}. This indicates that carbon sequestration in the forest of San Rossore was higher compared to the forest in Ispra during 2013.

Fig. 72 shows the latent (red) and sensible (blue) heat fluxes for 2013 as daily averages. As it is typical for dryer ecosystems, the sensible heat flux especially in summer is higher than the latent heat flux.
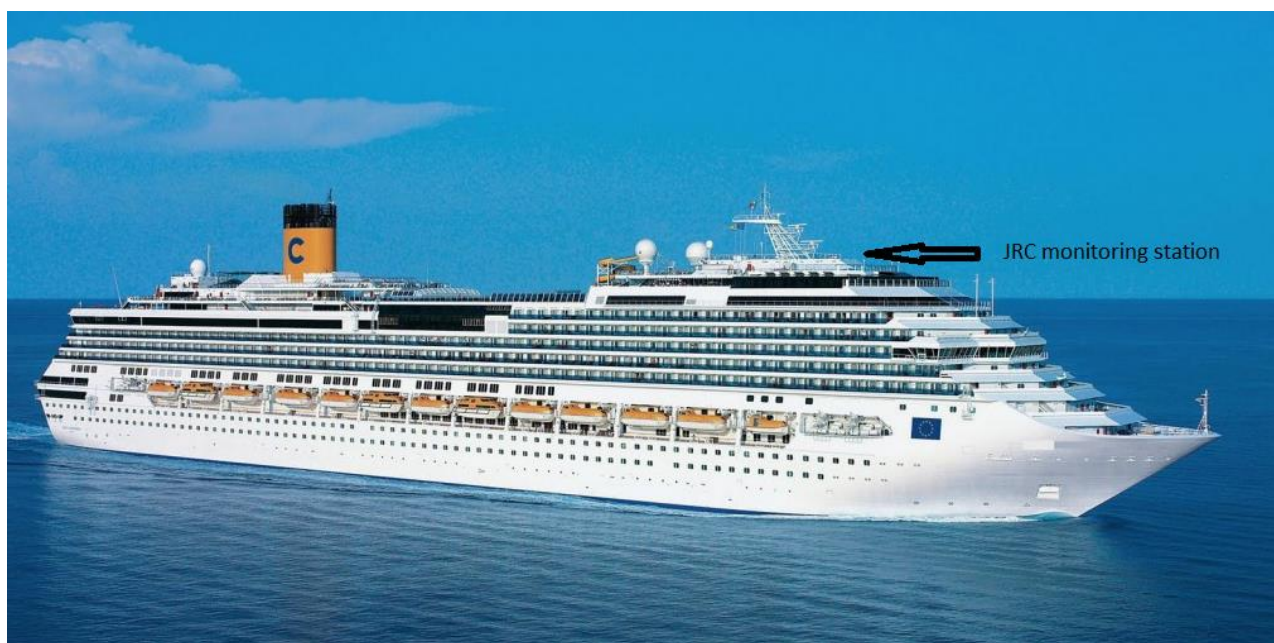
Fig.73: Costa Favolosa. The JRC air pollutant monitoring station is in the position at the top-front of the ship indicated on the picture.

Table 16. *Time schedule for Costa Favolosa in 2013 during the period of the measurements (local time).*

Day of the	Harbour	Arrival	Departure
Monday	Savona	09:00	17:00
Tuesday	Barcelona	13:30	19:30
Wednesday	Palma	09:00	18:00
Thursday	*At sea*		
Friday	Malta	08:00	18:00
Saturday	Catania	08:00	14:00
Sunday	Naples	08:00	14:00

Air pollution monitoring from a cruise ship

Introduction

Measurements of air pollutants over the Western Mediterranean have been carried out regularly since the autumn of 2005 during spring, summer and autumn from a monitoring station placed in a cabin on cruise ships belonging to the fleet of the Italian cruise line Costa Crociere. The basis for this monitoring activity is a collaboration agreement between Costa Crociere and the JRC. The scope of this activity is to obtain information about the concentration levels of air pollutants in this area, to improve the understanding of their sources and to test the performance of air pollution chemical transport models. Further, as this is intended as a long term monitoring activity, it is also potentially useful for analysis of trends and changes related to introduction of new legislation. So far four scientific papers have been published based on the data obtained from this monitoring activity (Marmer et al. 2009, Velchev et al. 2011, Schembari et al. 2012 and Schembari et al. 2014), where also more details about the instrumentation on board can be found.

In 2013 the measurement activities included a one-week campaign activity aiming at measuring the contents of Be-7 in particles in the area along the route of the ship. Be-7 is produced in the stratosphere and in the upper troposphere by interactions of cosmic radiation with nitrogen and oxygen and is thus a tracer of downwards transport of air masses to ground level. The half-life of Be-7 is 53 days.

In 2013 the JRC monitoring equipment was placed on Costa Favolosa.

Measurement platform location

In order to obtain a dataset that allows us to observe year-to-year variations, the measurements have, as far as possible, been performed on ships that follow the same weekly route in the Western Mediterranean. This implies that the monitoring instruments occasionally must be moved from one Costa Crociere ship to another. The measurements of air pollutants in 2013 were performed from June 17 until November 15 on the cruise ship Costa Favolosa, which was following a fixed weekly route in the Western Mediterranean (see Table 16).

Ambient air was sampled from inlets placed at the top front of the ship at appr. 50 m a.s.l. In order to test if this sampling point was equivalent to the ideal sampling point at the very front of the bow of the ship, a series of measurements of ozone and particle size distributions were carried out in July 2005 by the beginning of this monitoring activity. The results showed excellent agreement between ozone concentrations measured at the front of the bow and at the top of the cabin on Deck 14. For the aerosols, the agreement was generally also very good, discrepancies were only found in harbours with strong local emission sources and in a situation with fog and thus strong stable layering of the atmosphere.

Instrumentation

The automatic monitoring station on Costa Favolosa hosted the following measurement equipment

- Ozone Analyser (Model C49, Thermo Electron Instruments Inc., USA, S/N 0503110497),
- Trace level SO_2 Analyser (Model 43i-TLE, Thermo Electron Instruments Inc., S/N 0724324323)
- Trace level NOx-analyser (Model 42i-TL, Thermo Electron Instruments Inc., S/N 0710820808).
- Carbon monoxide IR analyser (Model 48, Thermo Electron Instruments Inc., S/N 68275-360).
- Aerosol Black Carbon Analyzer (Aethalometer, AE 21, 2 wavelengths, Magee Scientific, USA)
- Delta Ohm HD2003 ultrasonic anemometer (S/N 10007572); the built-in compass in this instrument allowed also to obtain the course of the ship.
- GPS Evermore SA320 instrument.

The inlets to the gas monitors and Aethalometer have a cut-off respectively at 1 μm and 10 μm particle diameter by a homemade inertial impactor. Before entering the gas analysers the air passes through 5 μm pore size PTFE Millipore membrane filters in order to remove particles. The measurement procedure complies with the recommendations in the EMEP manual (EMEP, 1996). The anemometer as well as the GPS were placed at the top of the cabin housing the other instruments.

Samples for the evaluation of Be-7 activity were taken on 102 mm quartz fibre samples using a Tecora ECHO PUF high volume sampler with a flow rate of approximately 180 L min^{-1}.

Data quality control and data processing

Calibrations are performed by use of certified standards of NO, CO, SO_2 and zero air from Air Liquide. Before being brought on the ship, the Air Liquide standards were certified by comparison to VSL (National Metrology Institute of The Netherlands) primary standards in the ERLAP laboratory in Ispra. Calibrations were performed automatically during the week while the measurements were running unattended. NOx and SO_2 were calibrated once per week while CO zero calibrations were performed daily because of rapid baseline drift. CO span calibration was performed once per week. Ozone was calibrated by comparison to a portable primary standard (Thermo Electron 49C PS).

The ozone analyser (Model C49) showed good stability: it was calibrated before the start of the measurements, during the measurements period and after getting back to the laboratory; no correction of the data was needed. This stability is related to the fact that the instrument is using a two-channel system: one channel measures ambient air while the other channel measures ambient air filtered by an ozone scrubber, and thus it provides a continuously updated zero point for the measurements.

Also the NOx and SO_2 analysers showed a good stability: NOx calibrations gave a zero value (+/- one standard deviation) of 0.09±0.02 ppbV and -0.04±0.04 for NO and NO_2, respectively; the measured span gas multiplication correction factor ($C_{measured}/C_{certified}$) varied from 0.94-0.99. For SO_2, the calibrations gave zero values of 0.05±0.03 ppbV while the measured span gas calibration multiplication factor was 1.05±0.01. CO showed by far the largest drift of the zero point (8 ppbV per day). Correction for the zero point drift were performed. The CO analyzer has also a much lower precision than the NOx, SO_2 and ozone instruments that have stated precisions of 1 ppbV or less, although the actually observed

precision was somewhat better than the 100 ppbV reported by the manufacturer. The actual precision of the instrument can be evaluated based on the observed standard deviations of the zero and the span measurements (calibration gas: 1,027 ppmV CO) during the period, corrected for zero point drift, which were 35 ppbV and 42 ppbV, respectively.

Raw data are averaged over 10 minute intervals and stored in a computer in an ACCESS database, using a LABVIEW software developed by NOS S.r.l. (Fabrizio Grassi). Using an internet connection available on the ship, the 10 minutes data averages are transmitted hourly to the JRC by ftp.

Aethalometer data were corrected for the effects of multiple scattering. This correction was performed using estimated values of the scattering coefficient and the single scattering albedo of the particles, based on the chemical composition of particles found in three measurement campaigns on Costa Ships in the Western Mediterranean. The values obtained were close to those found in the study by Arnott et al, (2005). The correction at 880 nm (used for calculating [BC]) is around 5%.

Measurement program in 2013

Measurements started on June 17th but during the first weeks, until July 8th, technical problems caused long interruptions of the data acquisition. The measurements were performed continuously until November 15th, apart from interruptions between August 19th and August 21st and between September 25th and October 7th. The aethalometer measurements were only performed in the periods before July 18th and after October 14th.

The information on course and speed of the ship as well as on wind speed and direction, obtained from the ultrasonic anemometer, was used to identify situations where the measurements might be influenced by emissions from Costa Favolosa: in all cases where the inlets to the measurement station were downwind of the stack of the ship within an angle of ± 40 degrees the data were discarded because of the risk of contamination from the stack. Episodes where aethalometer measurements of BC may be influenced by absorption by dust are identified by observing the cases where the ratio between absorption coefficients at 370 nm and at 880 nm exceeds 1.4.

Particle samples were collected on 24 quartz fibre filters, starting in Savona, during the week July 29 to August 5. Sampled volumes were typically in the range between 110 and 170 m^3. The filters were subsequently analysed for Be-7 by Federica Simonelli and Matteo Dalmiglio (JRC Unit I04), using a calibrated high purity germanium (HPGe) gamma-ray detector (EG&G Ortec, USA) available at the JRC cyclotron facility in Ispra. In order to test the experimental procedure and establish which would be the necessary sampling time for being able to observe a significant signal from Be-7, a series of 10 samples were taken at the Ispra site and analysed, all using the same procedure as subsequently applied on the ship. It was concluded that a sampling period of 12 hours with the Tecora high volume sampler were sufficient to quantify the Be-7 activity for the levels of Be-7 found at the Ispra site during this period.
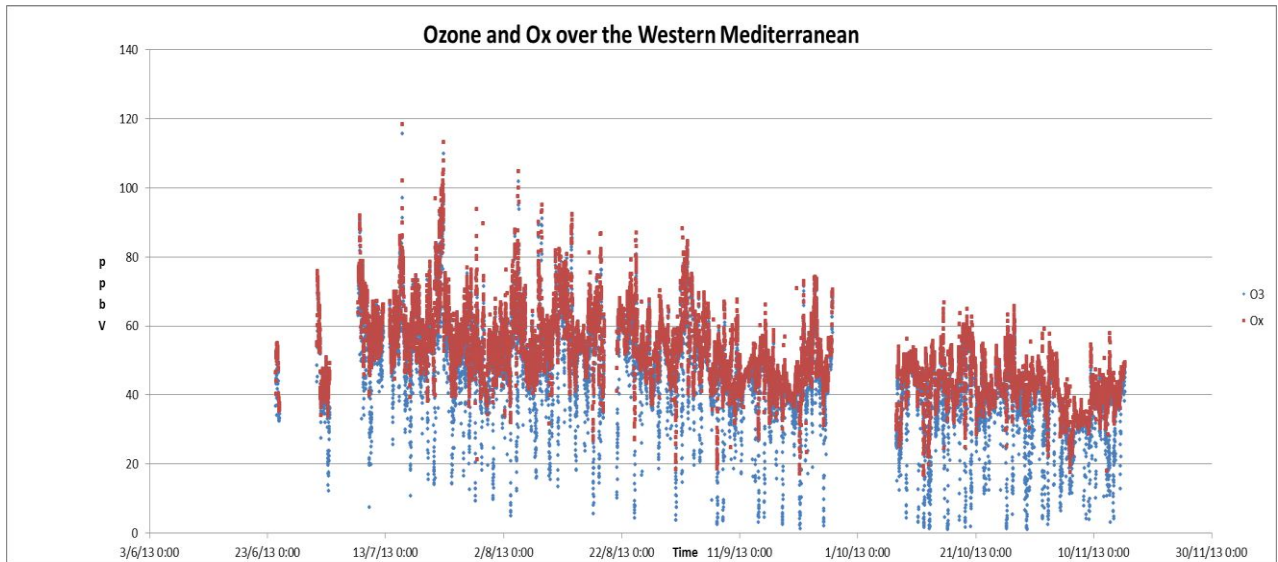
Figure 74. Day-to-day variations in ozone and Ox measured along the route of Costa Favolosa in the Western Mediterranean (including harbours).
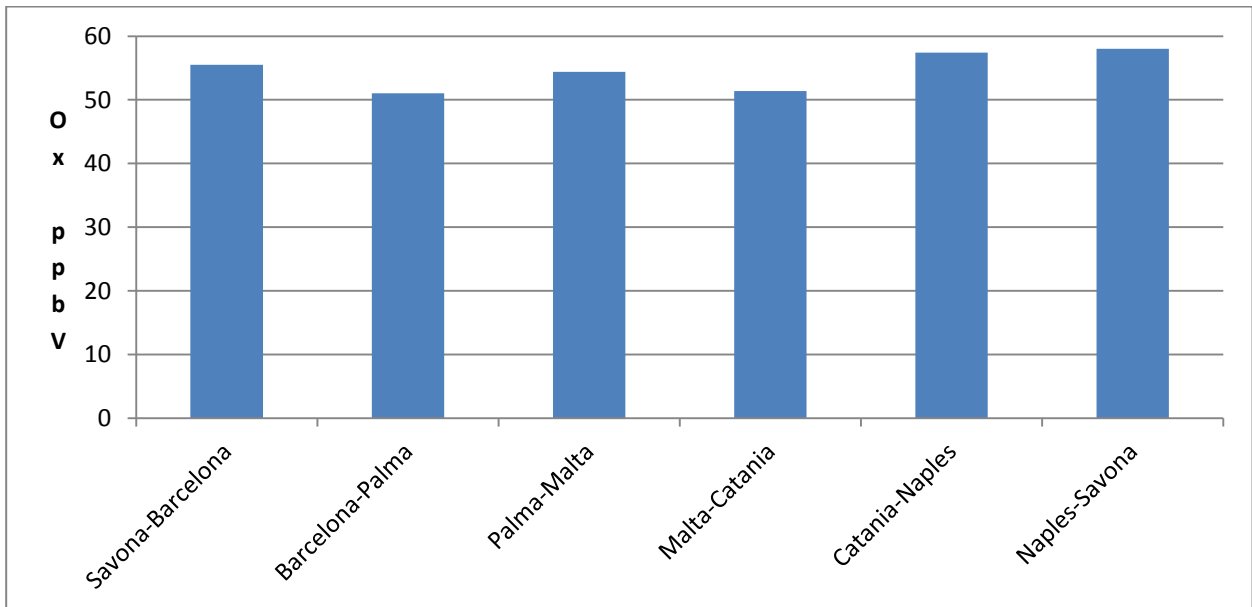

Figure 75. Average concentrations of Ox (the sum of O_3 and NO_2) for each leg of the ship route during the whole period of the measurements.

Results

The measured day-to-day variation of O_3 and O_x (the sum of O_3 and NO_2) along the route of the ship, including harbours, are shown in Figure 74. The parameter 'Ox' is used because the rapid changes in ozone are often caused by the reaction with NO, emitted from ships and other combustion sources:

$$O_3 + NO \rightarrow NO_2 + O_2$$
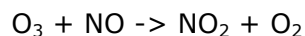
In this case the sum of O_3 and NO_2 (O_x) remains constant and corresponds to what the concentration of ozone would be if not influenced by near-by emissions of NO. Particularly in and around ports Ox is a convenient parameter to look at rather than ozone, which is frequently reduced due to the influence of local sources of NO.

The data show a maximum in the ozone and Ox concentrations in the month of July. The average concentrations of Ox for each leg of the route are shown in Figure 75, while Figure 76 (top of next page) shows an example of the distribution of the 10 minute average values of Ox along the route of the ship during a one-week cruise in July. It is seen that there can be large local variations in Ox within each leg of the route of the ship.

Figure 76 (bottom of next page) shows the distribution of SO_2 along the route of Costa Favolosa during the same week. SO_2 shows large variations because it is strongly influenced by the emissions from ships passing nearby. This influence is for instance seen in the part of the route between Sicily and the North African coast where Costa Favolosa crosses a main ship route in the Mediterranean, going from the Strait of Gibraltar to the Suez Channel.

The gamma-ray spectra of the particle samples collected during the week July 29 to August 5 along all of the legs of the cruise had a significant peak from Be-7, just above the detection limit, only in one case, which was the harbour of Savona on July 29; in all other cases Be-7 was not detected. The Minimum Detectable Activity for Be-7 by the conditions used for these measurements was between 0.5 and 1 Bq for 24 hours measurement time. Applying a measurement time as long 48 hours did not allow us to observe detectable activities of Be-7 in the filter samples. This indicates that transport of air masses from the upper troposphere or the stratosphere, which under some circumstances can be a relevant source of ozone at ground level, were not of importance during the period where the filter samples were collected. Ozone reached a maximum of 102 ppbV during the week of this cruise. The Be-7 concentrations over the sea were lower than those that could be observed at the Ispra site from the measurements performed during the month of May 2013.
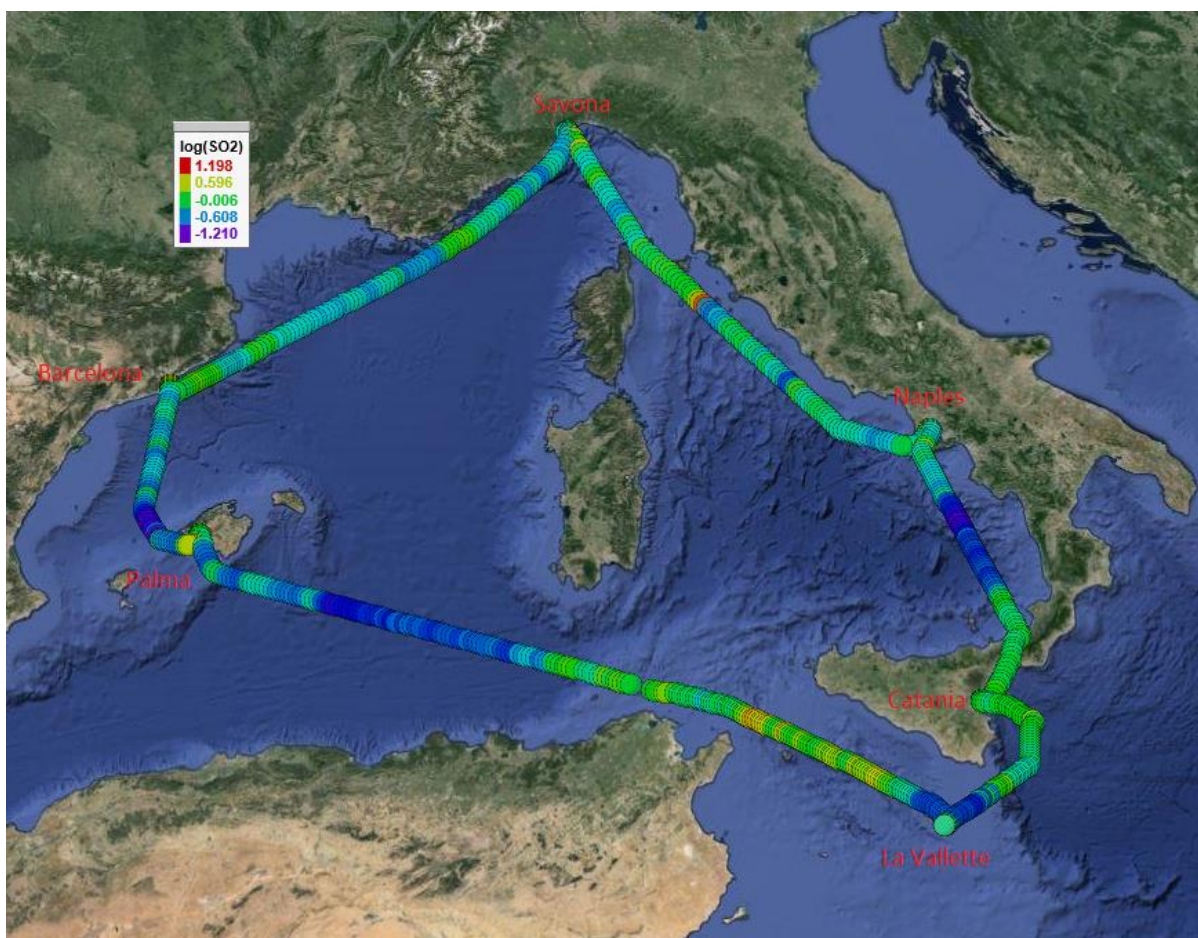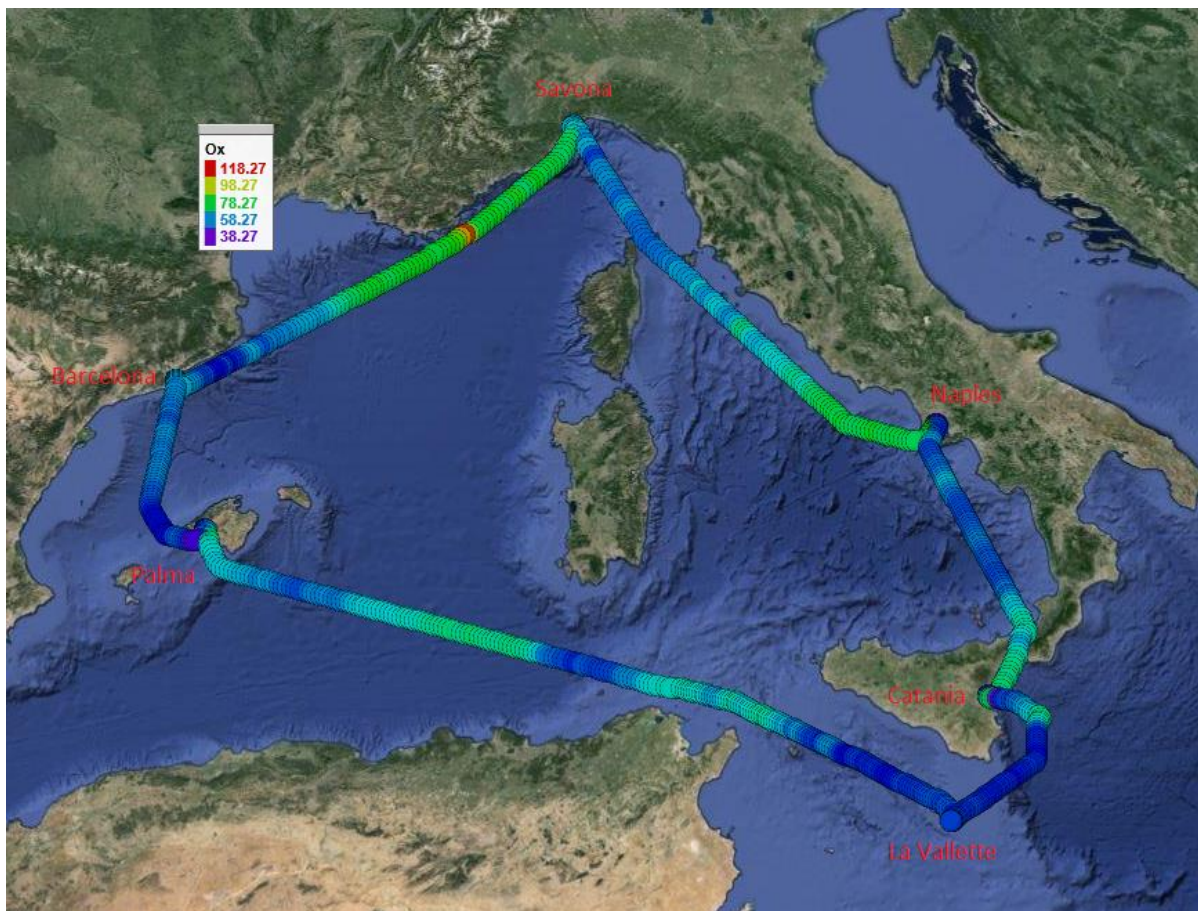
Figure 76. Measured concentrations of (top) Ox, outside of harbours, and (bottom) SO_2 (on a logarithmic scale) along the route of Costa Favolosa during the week July 15-21, 2013.

Ozone concentrations measured this year can be compared to those obtained during the previous years. Such a comparison for the case of ozone is shown in Figure 77 for the month of August. This month has been chosen because it is covered by the measurements without major interruptions during all of the years, apart from 2012. The routes in the Western Mediterranean of the ships on which the measurements were done during these years are similar, but not exactly the same. The largest change took place in 2011 where the ship started to go directly from Palma to Malta without calling at the port of Tunis, contrary to what was previously the rule.
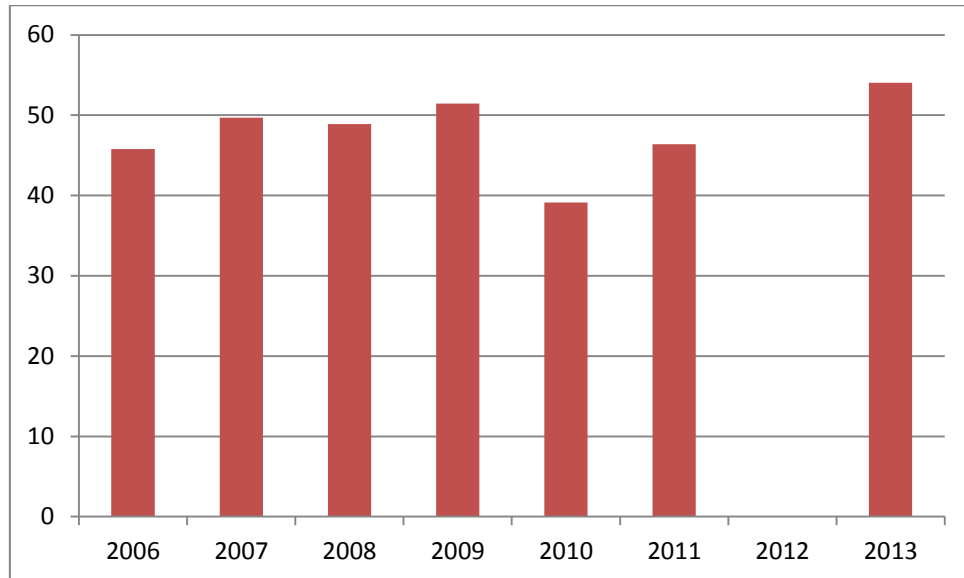
Figure 77. Average ozone concentrations, measured along the route of Costa ships in the Western Mediterranean, outside of ports, during the month of August.

Conclusions

The measurements provided information about the concentrations of ozone, NOx, SO_2 and CO at the sea and in harbours along the route of Costa Favolosa in the Western Mediterranean during summer and autumn of 2013. Due to technical problems Black Carbon data are only available for a brief period. The highest concentrations of ozone were found in the middle of July. Measurements of Be-7 activity during the week July 29 – August 5 indicated that transport from the upper troposphere or the stratosphere was not a relevant source of ozone at sea level.

References

Adam, M., J. P. Putaud, S. Martins dos Santos, A. Dell'Acqua, and C. Gruening, Aerosol hygroscopicity at a regional background site (Ispra) in Northern Italy, Atmos. Chem. Phys., 12, 5703–5717, 2012

Anderson, T.L., and Ogren, J.A., Determining aerosol radiative properties using the TSI3563 integrating nephelometer, *Aerosol Sci. Technol.*, **29**, 57-69, 1998.

Arnott, W.P., Hamasha, K., Moosmüller, H., Sheridan, P.J., and Ogren, J.A., Towards aerosol light-absorption measurements with a 7-wavelength Aethalometer: Evaluation with a photoacoustic instrument and a 3 wavelength nephelometer., *Aerosol Sci. Technol.*, **39**, 17-29, 2005.

Barnaba, F., Putaud, J.P., Gruening, C., Dell'Acqua, A., Dos Santos, S., Co-located in-situ, total-column and height-resolved aerosol observations: Implications for ground-level PM estimation from remote sensing. *J. Geophys. Res.*, **115**, D10204, doi:10.1029/2009JD012451, 2010.

Butterbach-Bahl K., R. Gasche, L. Breuer & H. Papen, Fluxes of NO and N_2O from temperate forest soils: impact of forest type, N deposition and of liming on the NO and N_2O emissions, Nutrient Cycling in Agroecosystems 48: 79–90, 1997.

Cavalli, F., Putaud, J.P., Toward a standardised thermal-optical protocol for measuring atmospheric organic and elemental carbon: the EUSAAR protocol, *Atmos. Meas. Tech.*, **3**, 79-89, 2010.

Chen, H., Harmon, M.E., Griffiths, R.P., Hicks, W., 2000. Effects of temperature and moisture on carbon respired from decomposing woody roots. Forest Ecology and Management, 138 (1-3), pp. 51-64

Cooke, W.F., Liousse, C., Cachier, H., and Feichter, J., Construction of a 1x1°fossil fuel emission data set for carbonaceous aerosol and implementation and radiative impact in the ECHAM4 model, *J Geophys. Res.*, **104**; 22,137-22, 1999.

Curiel Yuste, J., Janssens, I.A., Carrara, A., Ceulemans, R., 2004. Annual Q10 of soil respiration reflects plant phenological patterns as well as temperature sensitivity. Global Change Biology, 10 (2), pp. 161-169

Davidson, E.A., Keller, M., Erickson, H.E., Verchot, L.V., Veldkamp, E., 2000. Testing a conceptual model of soil emissions of nitrous and nitric oxides. BioScience, 50 (8), pp. 667-680.

Dell'Acqua, A., Putaud J.P., Gruening, C., Study of the JRC-Ispra EMEP site representativeness for short-lived atmospheric species measurements, *JRC report* EUR 24312 EN, 2010.

EMEP manual for sampling and chemical analysis (1995). *EMEP/CCC-Report 1/95. (Revised 1996; 2001; 2002).* 1995.

Erickson, H.E., Perakis, S.S., 2014. Soil fluxes of methane, nitrous oxide, and nitric oxide from aggrading forests in coastal Oregon. Soil Biology and Biochemistry 76, pp. 268-277

European Directive 2008/50/EC. On ambient air quality and cleaner air for Europe. 2008.

Firestone, M.K., Davidson, E.A., 1989.Exchange of Trace Gases Between Terrestrial Ecosystems and the Atmosphere, pp. 7-21.

Franzluebbers, K., Franzluebbers, A.J., Jawson, M.D., 2002. Environmental controls on soil and whole-ecosystem respiration from a tallgrass prairie. Soil Science Society of America Journal, 66 (1), pp. 254-262

Gruening C., Goded I., Jensen N.R., Cescatti A., Cieslik S., Project Document ABC-IS forest flux tower, ARES(2011)1288711, (2011)

Gruening C., Goded I., Cescatti A., D. Fachinetti, I. Fumagalli, M. Duerr, ABC-IS Forest Flux Station, Report on Instrumentation, Operational Testing and First Months of Measurements, EUR 25705 EN, (2012), JRC76928.

Gut, A., Scheibe, M., Rottenberger, S., (…), Müller, E., Piedade, M.T.F., 2002. Exchange fluxes of NO2 and O3 at soil and leaf surfaces in an Amazonian rain forest. Journal of Geophysical Research: Atmospheres 107 (20), pp. 27-1-27-15

Herich, H., Gianini, M. F. D., Piot, C., Močnik, G., Jaffrezo, J.-L., Besombes, J.-L., Prévôt, A. S. H. and Hueglin, C.: Overview of the impact of wood burning emissions on carbonaceous aerosols and PM in large parts of the Alpine region, Atmos. Environ., 89, 64–75, doi:10.1016/j.atmosenv.2014.02.008, 2014.

Hess, M., Koepke, P. Schult, I., Optical Properties of Aerosols and Clouds: The Software Package OPAC, *Bull. of Am. Meteorol. Soc.*, **79**; 831-844, 1998.

Horváth, L., Führer, E., Lajtha, K., 2006. Nitric oxide and nitrous oxide emission from Hungarian forest soils; linked with atmospheric N-deposition. Atmospheric Environment 40 (40), pp. 7786-7795

Jensen, N. R., Gruening, C., Adams, M., Cavalli, F., Cavalli, P., Grassi, F., Dell'Acqua, A., Martins Dos Santos, S., Roux, D., Putaud, J.-P. JRC Ispra EMEP – GAW regional station for atmospheric research, 2009 report, *EUR 24678 EN*, (2010), *JRC62602*.

Johansson, C., 1984. Field measurements of emission of nitric oxide from fertilized and unfertilized forest soils in Sweden. J. Atmos. Chem. 1, 429-442.Kiehl, J. T., Schneider, T. L., Rasch, P. J., Barth, M. C., Wong, J., Radiative forcing due to sulfate aerosols from simulations with the National Center for Atmospheric Research Community Climate Model, Version 3 (Paper 1999JD900495), *J. Geophys. Res.,* **105**; 1441-1458, 2000.

Marmer, E., Velchev , K., Hjorth, J., Vignati, E., Cavalli, F., Dentener, F., v. Aardenne,J., Raes, F. , Assessment of Impact of Ship Emissions Over the Summertime Mediterranean Sea, *Second International Conference on Harbours, Air Quality and Climate Change (HAQCC),*Rotterdam, the Netherlands, 29-30 May 2008.

Marmer, E., Dentener, F., Aardenne, J, Cavalli, F., Vignati, E., Velchev, K., Hjorth, J., Boersma, F. and Raes, F.: What can we learn about ship emission inventories from measurements of air pollutants over the Mediterranean Sea*,* Atmos. Chem. Phys., 9, 6815-6831, 2009.

McMurry, P., Wang, X., Park, K., and Ehara, K. The relationship between mass and mobility for atmospheric particles: A new technique for measuring particle density, *Aerosol Sci. Tech*., **36**, 227–238, 2002.

Mira-Salama, D., Van Dingenen, R., Gruening, C., Putaud, J.-P, Cavalli, F., Cavalli, P., Erdmann, N., Dell'Acqua, A., Dos Santos, S., Hjorth, J., Raes, F., Jensen, N.R. Using Föhn conditions to characterize urban and regional sources of particles, *Atmospheric Research* **90**, 159–16, 2008.

Paatero, P.: User's guide for the multilinear engine program "ME2" for fitting multilinear and quasimultilinear models, University of Helsinki, Finland, 2000.

Papen, H., Hellmann, B., Papke H. and Rennenberg H., 1993. Emissions of N-oxides from acid irrigated and limed soils of a coniferous forest in Bavaria. In Biogeochemistry of Global Change: Radiatively Active Trace Gases, edited by R. S. Oremland, pp. 95-103, Chapman and Hall, New York

Petzold, A., H., Schönlinner, M., Multi-angle absorption photometry - A new method for the measurement of aerosol light absorption and atmospheric black carbon, *Journal of Aerosol Science*, **35** (4), 421-441, 2004.

Putaud, J.-P., et al. (21 authors), 2004, A European aerosol phenomenology—2: chemical characteristics of particulate matter at kerbside, urban, rural and background sites in Europe. *Atmospheric Environment*, **38**, 2579-2595.

Putaud, J.-P., et al. (39 authors), 2010, A European aerosol phenomenology—3: Physical and chemical characteristics of particulate matter from 60 rural, urban, and kerbside sites across Europe. *Atmospheric Environment*, **44**, 1308-1320.

Putaud, J.P., F. Cavalli, S. Martins dos Santos, and A. Dell'Acqua, Long-term trends in aerosol optical characteristics in the Po Valley, Italy, Atmos. Chem. Phys., 14, 9129–9136, 2014.

Russell, L.M.: Aerosol organic-mass-to-organic carbon ratio measurements, *Environ. Sci. Technol.*, **37**, 2982-2987, 2003.

Schaufler, G., Kitzler, B., Schindlbacher, A., Skibab, U., Sutton, M. A. & Zechmeister-Boltenstern S., 2010. Greenhouse gas emissions from European soils under different land use: effects of soil moisture and temperature. European Journal of Soil Science, October 2010, 61, 683–696

Schindlbacher, A., Zechmeister-Boltenstern, S., Butterbach-Bahl, K., 2004. Effects of soil moisture and temperature on NO, NO2, and N 2O emissions from European forest soils, Journal of Geophysical Research D: Atmospheres 109 (17), pp. D17302 1-12.

Schmid, O., et al., Spectral light absorption by ambient aerosols influenced by biomass burning in the Amazon Basin I: comparison and field calibration of absorption measurements techniques, *Atmos. Chem. Phys.*, **6**, 3443-3462, 2006.

Scheeren, H. A., P. Bergamaschi, N. R. Jensen, C. Gruening, I. Goded, and J. van Aardenne, First results from the new JRC greenhouse gas monitoring site at Ispra, Italy. In Willi A. Brand (ed.) Report of the 15th WMO/IAEA Meeting of Experts on Carbon Dioxide, Other Greenhouse Gases and Related Tracers Measurement Techniques, Jena, Germany, 7-10 September 2009, WMO GAW report N. 194, 2010.

Scheeren, H. A., P. Bergamaschi et al., An analysis of four years of CO_2, CH_4, N_2O and SF_6 observations and [222]Radon-based emission estimates from the monitoring station at Ispra (Italy), for submission to Atmos. Chem. Phys. Discuss., 2013.

Schembari, C., F. Cavalli, E. Cuccia, J. Hjorth, G. Calzolai., N. Pérez, J. Pey, P. Prati, F. Raes: Impact of a European directive on ship emissions on air quality in Mediterranean harbours, Atmospheric Environment (2012), doi: 10.1016/j.atmosenv.2012.06.047.

Schembari, C., M.C. Bove, E. Cuccia, F. Cavalli, J. Hjorth, D. Massabò, S. Nava, R. Udisti, P. Prati, Source apportionment of PM10 in the Western Mediterranean based on observations from a cruise ship. Atmospheric Environment 98, 510–518, 2014.

Skiba, U., Fowler, D. and Smith, K.A. 1994. Emissions of NO and N2O from soils. In: Non-CO2 Greenhouse Gases (Ed. J. van Ham, L.J.H.M. Janssen and R.J. Swart), Kluwer, Dordrecht, 153–158

Stark, J.M., Smart, D.R., Hart, S.C., Haubensak, K.A., 2002. Regulation of nitric oxide emissions from forest and rangeland soils of Western North America. Ecology, 83 (8),pp. 2278-2292

Stratmann, F., Wiedensohler, A. A new data inversion algorithm for DMPS-measurements. *J. Aerosol Sci.*, **27** (Suppl 1), 339-340, 1996.

Sulzman, E.W., Brant, J.B., Bowden, R.D., Lajtha, K., 2005. Contribution of aboveground litter, belowground litter, and rhizosphere respiration to total soil CO2 efflux in an old growth coniferous forest. Biogeochemistry,73(1),pp. 231-256

Van Dingenen, R., et al. (28 authors), 2004, A European aerosol phenomenology −1: Physical characterization of particulate matter at kerbside, urban, rural and background sites in Europe, *Atmospheric Environment*, **38**, 2561-2577.

Velchev, K., Cavalli F., Hjorth J., Vignati E., Dentener F., Raes F., Ozone over Western Mediterranean Sea-results from two years of shipborne measurements., Atmospheric Chemistry and Physics, 11, 675-688, 2011.

Venterea, R.T., Groffman, P.M., Verchot, L.V., Magill, A.H., Aber, J.D., Steudler, P.A., 2003. Nitrogen oxide gas emissions from temperate forest soils receiving long-term nitrogen inputs. Global Change Biology,9 (3),pp. 346-357.

Weingartner, E., Saathoff, H., Schnaiter, M., Streit, N., Bitnar, B., and Baltensperger, U., Absorption of light by soot particles: determination of the absorption coefficient by means of aethalometers, *J. Aerosol Sci.*, **34**, 1445-1463, 2003.

Weitkamp, C. (editor), LIDAR Range-Resolved Optical Remote Sensing of the Atmosphere, *Springer*, New York, 2005.

WHO, Health risks of ozone from long-range transboundary air pollution, 2008.

Williams, E.J., and F.C. Fehsenfeld, 1991. Measurement of soil nitrogen oxide emissions at three North American ecosystems, J. Geophys. Res., 96, 1033-1042

Williams, E.J., Hutchinson, G.L., Fehsenfeld, F.C. , 1992. NOx and N2O emissions from soil. Global Biogeochemical Cycles. Volume 6, Issue 4, Pages 351-388

Worthy, D. E. F., I. Levin, N. B. A. Trivett, A. J. Kuhlmann, J. F. Hopper, and M. K. Ernst, Seven years of continuos methane observations at a remote boreal site in Ontario, Canada, J. Geophys. Res., 103 (D13), 15995-16007, 1998.

Zahorowski, W., S. D. Chambers, A. Henderson-Sellers, Ground based radon-222 observations and their application to atmospheric studies, J. Environm. Radioact., 76, 3-33, 2004.

Zhang, Q., Jimenez, J. L., Canagaratna, M. R., Ulbrich, I. M., Ng, N. L., Worsnop, D. R. and Sun, Y.: Understanding atmospheric organic aerosols via factor analysis of aerosol mass spectrometry: a review, Anal. Bioanal. Chem., 401(10), 3045–3067, doi:10.1007/s00216-011-5355-y, 2011.

Links

ACTRIS, *www.actris.net*

ARPA Lombardia, *ita.arpalombardia.it/ITA/qaria/doc_RichiestaDati.asp*

Calipso, *www.nasa.gov/mission_pages/calipso/main*

Chemical Co-ordinating Centre of EMEP, *www.nilu.no/projects/ccc*

CLRTAP, *www.unece.org/env/lrtap/welcome.html*

EARLINET, *www.earlinet.org*

ECLAIRE: www.eclaire-fp7.eu

EMEP, *www.emep.int*

EPTR*,* European Pollutant Release & Transfer Register*,* prtr.ec.europa.eu/MapSearch.aspx

European Committee for Standardisation (CEN), *www.cen.eu/cen/pages/default.aspx*

EUSAAR, *www.eusaar.net/*

Global Atmosphere Watch (GAW), *www.wmo.int/pages/prog/arep/gaw/gaw_home_en.html*

ICOS, www.icos-infrastructure.eu

InGOS, www.ingos-infrastructure.eu

WDCA, *www.gaw-wdca.org*

World Meteorological Organization (WMO), *www.wmo.int/pages/index_en.html.*

JRC Mission

As the Commission's
in-house science service,
the Joint Research Centre's
mission is to provide EU
policies with independent,
evidence-based scientific
and technical support
throughout the whole
policy cycle.

Working in close
cooperation with policy
Directorates-General,
the JRC addresses key
societal challenges while
stimulating innovation
through developing
new methods, tools
and standards, and sharing
its know-how with
the Member States,
the scientific community
and international partners.

Serving society
Stimulating innovation
Supporting legislation

Publications Office